



<https://theses.gla.ac.uk/>

Theses Digitisation:

<https://www.gla.ac.uk/myglasgow/research/enlighten/theses/digitisation/>

This is a digitised version of the original print thesis.

Copyright and moral rights for this work are retained by the author

A copy can be downloaded for personal non-commercial research or study,  
without prior permission or charge

This work cannot be reproduced or quoted extensively from without first  
obtaining permission in writing from the author

The content must not be changed in any way or sold commercially in any  
format or medium without the formal permission of the author

When referring to this work, full bibliographic details including the author,  
title, awarding institution and date of the thesis must be given

Enlighten: Theses

<https://theses.gla.ac.uk/>  
[research-enlighten@glasgow.ac.uk](mailto:research-enlighten@glasgow.ac.uk)

# **M.Sc. Thesis**

**An**

# **Interferometric Auto- Correlator.**

Norman Macdonald Bett, submission for the degree of Master of  
Science in the Department of Electronic and Electrical  
Engineering in the University of Glasgow. October 1990.

Copyright : N. M. Bett, 1990.

ProQuest Number: 11007982

All rights reserved

INFORMATION TO ALL USERS

The quality of this reproduction is dependent upon the quality of the copy submitted.

In the unlikely event that the author did not send a complete manuscript and there are missing pages, these will be noted. Also, if material had to be removed, a note will indicate the deletion.



ProQuest 11007982

Published by ProQuest LLC (2018). Copyright of the Dissertation is held by the Author.

All rights reserved.

This work is protected against unauthorized copying under Title 17, United States Code  
Microform Edition © ProQuest LLC.

ProQuest LLC.  
789 East Eisenhower Parkway  
P.O. Box 1346  
Ann Arbor, MI 48106 – 1346

Acknowledgements :-

This work has been made possible by the kind support and co-operation of Professor J. Lamb. Thanks are also due to Professor De La Rue and Dr. C. Ironside for their advice and assistance throughout the project. The fine mechanical engineering work was carried out under the supervision of Mr. H. Anderson and the practical success of the instrument built is due to the skill of the mechanical engineering workshop staff. The work on semiconductor lasers was carried out with the co-operation of Brian Graham who kindly allowed me access to his equipment and provided useful advice and discussion.

Thanks are also due to the Chairman of the Department of Physics in the King Saud University, Professor Ahmed Suraiya and his successor Professor Ahmed Harkan who allowed me free access to laboratory and library facilities. Within the department Dr. Abdullah Azeer made me very welcome and reviewed and discussed my work.

Lionel Edwards of the National Guard School of Signals provided invaluable assistance with the computer simulations and Cable & Wireless allowed me considerable freedom to carry on my work.

TABLE OF CONTENTS :-

Summary - page(x)

CHAPTER ONE :

	<u>PAGE</u>
1.1 Introduction.	1.
1.2 Chirp in ultra-short pulses.	4.
1.3 Generation of ultra-short pulses.	7.
1.3.1 Elements necessary for ultra-short pulse generation.	7.
1.3.2 Spontaneous mode-locking.	10.
1.3.3 Active mode-locking.	11.
1.3.4 Passive mode-locking.	12.
1.4 Theory of mode-locking.	13.
1.4.1 Pulse width.	21.
1.4.2 Gaussian amplitude distribution.	21.
1.5 Structure of ultra-short pulses.	24.
1.6 Summary.	27.

CHAPTER TWO :

2.1 Methods of detection and measurement.	29.
2.1.1 Streak camera.	30.
2.1.2 Two-photon fluorescence.	33.

CHAPTER TWO (CONT) :

	<u>PAGE</u>
2.1.3 Pressure scan.	36.
2.1.4 Resonant vapour cell.	37.
2.1.5 Intensity auto-correlator.	40.
2.2 Summary.	

CHAPTER THREE :

3.1 Auto-correlation techniques.	45.
3.1.1 Linear auto-correlation of two pulses.	47.
3.1.2 Nonlinear auto-correlation of two pulses - 'slow' correlation.	49.
3.1.3 Background-free correlation.	51.
3.1.4 Nonlinear interferometric auto- correlation of two pulses - 'fast' correlation.	51.
3.1.5 Background-free interferometric auto-correlation.	53.
3.2 Interferometric auto-correlation and pulse shape.	56.
3.2.1 Linearly chirped pulses.	57.

TABLE OF CONTENTS (CONT)

<u>CHAPTER THREE (CONT) :</u>	<u>PAGE</u>
3.2.2 Correlation of pulses of unknown chirp.	57.
3.3 Summary.	59.
 <u>CHAPTER FOUR :</u>	
4.1 Interferometric measurement.	61.
4.2 Instrument design.	62.
4.2.1 Basic framework.	62.
4.3 Components used in the construction of the instrument.	65.
4.3.1 Optical components.	65.
4.3.2 Mechanical components.	71.
4.4 Factors affecting instrumental accuracy.	74.
4.4.1 Mechanical factors.	74.
4.4.2 Optical factors.	75.
4.4.3 Signal detection.	76.
4.5 Instrument operation.	76.
4.6 Instrument resolution.	77.

TABLE OF CONTENTS (CONT)

<u>CHAPTER FOUR (CONT) :</u>	<u>PAGE</u>
4.7 Instrument Assembly.	79.
4.8 Calibration of the "Inchworm" movement.	79.
4.9 Glitch in the "Inchworm" movement.	82.
4.10 Summary.	83.
 <u>CHAPTER FIVE :</u>	
5.1 Performance evaluation.	84.
5.2 Applications using the Michelson configuration.	84.
5.2.1 Interferogram and visibility curve from the output of a semiconductor laser.	85.
5.2.2 Sharp semiconductor laser LTO 15MFO.	86.
5.2.3 Theory of operation of a Sharp semiconductor laser.	87.

TABLE OF CONTENTS (CONT)

<u>CHAPTER FIVE (CONT) :</u>	PAGE
5.2.4 Experimental method used in recording a diode laser output.	90.
5.2.5 Visibility curve for a semiconductor laser diode.	92.
5.2.6 Semiconductor laser as part of phase combined array.	95.
5.2.7 Phase combination of two semiconductor lasers.	98.
5.2.8 Interferogram and visibility curve for a semiconductor laser mounted as part of a phase-combining experiment.	100.
5.2.9 Further experiments using the Michelson configuration.	105.
5.2.10 Instability and self-pulsing in a semiconductor laser.	106.
5.2.11 Effect of an external cavity on a semiconductor laser.	109.
5.3 Intensity auto-correlation.	111.

TABLE OF CONTENTS (CONT)

<u>CHAPTER FIVE (CONT) :</u>	<u>PAGE</u>
5.3.1 Intensity auto-correlation of a mode-locked Nd.YAG laser output.	112.
5.4 Interferometric auto-correlation	117.
5.4.1 Interferometric auto-correlation of part of an Nd.YAG pulse.	117.
5.4.2 Sampling interferometric auto- correlation of sections of an Nd.YAG pulse.	121.
5.5 Instability in an Nd.YAG laser output.	125.
5.6 Summary	127.
<u>CHAPTER SIX :</u>	
6.1 Conclusions drawn from the work completed.	128.
6.2 Suggestions for future applications.	129.
6.2.1 Fast Fourier transforms.	129.
6.2.2 Application of F.F.T. to pulse analysis.	130.

TABLE OF CONTENTS (CONT)

<u>CHAPTER SIX (CONT) :</u>	<u>PAGE</u>
6.2.3 System modifications.	131.
6.2.4 Research applications.	132.
6.3 Summary	133.

SUMMARY OF THESIS CONTENTS.

This work concerns the design and building of an interferometric auto-correlator for use in the analysis of ultra-short pulses and their sources. The need for such an instrument is explained with particular reference to optical communications. The evidence for the existence of frequency change within ultra-short pulses and methods used to investigate such changes is reviewed.

The production of ultra-short pulses is briefly described and the basic theory of mode-locking treated. The relationship between pulse width and bandwidth is established. A brief theoretical treatment of a bandwidth limited pulse is given.

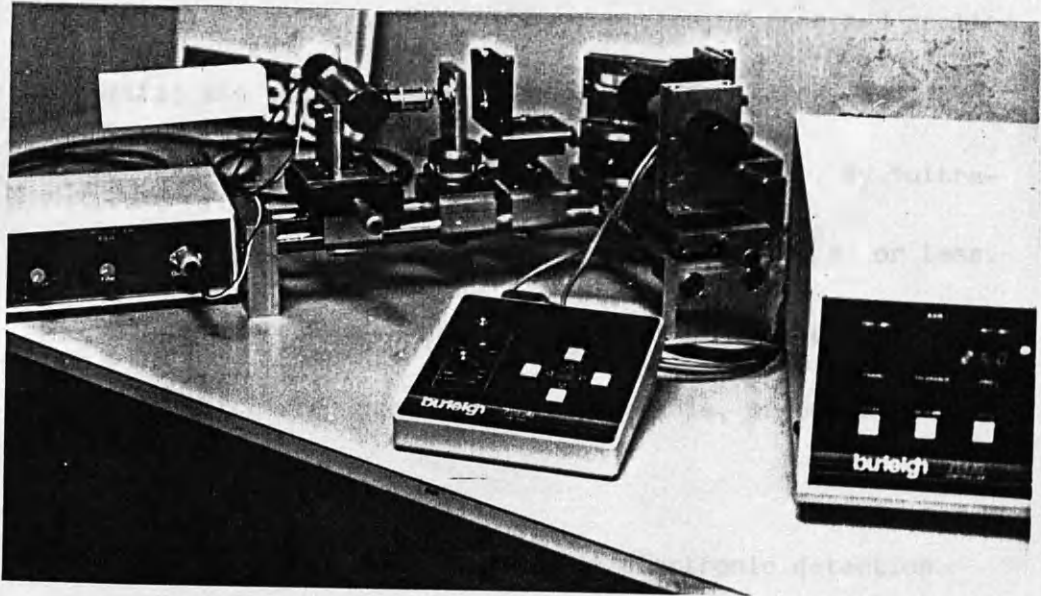
Methods used for the detection and measurement of ultra-short pulses are described. Their areas of applicability and their limitations are discussed. Linear and nonlinear correlation techniques are described. Fast and slow correlations are differentiated. Background-free correlation methods for intensity and interferometric scans are described. The necessity for interferometric correlations in the investigation of pulse structure is discussed. The effect of pulse chirp on the correlation obtained is described.

The difficulty in interpreting auto-correlations without assumptions regarding the pulse shape and structure, is noted.

The construction of an interferometric auto-correlator is described and the functions of the individual components detailed. The mechanical and optical factors affecting instrumental accuracy are discussed. The operation of the instrument is described and its resolution estimated. The results of initial calibration tests are presented and the presence of 'glitch' in the obtained traces is noted. The source of the 'glitch' is identified.

The operation of the instrument is demonstrated in three modes. In the first mode it is used as a Michelson interferometer to investigate the output of a semiconductor laser. Visibility curves are presented and several laser parameters estimated from them. Evidence is presented for instability and self-pulsing during cw operation. In the second mode, its use as an intensity auto-correlator is demonstrated. Pulse width measurements are recorded for a mode-locked Nd.YAG laser. In the third mode of operation interferometric auto-correlations are carried out on part of an Nd.YAG pulse and samples of the pulse are taken at different points throughout the pulse length. Indication

of chirp within the pulse is demonstrated by the latter.



AN INTERFEROMETRIC AUTO-CORRELATOR.CHAPTER ONE.1.1 INTRODUCTION.

Physical investigations in many branches of pure and applied scientific and technological research are now being carried out using ultra-short optical pulses (1), (2), (3). By "ultra-short pulse" is meant a pulse of picoseconds ( $10^{-12}$ s) or less. They have made possible the direct observation of physical processes which were previously unobservable, or observed only by indirect methods.

The physical processes involved in electronic detection methods, are in general slow when observed on a picosecond time scale. For example, picosecond electro-optic sampling provides a time resolution which is almost ten times better than that which can be achieved by purely electronic instruments such as the sampling oscilloscope. Practical applications for short optical pulses are now emerging. They are encroaching on areas which have been traditionally regarded as exclusive to electronic engineering. Major examples would include electronic device characterization, communications signal processing and computing.

In communications applications, short pulses imply high data transmission rates. At present, pulse repetition rates in the gigabits( $10^9$  bits) per second range are possible over considerable distances using optical fibre as the transmission medium (4). The potential major advantage of optical communications is the large bandwidth available. The bandwidth-distance product in fibre communication systems is capable of handling 1000GHz over one kilometre of fibre length (4). There is also substantial avoidance of the distortion suffered by ultra-short electrical pulses in even small lengths of coaxial cable or micro-strip line. Bandwidth-limited pulses of five picoseconds duration have been shown to propagate in a fused silica fibre without distortion (5 ). The optical wavelength transmitted was  $1.30\mu\text{m}$  and the measured distances of propagation were 0.76km and 2.5km. The measured loss was only 0.5db/km. Other advantages of an optical communication system are greater security from listening devices and less liability to interference where a closed system is used.

The increase in transmission rates requires improved signal processing speeds. Current systems operate at 2.24GHz, while signal transmission at 10 gigabits per second has been demonstrated. Several applications indicate that the demand on information capacity, transmission and processing rates

will increase to a level requiring such high signalling rates. An example of this is the video telephone which would require a thousandfold increase in signalling speed in comparison with its audio counterpart if universally adopted. Frequency domain phase coding of individual short pulses has been proposed as a basis for an ultra high speed optical spread communications network (6). This allows a higher bit rate than is obtainable using time domain encryption, and decoding using direct laser modulation and electronic processing.

Whilst it has been realized that ultra-short pulses can be used in a wide range of applications, the problems of measuring such short pulses, identifying their structure and extracting the maximum information from them remains (7). The areas of application of ultra-short pulses have multiplied and the means of producing such pulses have become more readily available. However, the instrumentation for measuring pulse widths and more importantly, pulse shape and internal structure has not kept pace with the expansion of possible applications. Much effort has gone into modifying pulse structure using pulse compression techniques to approach the bandwidth limited 'ideal pulse'. The desire to produce ever shorter pulses may have overshadowed the need to investigate pulse structure more thoroughly.

Pulse structure has its origins in the method used to produce the pulse in the first instance. This is a laser which is inherently nonlinear in operation. The pulsed mode of operation can be achieved by a variety of means including 'Q' switched operation, active mode-locking, passive mode-locking or a combination of such methods. The pulse so produced will have its structure influenced by its subsequent history. In particular, its passage through optical materials and devices, both linear and nonlinear, will modify the spectral components in the pulse and may change their phase relations. Most pulse measurement techniques were developed originally to study the mechanism of laser mode-locking (8).

The existence of substructure in picosecond pulses was inferred from the discrepancy observed between measured and expected pulse widths in a passively mode-locked Neodymium-glass laser(3). It was confirmed by E. B. Treacy who built a grating pulse compressor which compensated for positive carrier frequency sweep ('chirp'). Using this instrument he obtained output pulse widths close to the bandwidth-limited values(9). He extended the usefulness of his method by combining it with a two-photon fluorescence technique which measured the positive frequency sweep (10),(11),(12). The first unambiguous proof of pulse chirp was also given by

Treacy who produced and directly displayed dynamic spectrograms of mode locked Nd-glass laser pulses (12). The presence of chirp in the pulse train emitted by a passively mode locked dye laser was indicated by asymmetry in the temporal pulse shape observed using auto-correlation methods (13). A background free auto-correlation was combined with spectral filtering which showed the presence of frequency sweep (14). It was later shown that an auto-correlation carried out with interferometric accuracy could contain information on the nature of chirp which might be present in a pulse(15). If individual interference fringes were recorded, measurements made on the pulse envelope yielded information on the nature of chirp present.

An instrument constructed by Toshio Kurobori and co-workers produced both phase and intensity correlations in a single run (16). This incorporated a piezo-electric movement which allowed very fine scanning of the pulse to be carried out. The interferometric trace obtained was compared with a computer simulation of possible chirped pulse correlations.

To avoid the assumption of pulse shape which is inherent in the above methods T. Kobayashi and co-workers combined second order auto-correlation with simultaneous profile scanning using a Fabry-Perot (17). A 'best fit' process was carried

out between the calculated correlation curve and the experimental curve. This yielded parameters which indicated the pulse shape. An interferometric auto-correlation then provided information on pulse chirp.

Rothenberg and Grischkowsky showed that it was possible to measure the time dependent relative phase of a frequency swept pulse by propagating it through a resonant vapour (sodium). This produced a heterodyne signal which was subsequently cross-correlated with a compressed version of the original pulse (18). The applicability of this was restricted by the difficulty of finding suitable two-level ensembles for the heterodyning process and the problems of interpretation when amplitude fluctuations were present in the input pulses.

A modified version was produced where the resonant vapour was replaced by a Mach-Zehnder incorporating a Fabry-Perot etalon in one arm. The latter produced a monochromatic reference pulse which could be heterodyned with the original pulse by adjusting the delay in one arm of the Mach-Zehnder. The heterodyned output pulse was then cross-correlated with a compressed version of the original pulse (19).

A general method for the measurement of chirp in ultra-short light pulses was proposed by Kazumori Naganuma and co-workers (20). A mathematical foundation for an assumption-

free pulse reconstruction based on the measurable auto-correlation functions was laid down. The sufficient conditions for the data set required were presented. An iterative technique making use of 'Fast Fourier Transforms' produced a reconstructed pulse form, including chirp, from the data gathered.

The object of the work presented here was to build an instrument capable of producing the necessary data set from which the nature of any chirp present in a pulse would be revealed.

1.3 Generation of ultra-short pulses.

Ultra-short pulses are generated by 'mode-locking' techniques. These range from spontaneous effects within the lasing medium, to induced effects which modify the gain characteristics of the laser. Once such a pulse has been produced, it may be further modified by its linear and nonlinear interactions with intra-cavity and extra cavity transparent elements. The original structure of the pulse and its subsequent modification by physical interaction with optical devices are matters of considerable interest. It is in this area that a stable and sensitive interferometric auto-correlator should prove useful.

1.3.1. Elements necessary for pulse generation. (See fig. 1.1).

A feedback loop consisting of an amplifier, a filter, a delay line and a nonlinear element which attenuates a low-level signal more than a high-level signal, behaves as a regenerative

pulse amplifier (3). If the loop gain is greater than unity, a pulse re-circulates indefinitely around the loop and each traversal gives rise to an output pulse at the output terminal. The nonlinear element emphasises the peak region while reducing the lower amplitude regions. It also discriminates against noise and unwanted reflections, and shortens the pulse to a width limited by the frequency response of the circuit. Microwave pulses of the order of nanoseconds in temporal length have been generated by this technique.

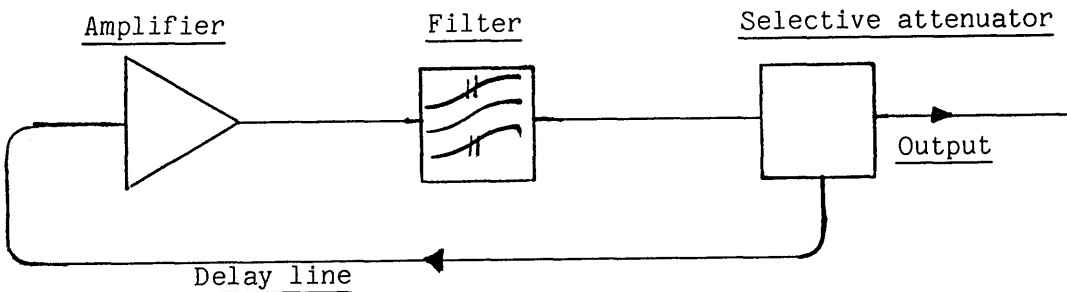


Fig 1.1. Essential elements in pulse generation.

A laser contains all the essential elements for regenerative pulse production with the possible exception of the nonlinear element described above. Most lasers consist of a region of material which exhibits gain over a narrow range of frequencies, and which is placed between two mirrors forming a resonant cavity. The lasing medium serves as an amplifier. The mirrors form an optical cavity which allows the formation of resonant

structures of the electro-magnetic field within it. The structures are essentially those provided by a Fabry-Perot cavity. The resonances, together with the linewidth of the laser transition, act as a filter.

A finite time is required by any pulse to traverse the cavity. The latter acts as a delay line. One end mirror allows a percentage of the incident pulse to be transmitted and hence forms an output. The temporal separation of the output pulses depends directly on the optical length of the cavity, being proportional to twice this length, as shown in figure 1.2.

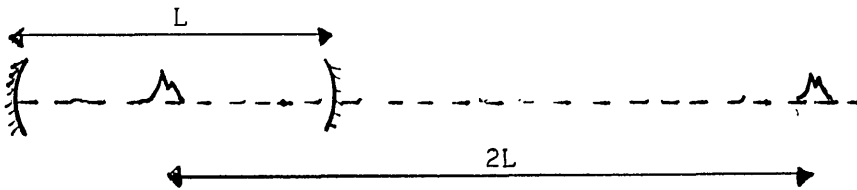


Fig.1.2. Output pulse separation for a mode-locked laser.

In a continuous wave (cw) laser the radiation field is spread out fairly uniformly between the mirror, although there may be random space-time fluctuations in the intensity. The generation of ultra-short pulses is based on the confinement of the energy in the cavity to a small spatial region or reducing the many fluctuations into one. This then forms the pulse which is reflected back and forth within the cavity.

If one mirror is partially transmitting, or a suitable beam splitter is placed within the cavity, a replica of each

pulse will be transmitted. The stream of pulses so generated will be spatially separated as shown in Fig.1.2 above. If this condition can be achieved and maintained, the laser is said to be mode-locked.

To achieve the mode-locked condition, selective attenuation must be applied. There are several ways in which this can be done. These will be considered briefly.

### 1.3.2. Spontaneous mode-locking.

Mode-locking can be spontaneous because the lasing medium is itself nonlinear in nature. This can affect the otherwise smooth spatial intensity distribution within the cavity. Experiments with helium-neon lasers operating on three longitudinal modes, showed that, when the mode frequency difference was identical for successive modes, mode-locking did occur (8). Solid state systems do not appear to exhibit self mode-locking, although there are conflicting viewpoints on this (2). It is interesting to note that the confusion on this matter relates in part to the method used in the relevant experiments to measure the pulses produced (15).

### 1.3.3 Active mode-locking.

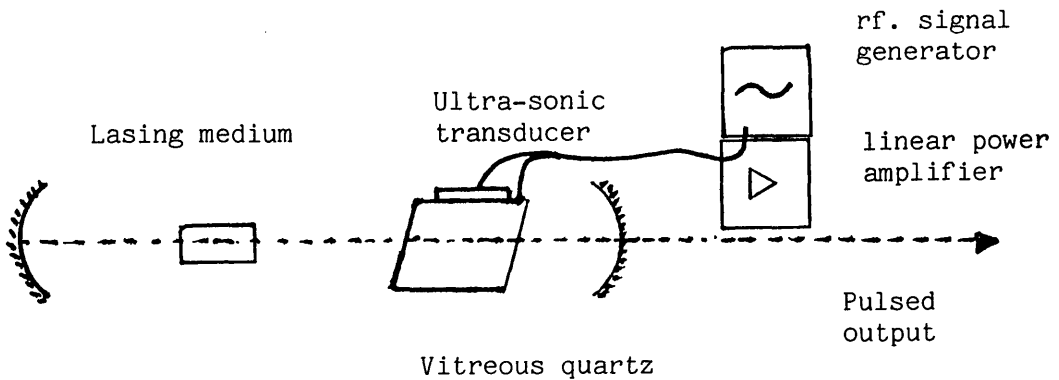


Fig. 1.3. Active mode-locking using an intra-cavity acousto-optic modulator.

Fig 1.3 above shows the basic elements required for the production of ultra-short optical pulses by intra-cavity intensity modulation. In this method the intensity within the lasing cavity is modulated by the application of an external signal at a frequency matched to the pulse reproduction rate dictated by the cavity length. In a semiconductor laser this can be achieved by modulating the drive current with a radio frequency (rf) signal. In a solid state laser an acousto-optic element is placed within the cavity, usually close to one mirror, as shown in Fig 1.2 above. This element is driven by an rf signal to act as a loss or phase modulator. This is a reliable method which is suitable for incorporation into a synchronous system. The Niodymium.YAG. laser used in this work produced 100 picosecond pulses by this method.

#### 1.3.4. Passive mode-locking.

A favoured method for the production of pulses shorter than one picosecond is by use of saturable absorbers. Such absorbers have the property that they are opaque to low intensity signals but become transparent at high intensities. They must also have recovery times which are faster than the cavity round trip time, an absorption line at the laser wavelength and a bandwidth greater than that of the laser.

Random fluctuations within the cavity initiate the mode-locking process. The usual cavity configuration is shown in Fig. 1.4 below. The saturable absorber is placed close to one mirror. Large fluctuations cause greater saturation than smaller ones and hence are preferentially transmitted. Ultimately one such fluctuation dominates all others. This forms a stable pulse which is reflected back and forth in the cavity at a rate dictated by the cavity length. A replica of the pulse may be output as previously described.

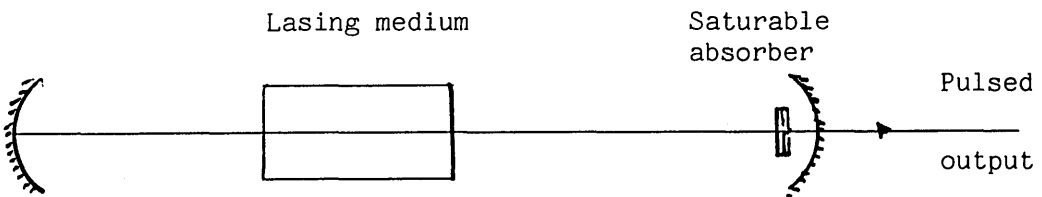


Fig. 1.4. Basic cavity for passive mode-locking.

#### 1.4. Theory of mode-locking. (2)

The complex electric field within the resonant cavity may be written in the form :-

$$V(t) = \sum_n \tilde{E}_n \exp(i\omega_n t) = \sum_n E_n \exp[i(\omega_n t + \phi_n)] \quad (1.1)$$

where  $\omega_n = q\delta\omega = (q_0 + n)\delta\omega$ ,  $\delta\omega = 2\pi\delta\nu$  and  $q_0$  is the longitudinal mode number of an appropriate centre frequency. In the frequency description the signal is determined by specifying the amplitudes  $E_n$  and the phases,  $\phi_n$ . The time description is based on the parameters in the equation :-

$$V(t) = \tilde{E}(t) \exp(i\omega_0 t) = E(t) \exp[i(\omega_0 t + \Phi(t))] \quad (1.2)$$

where  $\tilde{E}(t)$  is the slowly varying complex field and  $E(t)$ ,  $\Phi(t)$  are the corresponding slowly varying amplitude and phase respectively. The two descriptions are related through the equation :-

$$E(t) \exp[i\Phi(t)] = \sum_n E_n \exp[i(n\delta\omega t + \phi_n)]. \quad (1.3)$$

The output from the laser is said to be mode-locked if any definite phase relationship exists throughout the cavity modes. Normally this condition is taken to mean that the phase difference between adjacent modes is a constant. If three or more modes are phase-locked in this manner then pulses

can be produced. The term 'mode-locking' defines a condition where several longitudinal modes are made to oscillate with comparable amplitudes and a fixed phase relation.

Consider the case of  $2n + 1$  longitudinal modes of fixed amplitude  $E_0$ . The phases  $\phi_l$  of the various modes are assumed to be 'locked' in phase in such a way that the phase difference between successive modes is a constant. Summing the contributions to the electric field by the various modes at any point either within or without the lasing cavity gives the electric field at that point. This can be written as follows :-

$$E(t) = \sum_{-n}^n E_0 \exp[i(\omega_0 + l\Delta\omega)t + l\phi] \quad (1.4)$$

where  $\omega_0$  is the central frequency and  $\Delta\omega$  is the frequency difference between subsequent modes.

Considering the field at that point where the phase of the centre frequency is zero, the frequency difference for consecutive longitudinal modes associated with the same transverse mode is given by :-

$$\Delta\omega = \frac{\pi c}{L} \quad \text{where } L \text{ represents the cavity length.}$$

The above result applies to a stable confocal resonator in which the field is tightly confined down the resonator axis and diffraction losses are small.

Carrying out the summation in (1.4) above leads to :-

$$E(t) = A(t)\exp(i\omega_0 t) \quad (1.5)$$

where  $A(t)$  is given by :-

$$A(t) = E_0 \frac{\sin[(2n + 1)(\Delta\omega t + \phi)/2]}{\sin[(\Delta\omega t + \phi)/2]} \quad (1.6)$$

$E(t)$  therefore represents a sine wave with modulated amplitude varying in time and described by  $A(t)$ . As a result of the mode-locking condition between adjacent modes, the oscillating modes tend to interfere to produce short pulses of light. These occur when the arguments of the sine function above both tend to zero. The angular separation between successive maxima is given by :-

$$[(\Delta\omega t' + \phi)/2] - [(\Delta\omega t + \phi)/2] = \pi. \quad (1.7)$$

Thus  $\Delta\omega(t' - t) = 2\pi$ , and the time separation

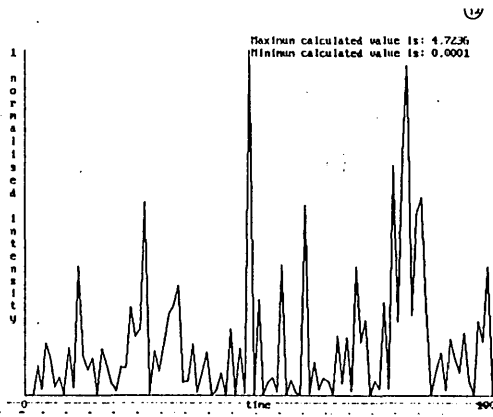
between successive maxima is therefore :-

$$\tau = \frac{2\pi}{\Delta\omega} = \frac{2L}{c}. \quad (1.8)$$

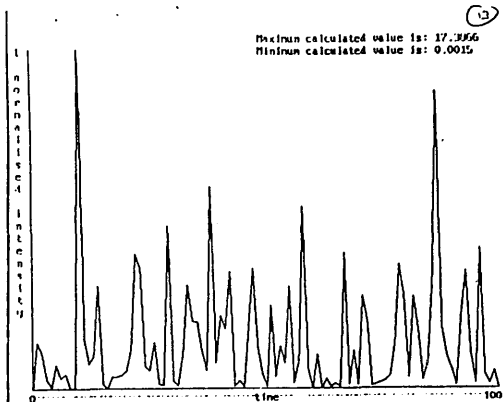
This is of course the round trip time for a cavity of length  $L$ .

The following diagrams are computer simulations of laser outputs for a variety of conditions. An original basic version of the program was provided by Dr. C. Ironside. This was translated into 'C' in the National Guard School of Signals with modifications and graphics added.

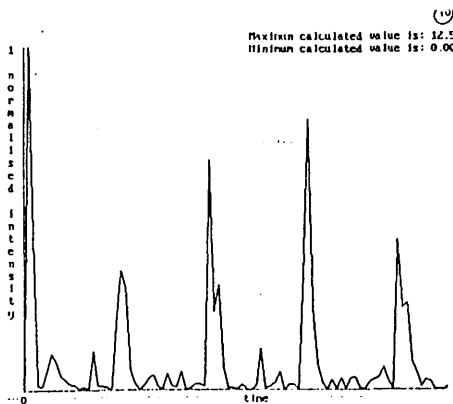
The following diagrams show the effect of locking 5 cavity modes under a variety of conditions. All vertical axes represent intensity, all horizontal axes represent time.



1.5. Random phase and random amplitude.



1.6. Random phase and fixed amplitude.



1.7 Fixed phase and random amplitude.

The following diagrams compare the effect of mode-locking a variety of numbers of modes of fixed phase relationship and whose amplitudes follow a Gaussian form. Where two examples are given below, the first has amplitudes described by the equation :-

$$A = \exp\left[-4\frac{(j-J)^2}{J}\right].$$

J represents the number of modes and  $0 < j \leq J$ .

The second version is similar but has amplitudes described

by :- 
$$A = \exp\left[-8\frac{(j-J)^2}{J^2}\right].$$

The phase is fixed by a cosine function of the form :-

$$f = \cos\left(\frac{N}{10} + 2\pi t\right); \text{ where } N \text{ is an integer which}$$

is the product of the mode number and an integer proportional to the time. The vertical axes are again intensity and the horizontal axes time.

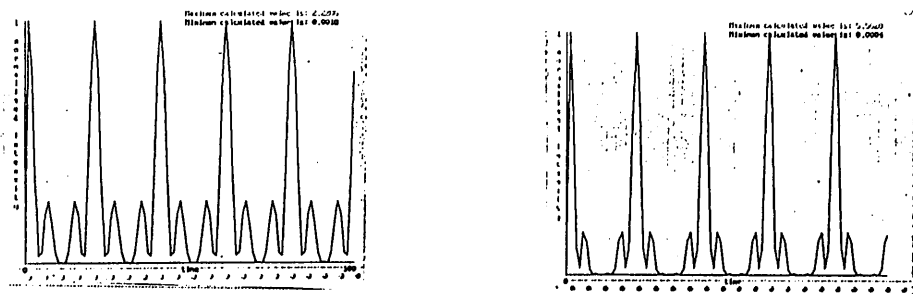


Fig. 1.8. Fixed phase, Gaussian amplitude, 3 cavity modes.

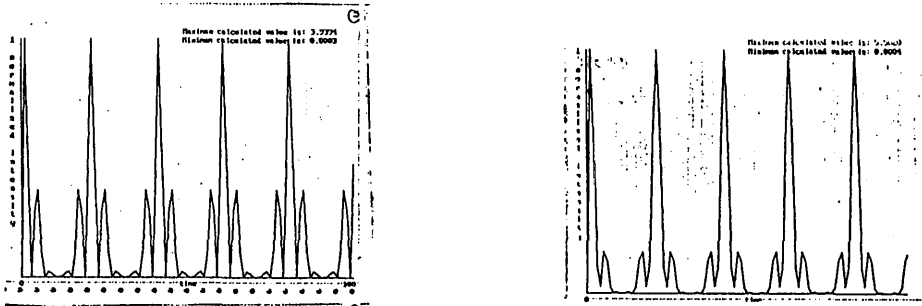


Fig.1.9.Fixed phase, Gaussian amplitude, 5 cavity modes.

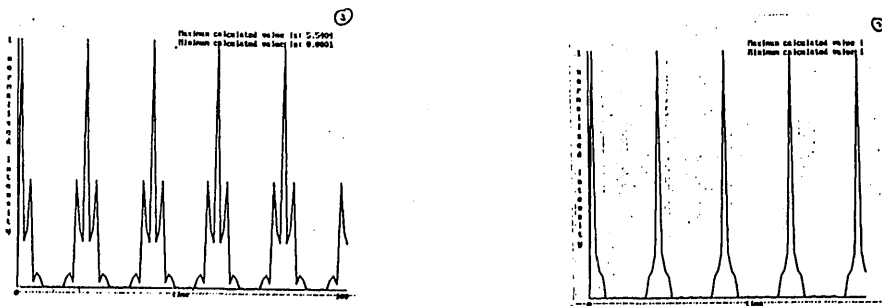


Fig.1.10.Fixed phase, Gaussian amplitude,7 cavity modes.

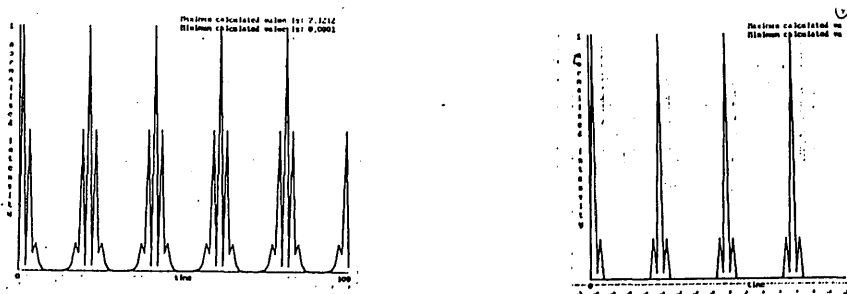


Fig.1.11 Fixed phase, Gaussian amplitude, 9 cavity modes.

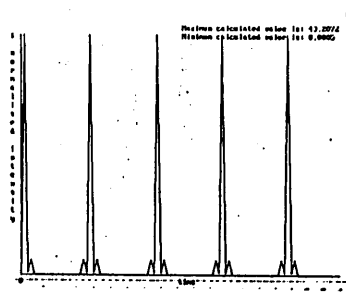
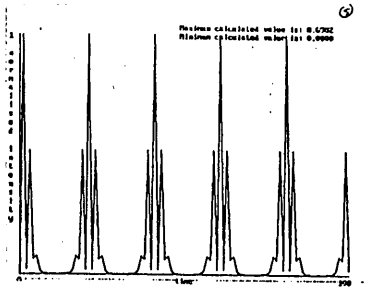


Fig 1.12. Fixed phase, Gaussian amplitude, 11 cavity modes.

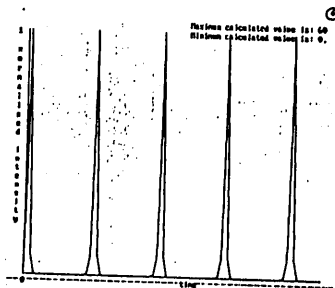
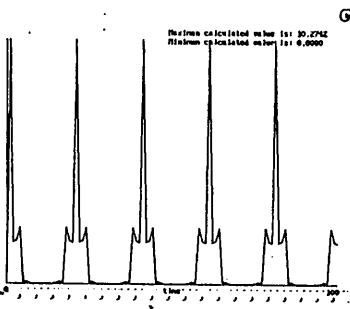


Fig. 1.13. Fixed phase, Gaussian amplitude, 13 cavity modes.

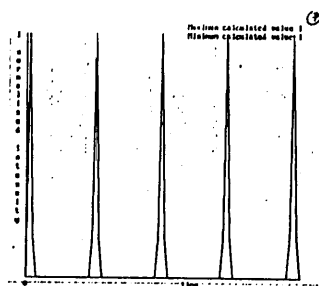
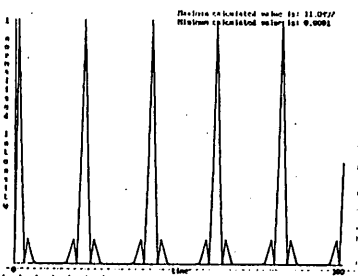


Fig. 1.14. Fixed phase, Gaussian amplitude, 15 cavity modes.

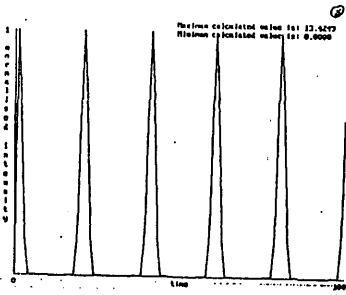


Fig. 1.15. Fixed phase, Gaussian amplitude, 17 cavity modes.

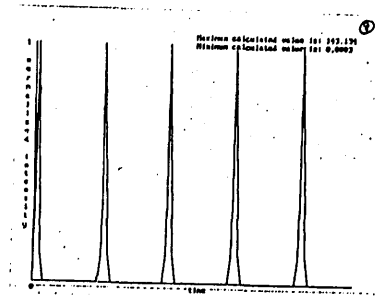
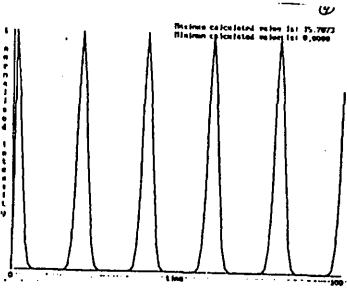


Fig. 1.16. Fixed phase, Gaussian amplitude, 20 cavity modes.

#### 1.4.1. Pulse width.

The pulse width at half maximum intensity (FWHM) is found from  $A^2(t)$  to be given approximately by :-

$$\Delta \tau_p = \frac{2 \kappa}{(2n + 1) \Delta \omega} \quad (1.9)$$

This represents the inverse of the oscillating bandwidth. Thus if the latter is wide, the pulse time will be short. The bandwidth is restricted by the gain bandwidth of the lasing medium. Thus broad bandwidth lasers (e.g. dye lasers), are used to obtain pulses in the sub-picosecond regime. A further advantage of mode-locking lies in the large peak powers produced in ultra-short pulses. These are proportional to :-

$$(2n + 1)^2 A^2,$$

as compared with  $(2n + 1)A^2$  for random phases (21).

It follows that the mode-locked peak power is  $(2n + 1)$  times the random phases power. For a solid state laser the multiplying factor may be as much as  $10^3$  or  $10^4$ . Note, in theory, the average power is unaffected.

#### 1.4.2. Gaussian amplitude distribution.

It is unlikely, as assumed by the above derivation, that the mode amplitudes would be identical. A more realistic

analysis, based on a Gaussian distribution of mode amplitudes, is as follows (2),(21). The intensity of the  $l$ th longitudinal mode is given by :-

$$E_l^2 = E_0^2 \exp[-\ln 2 \left\{ \frac{2l\Delta\nu}{\Delta\nu_{osc}} \right\}^2] \quad (1.10)$$

where  $\Delta\nu_{osc}$  is the FWHM of the spectral intensity profile

$E_l^2$ . We assumed the phases to be locked as above.

Taking  $\phi = 0$ , the total electric field becomes :-

$$E(t) = \exp(i\omega_0 t) \sum_{-\infty}^{+\infty} E_l \exp(il\Delta\omega t) \quad (1.11)$$

$$= A(t) \exp(i\omega_0 t). \quad (1.12)$$

Making the approximation  $A(t) = \int E_l i(l\Delta\omega t) dl$ ,

it follows that  $A^2(t)$  varies as  $\exp\left[-\ln 2 \left(\frac{2t}{\Delta\tau_p}\right)^2\right]$ , since  $A(t)$

is proportional to the Fourier transform of the spectral amplitude  $E_l$ . The pulse width is given by :-

$$\Delta\tau_p = \frac{2\ln 2}{\pi \Delta\nu_{osc}} = \frac{0.441}{\Delta\nu_{osc}}. \quad (1.13)$$

We conclude from the above that when the laser is mode-locked, the following conditions apply.

(1) the field amplitude is proportional to the Fourier transform of the spectral amplitude;

(2) the pulse width  $\Delta\tau_p$ , is related to the width of the spectral intensity  $\Delta\nu_{osc}$ , by the relation:-

$$\Delta\tau_p = \frac{k}{\Delta\nu_{osc}}. \quad (1.14)$$

The constant  $k$  is approximately equal to 1 and depends on the shape of the spectral intensity distribution. This is described as a 'transform limited' pulse or 'bandwidth limited' pulse and represents the ideal.

In practice it is unlikely that the mode-locking conditions are as simple as those described above. Taking for example a phase relation of the form  $\phi_1 = 1\phi + 1^2\phi_2$ , and again assuming a Gaussian distribution of amplitudes, the total electric field becomes :-

$$E(t) = A(t)\exp[i(\omega_0 t + \beta t^2)]. \quad (1.15)$$

$A^2$  is unaffected in form and remains a Gaussian function.

The pulse width becomes :-

$$\Delta\tau_p = \left[ \frac{2\ln 2}{\kappa\Delta\nu_{osc}} \left[ 1 + \left( \frac{\beta\Delta\tau_p^2}{2\ln 2} \right)^2 \right] \right]^{\frac{1}{2}}. \quad (1.16)$$

Note that in this case  $\Delta\tau_p \Delta\nu_{osc} > 0.441$ . This is due to the term  $\beta t^2$  in the expression for  $E(t)$ . This corresponds physically to a linear sweep of the carrier frequency (linear frequency chirp). The spectral amplitude now arises from both the amplitude and frequency modulation of  $E(t)$ .

Note also the output from a 'real' laser is never perfectly repetitive. In a pulsed laser the signal structure inevitably changes to some extent from one round trip to the next(14).

The magnitude of the electric field vector of a plane wave optical pulse at a fixed point in space may be expressed as the Fourier integral :-

$$E(t) = \frac{1}{\sqrt{2\pi}} \int_{-\infty}^{\infty} e(\omega) \exp(-i\omega t) . d\omega. \quad (1.17)$$

The Fourier inversion yields :-

$$e(\omega) = \frac{1}{\sqrt{2\pi}} \int_{-\infty}^{\infty} E(t) \exp(i\omega t) . dt \quad (1.18)$$

It is convenient to integrate over positive frequency components only. To do this a complex function  $V(t)$  is defined such that  $E(t) = \text{Re}[V(t)]$ . This leads to :-

$$V(t) = \frac{1}{\sqrt{2\pi}} \int_0^{\infty} 2e(\omega) \exp(-i\omega t) . d\omega. \quad (1.19)$$

Further we may write :-

$$V(t) = \frac{1}{\sqrt{2\pi}} \int_{-\infty}^{\infty} v(\omega) \exp(-i\omega t) . d\omega, \quad (1.20)$$

where

$$\begin{aligned} v(\omega) &= \frac{1}{\sqrt{2\pi}} \int_{-\infty}^{\infty} V(t) \exp(i\omega t) . dt & (1.21) \\ &= 2e(\omega) \quad (\omega > 0); \\ &= 0 \quad (\omega < 0). \end{aligned}$$

Note since  $E(t)$  is real,  $e(-\omega) = e^*(\omega)$ .

Since  $V(t)$  and  $v(\omega)$  are complex functions of time and frequency respectively, we may write :-

$$v(\omega) = a(\omega)\exp[i\phi(\omega)] \quad (1.22)$$

where  $a(\omega)$  and  $\phi(\omega)$  are called the spectral amplitude and spectral phase respectively.

Assuming  $\Delta\omega \ll \omega_0$ , the mean frequency, and defining  $A(t)$  and  $\Phi(t)$  as the temporal amplitude and temporal phase of the carrier wave, we may write :-

$$V(t) = A(t)\exp[i\Phi(t)]\exp(-i\omega_0 t). \quad (1.23)$$

With the above restrictions,  $A(t)$  and  $\Phi(t)$  are (assumed to be) slowly varying functions of time.

The instantaneous intensity  $I(t)$  can be defined as :-

$$I(t) = V(t) \cdot V^*(t) = A^2(t). \quad (1.24)$$

Note: In general,  $I(t)$  is not strictly proportional to the square of the real field  $E(t)$ , but in the quasi-monochromatic case, over a few optical cycles :-

$$\frac{1}{2}I(t) = \langle E^2(t) \rangle_{\text{time}} \quad (22) \quad (1.25)$$

Similarly the spectral intensity  $i(\omega)$  is given by :-

$$i(\omega) = v(\omega) \cdot v^*(\omega) \quad (1.26)$$

$$= a^2(\omega). \quad (1.27)$$

From Parseval's theorem, the total energy of the pulse is proportional to the area under either the temporal or spectral intensity profile. Thus the structure of a pulse

is completely defined by a phase and an amplitude.

Whilst these can be referred to the time or frequency domain and inter-related by Fourier transform, there is not a one to one correspondence between the two intensity profiles  $I(t)$  and  $i(\omega)$ . These depend also on their associated phase function. There is a general relationship between the FWHM values of  $I(t)$  and  $i(\omega)$ , viz.  $\Delta t$  and  $\Delta \omega$ , which are related by the inequality :-

$$\frac{\Delta \omega \Delta t}{2\pi} \geq k; \quad (k \approx 1). \quad (1.28)$$

The shortest pulse obtainable for a given spectral bandwidth is therefore :-

$$\Delta t_{\min} = \frac{2\pi k}{\Delta \omega}. \quad (1.29)$$

Such a pulse, as indicated earlier is said to be bandwidth or transform limited. In practice, measured pulse widths tend to exceed the transform limited values. The reasons for this form part of this investigation.

## 1.6. Summary

A definition of an ultra-short pulse has been given. The utility of such pulses to current research has been outlined. The limitation of present electronic means for measurements on a picosecond timescale has been indicated. Some areas where ultra-short light pulses may replace their electronic equivalents have been discussed, with particular reference to signal processing and communications.

The importance of identifying pulse structure has been stressed. The history of pulse structure investigations has been traced from the discovery of chirp in mode-locked laser pulses. The various methods used to investigate pulse chirp have been briefly described in chronological order.

The basic principles for the generation of ultra-short pulses have been stated and the components necessary in making a pulse generator described. It has been shown that a laser may be suitable for the generation of short pulses if a mechanism for the preferential selection of large amplitude pulse components is added. Such mechanisms, which produce short pulses in laser cavities are briefly described.

The theory of short pulse generation using active mode-locking techniques has been developed, and a computer

simulation of a laser output under various conditions restricting phase and amplitude of the pulse components, has been presented. The mode-locking conditions relating field and spectral amplitudes, pulse width and spectral width, have been established. An example of a phase relationship which leads to the presence of linear chirp within a pulse, has been described.

A brief theoretical treatment of the structure of an ultra-short pulse has been given which leads to the concept of a bandwidth-limited pulse. It shows the relationship between spectral bandwidth and temporal pulse width, indicating the limits attainable in the production of ultra-short pulses.

CHAPTER TWO.2.1 METHODS OF DETECTION.AND MEASUREMENT.

Nanosecond ( $10^{-9}$ s) pulses can be measured by electronic means. Fast photodiodes are available which, when used in conjunction with a sampling oscilloscope of gigahertz ( $10^9$ Hz) bandwidth, can measure pulses of 25 picoseconds duration. Pulses of less than 25 picoseconds require optical measurement methods.

Picosecond pulse sources fall into two categories. Systems which are flashlamp pumped at low repetition rates of a few hertz, and those which are continuously operated at high repetition rates using mode-locked cw lasers. The source of the pulse will influence the type of detection, measurement and display devices employed. The methods most commonly used for ultra-short pulse measurement are the streak camera (23), the intensity auto-correlator (24) and two-photon fluorescence (TPF) (3), (8). Other methods which have been tried include a pressure scan technique (15) and an interferometric method based on Young's Slits experiment (25).

2.1.1. Streak camera.(8)

The figure below shows the essential components of a streak camera. The input pulse illuminates a diffusing screen in front of a narrow slit. The light from the slit is collected by a short focal length lens and focussed on to the photocathode of an image tube.

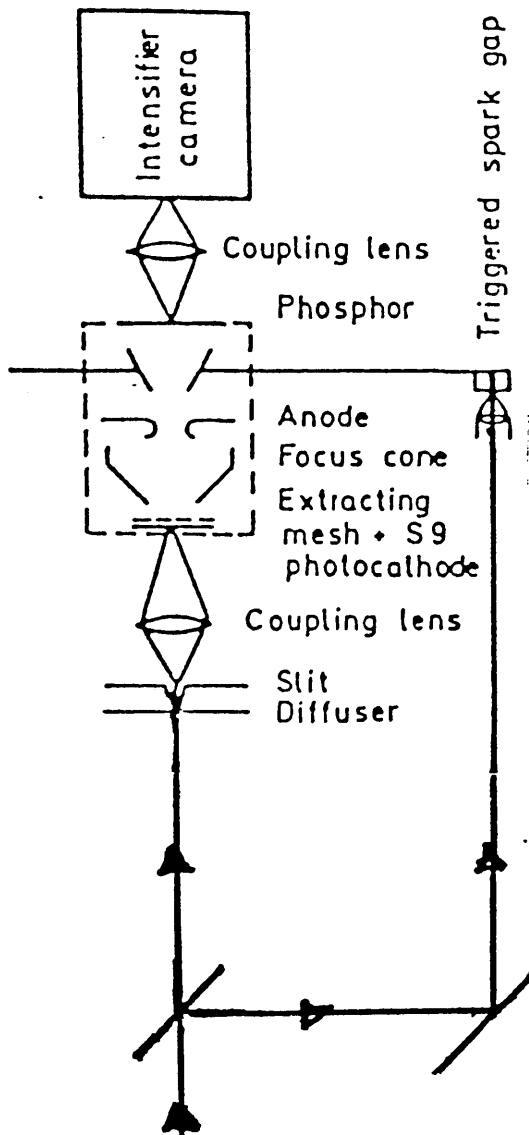


Fig. 2.1. Basic streak camera design. (After ref. 8).

The photo-electrons produced are accelerated rapidly by a strong electric field maintained by a mesh close to the photocathode. Focussing plates and a hollow anode direct the electron beam between two deflection plates. A ramp voltage is generated between these electrodes by a spark gap. The latter is triggered by part of the original pulse energy which has been removed from the pulse by a beam splitter. The ramp voltage and incident pulse are thus synchronized. The electron beam strikes a luminescent surface whose output is coupled by a short focal length lens to an image intensifier camera. The latter records the event for analysis.

The time resolution of the streak camera is ultimately limited by the spread of photo-electron transit times through the first image tube. This is due to variations in the initial ejection velocities of the photo-electrons (8). The spread of transit times through the first image tube is related to the initial velocity distribution as follows:-

$$\delta T_d = \frac{m \delta U}{eE} , \quad (2.1)$$

where  $\frac{e}{m}$  is the charge to mass ratio for an electron,  $E$  is the field strength near the photocathode and  $\delta U$  is the half width of the initial velocity distribution.

It follows that  $E$  must be maximized to reduce  $\delta T_d$ .

$\delta U$  depends on the wavelength of the illuminating light and on the nature of the photocathode material. Thus the ultimate resolution of the streak camera depends on the extraction field strength, the illumination wavelength and the nature of the photocathode.

The pulse half-width recorded by a streak camera is given approximately by :-

$$\delta T_r = \sqrt{\delta T_s^2 + \delta T_d^2 + \delta T_p^2} \quad , \quad (2.2)$$

where  $\delta T_s$  is the time resolution limit determined by the finite spatial resolution of the image tube camera at a given writing speed and  $\delta T_p$  is the laser pulse width.

Since the latter is determined by the laser in use, and  $\delta T_s$  is determined by the design of the camera tube and associated switching electronics,  $\delta T_r$  is controlled by  $\delta T_d$  and hence by  $E$ , the field intensity close to the photocathode. The latter is limited by the onset of cold emission at fields of the order of  $10^6$  V/cm.(26). Such fields are more likely if there are irregularities in the photocathode surface. It would appear from the inverse relationship between  $\delta T_r$  and  $E$  that the streak camera is limited in resolution to pulses of one picosecond. The streak camera is expensive, and difficult to use in practice. In particular, the time delay, jitter and dynamic range have proved difficult to adjust in preparation

for a measurement (23),(27).

### 2.1.2. Two-photon fluorescence.

This method employs two pulses travelling in opposite directions which are made to overlap in an organic dye solution which exhibits two-photon absorption (8). The basic optical layout is shown in figure 2.2 below.

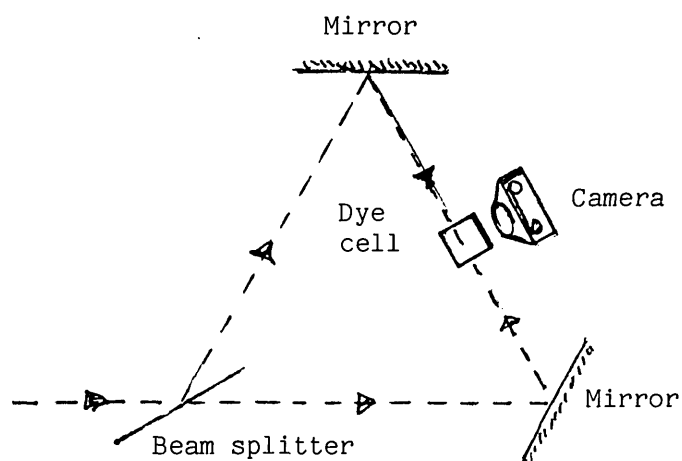


Fig. 2.2. Schematic diagram showing the combination of two photons within a fluorescent dye.

Where the two pulses overlap or where fluctuations within pulses overlap enhanced fluorescence is produced. The spatial distribution of this fluorescence is directly related to the second order correlation function and hence the complete auto-correlation profile is displayed as a function of distance from the centre of the overlap region. Since it is impossible to obtain zero background signal in this type of experiment, the profiles obtained are insensitive to the form of the

incident signal.

The fluorescent signal is directly related to the time-averaged fourth power of the electric field and may be written as follows :-

$$F(\tau) = k[G_2(0) + 2G_2(\tau) + R_{\text{TPF}}(\tau)]. \quad (2.3)$$

$G_2(\tau)$  is the second order correlation function and  $R_{\text{TPF}}(\tau)$  contains rapidly varying terms. The constant  $k$  depends on the photo-chemical properties of the dye and the geometry of the detection system. Far from the region of overlap,  $F(\tau)$  becomes equal to  $kG_2(0)$ , which represents the background level.

Relative to this level, the TPF signal is given by :-

$$S(\tau) = [1 + \frac{(2G_2(\tau) + R_{\text{TPF}}(\tau))}{G_2(0)}]. \quad (2.4)$$

The spatial resolution of the recording camera averages out the fine fringe structure and  $R_{\text{TPF}}$  can often be neglected. A contrast ratio of 3:1 is possible but, to achieve this, stable, high input power pulses are required and the alignment of the optical system is critical (8).

There seems to be some discrepancy between auto-correlation measurements of pulse widths and those obtained using a streak camera (23). This is attributed to triggering difficulties and long term jitter. It should be noted, however, that all methods of pulse width measurement involve some interpretation

on the part of the experimenter and there remains some disagreement with respect to what is actually measured (23).

The TPF method is an imperfect technique in that it records  $G_2(\tau)$  which does not uniquely determine the temporal intensity of the pulse. To record the higher order correlations which contain evidence of phase changes taking place within the pulse, a more elaborate experimental procedure is required. It has proved convenient to use pulse compression and correlation techniques to this end (28).

Whilst auto-correlation techniques (to be described later) pre-date the TPF method, the latter was found to be more suited to examination of single pulses produced at relatively long time intervals (29),(30). Single pulse measurements are generally made on pulses selected from flashlamp-pumped laser outputs. Such pulses are individual in nature. The entire event must be detected and recorded in one measurement. The TPF technique enables single shot, single pulse measurements to be made.

### 2.1.3. Pressure scan.

An interferometric device making use of a pressurized chamber has been used by J. C. Diels to study the femto-second structure of ultra-short pulses at 612nm (15).

The basic components are show in figure 2.3 below.

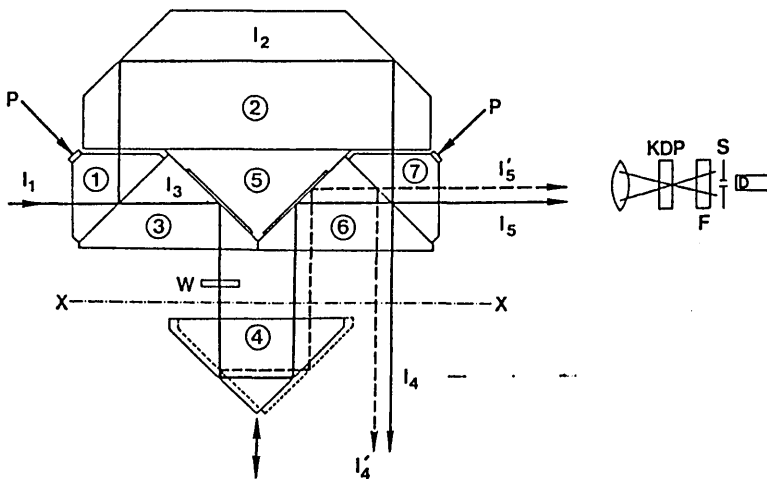


Fig. 2.3. Gas pressure controlled interferometer using a Mach-Zehnder configuration. (After ref. 15)

The device operates as follows. The input pulse is split into two at the first reflecting surface. One part is directed around a delay line formed by two reflecting surfaces to recombine with the other part at the output as in a Mach-Zehnder arrangement. The latter part reaches the output via a series of right-angled prisms which form a delay line where part of the path traverses a pressurized chamber.

The optical path difference between the two beams is altered by translating one of the prisms. The intervening medium between the prisms is the gas sulphur hexafluoride ( $\text{SF}_6$ ). The fine scanning in this device is achieved by altering the effective path length difference using pressure controlled refractive index changes within the instrument chamber.

A correlation of the output pulses can be carried out with considerable sensitivity. This instrument is not suitable for the investigation of chirped pulses as the intensity correlation information is masked by the phase correlation component (16). However Diels interpreted his results as indicating that the dye laser pulses observed were unchirped.

#### 2.1.4. Resonant vapour cell.

A method used by Rothenberg and Grischowsky to measure the phase of a frequency-swept pulse involves the use of a resonant vapour, together with a pulse compression technique (18). The compressed pulse is used as a reference in a cross-correlation measurement. The frequency-swept pulse is introduced into a sodium vapour cell and excites the resonant frequency. This resonant excitation then interferes with the propagating pulse to produce a heterodyne signal. This signal provides a measure of the time dependent

relative phase between the propagating pulse and the oscillation created in the vapour. This allows the instantaneous frequency to be obtained by cross correlation with the compressed pulse. Figure 2.4 below illustrates this technique.

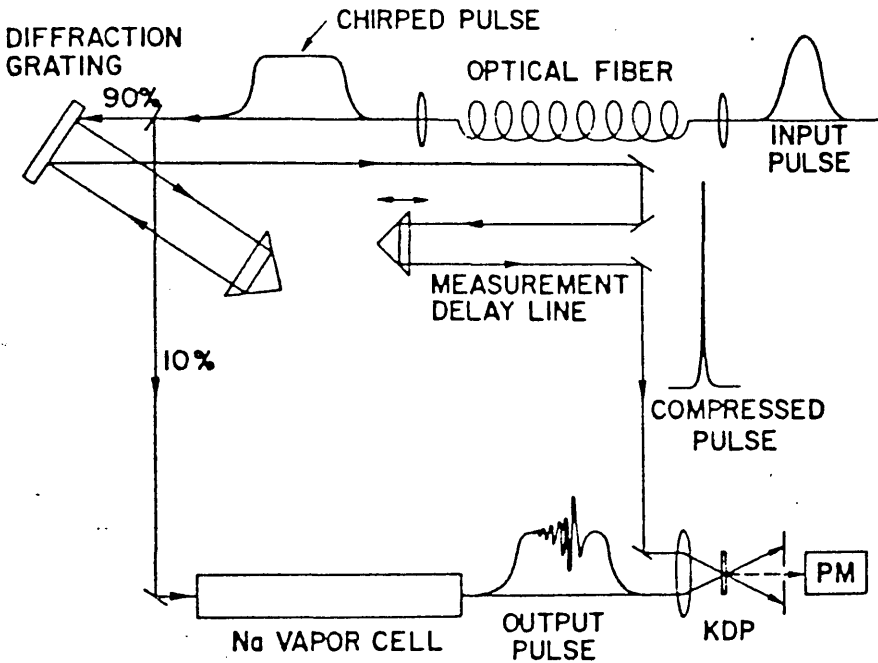


Fig. 2.4. Heterodyne technique for phase measurement of a frequency-swept pulse. (After ref. 18).

The input pulse is first chirped by linear group velocity dispersion and nonlinear self-phase modulation in a length of optical fibre. It is then compressed by a grating-prism arrangement which is equivalent to the grating pair originally used by E. B. Treacy (10). A beam splitter removes 10% of the intensity of the frequency-swept pulse for use as the

input to a sodium vapour cell. The compressed pulse is sent via a delay line to combine with the output heterodyned pulse from the vapour cell, in a frequency doubling crystal. The correlation between the compressed reference pulse and the phase dependent intensity of the heterodyned pulse constitutes the signal at the photomultiplier which acts as a detector. The use of sodium as the reference medium results in two sets of beats being present during the heterodyning process. This complicates the analysis to determine the phase relations. Moreover if the amplitude is changing more rapidly than the phase, error may occur in the measured phase (19).

A modification of the above experiment is shown in figure 2.5 below. The resonant vapour cell is replaced by a Mach-Zehnder which incorporates a Fabry-Perot etalon in one arm. The Fabry-Perot selects a resonance from within the chirped pulse. This monochromatic signal is then heterodyned with the original chirped pulse which traverses the other arm of the Mach-Zehnder. The resultant output is then correlated with a compressed reference pulse as before. This method introduces more flexibility into the selection of the heterodyning signal, and the ease of adjustment of the delay allows the complete pulse to be scanned. Amplitude variations in

the modulation again pose a problem for the observation of higher frequency oscillations.

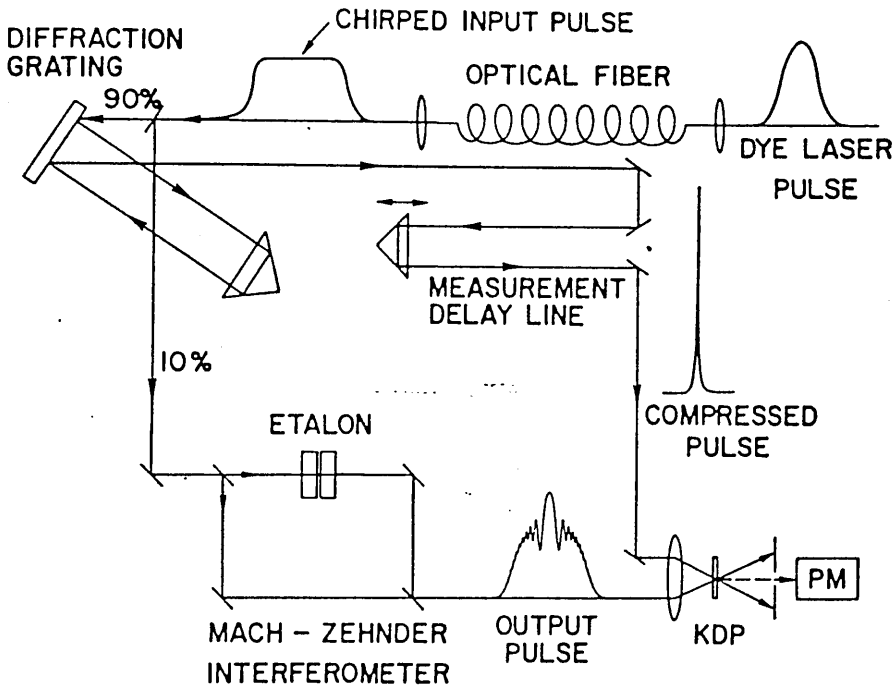


Fig. 2.5. Heterodyne technique incorporating a Fabry-Perot for frequency selection. (After ref. 19).

#### 2.1.5. Intensity Auto-correlator.

The Michelson interferometer is already well established as a means of investigating coherence lengths of light sources (22). With the development of semiconductor lasers, whose coherence length can be tailored to suit their particular application, the Michelson interferometer has

continued to be appreciated for its reliability in operation (31),(32). Laser diodes with coherence lengths of a millimetre are used in conditions where it is essential to limit optical feedback. The verification of such a coherence length is readily carried out using a Michelson interferometer.

The use of this instrument has been extended to the measurement of the temporal width of ultra-short pulses. When used in this application it normally incorporates frequency-doubling of the output and is then described as an intensity auto-correlator. The lay-out of the optical components is shown in figure 2.6 below.

The instrument operates as follows. The input pulse train is split into two by a 50-50 beam splitter. After reflection from a corner cube or retro-reflector, each beam is rendered parallel but not collinear at the beam-splitter. These beams are focussed by a short focal length lens on to a suitable second harmonic generating crystal. The output from the crystal is filtered to remove the fundamental radiation. The second harmonic signal passes through an aperture before falling on a suitable detector. The latter is normally a photomultiplier tube whose output goes to an oscilloscope.

The crystal is angle-tuned to find the best phase matching condition for each individual beam and then the combined

beam. The aperture serves to block that harmonic radiation which is not produced by the combined beams.

When making a measurement, the optical path length is varied in one arm around the zero-delay position. A linear vibrator is used to scan around this position at low frequency while a linear translation of the other reflector takes place. This provides a means of calibrating the pulse spacing and hence find the pulse width from the auto-correlation trace.

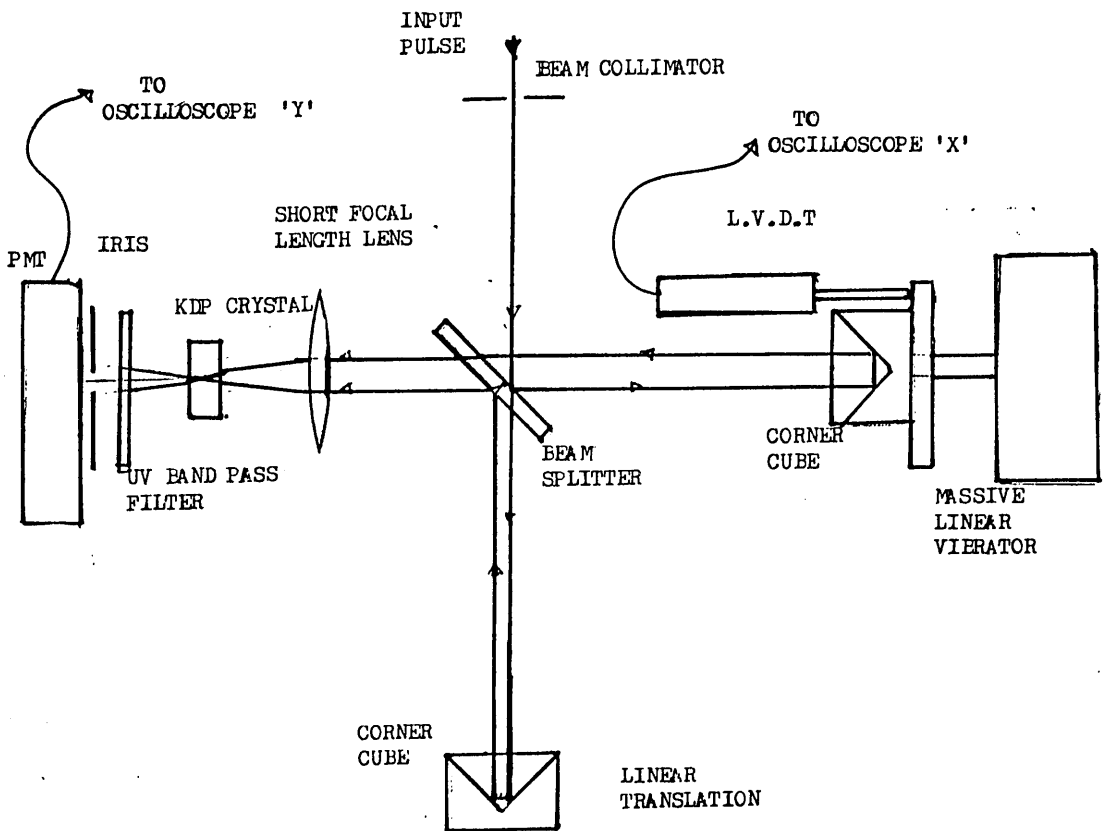


Fig. 2.6. Basic design of an intensity auto-correlator

built in the Department of Electronic and Electrical Engineering of the University of Glasgow.

The second order auto-correlation of the input pulse produced by this technique is symmetric in nature. It cannot provide unequivocal information regarding pulse shape or possible asymmetry. The conventional intensity auto-correlation is very insensitive to pulse shape. Measurements based on this technique are difficult to interpret (2). In order to overcome these limitations, interferometric techniques have been developed (16),(28). These provide some phase information and are more sensitive to pulse shape than intensity correlations.

An intensity auto-correlator was built in the Department of Electrical Engineering in the University of Glasgow and was used successfully in the initial pulse width measurements made when setting up the laser system. Figure 2.7 below shows the output pulse from a dye laser pumped by a mode-locked Nd.YAG laser.

Autocorrelation of  
dye-laser pulse

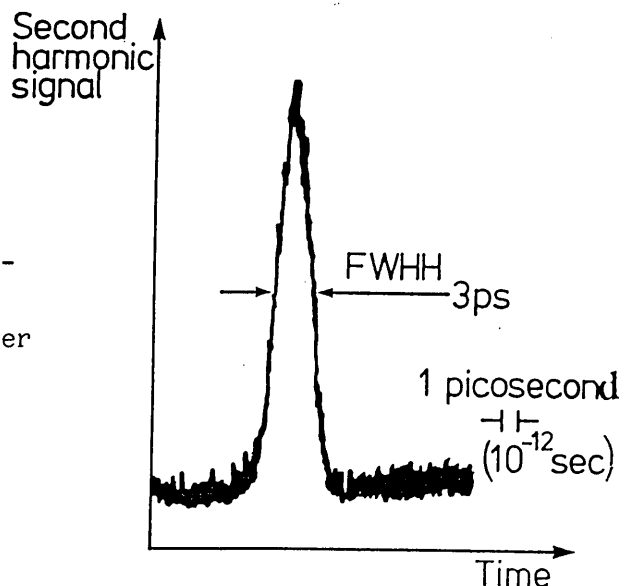


Fig. 2.7. Intensity auto-correlation of a dye laser pulse.

## 2.2 Summary.

Methods of detection and measurement of ultra-short pulses have been introduced. The temporal limits of electronic measurement of optical pulse widths using an opto-electronic detector in conjunction with a sampling oscilloscope have been quantified. The relationship between the method of generation of a short optical pulse and the method chosen for its measurement has been noted. Several methods used for the measurement of ultra-short pulses have been described in detail. Their areas of applicability and their limitations have been outlined. The information available from each method has been noted. An intensity auto-correlator built by the author has been described and a sample pulse measurement displayed.

## CHAPTER THREE.

### INTERFEROMETRIC AUTO-CORRELATOR DESIGN.

#### 3.1. Auto-correlation techniques.

The most commonly used method for measuring ultra-short pulse widths in high repetition rate pulsed laser systems is by the correlation of two pulses. Correlations may be carried out in a variety of ways , each producing a distinctive correlation function. These functions may include background levels from uncorrelated signals, or be background free. One pulse may be compressed and used to produce a cross correlation with the uncompressed pulse. The correlation technique employed may react slowly to the fast optical changes taking place during the correlation. All information regarding phase is lost as a consequence. In order to retain phase information, the technique employed must be able to resolve the fast optical variations. In practice this means the spatial variation during correlation must be resolved to about one tenth of the shortest wavelength involved (32).

The auto-correlation of two pulses is often carried out within a second-harmonic generating crystal. This is

necessary if an accurate measurement of pulse width is to be obtained. Any linear interferometer applied in pulse measurement records the auto-correlation function of the pulse amplitude (3). The power density spectrum and the amplitude correlation function form a Fourier transform pair. Thus complete knowledge of one, completely specifies the other. A spectrometer may be used to measure the power density spectrum. An instrument such as the Michelson interferometer may be used to measure the amplitude correlation function.

The linear interferometer can also be used to measure the coherence length and coherence time for a pulse. The coherence time and the spectral bandwidth are related by the following :-

$$\Delta\omega \cdot \Delta\tau_c \geq 2\pi. \quad (3.1)$$

As was indicated earlier, this represents the lower limit to the possible measurement of pulse duration. One concludes that a measurement taken with a linear optical system can provide information establishing a lower limit to the pulse duration. In order to measure pulse widths accurately, a nonlinear instrument such as an intensity auto-correlator may be used. However, even in this case, the measured pulse width depends to a degree on the assumption of pulse shape (8). Since the instrument constructed could be used in the linear

or nonlinear mode of operation, these applications will be considered in turn.

### 3.1.1. Linear auto-correlation of two pulses.

In this application the input pulse is split into two pulses of approximately equal amplitude by a beam splitter. Each pulse traverses one arm of a Michelson interferometer which introduces a phase shift between the pulse pair proportional to the path difference in the arms. The pulses are directed to the detector along a collinear path where they are re-combined. The detector records the intensity of the combined signal which changes as the path difference between the arms is varied. This is illustrated in figure 3.1. below.

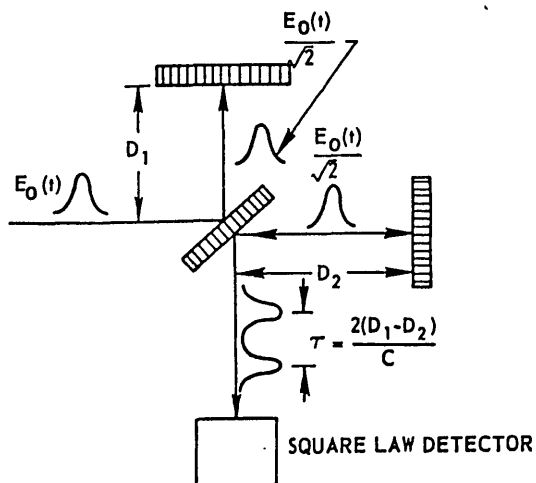


Fig. 3.1. Schematic diagram of a linear auto-correlation

(After ref. 3.)

Consider a pulse of amplitude  $E(t)$  which is split into two pulses of equal amplitude  $\frac{1}{\sqrt{2}}E(t)$ . Assuming a delay in time of  $\tau$  between the pulses, they may be represented by :-

$$E_1(t) = \frac{1}{\sqrt{2}}E_0(t)e^{i\omega t}; \quad E_2(t) = \frac{1}{\sqrt{2}}E_0(t - \tau)e^{i\omega(t - \tau)}.$$

It is assumed that  $E_0(t)$  is the slowly varying pulse envelope with respect to the frequency  $\omega$ .

The detector records the intensity of the combined signal as follows :-

$$I(t, \tau) = \frac{1}{2}[E_0(t) + E_0(t - \tau)]^2. \quad (3.2)$$

If the response of the detector is assumed to be slow in comparison to  $\tau$ , the delay time, or  $\Delta\tau$ , the pulse width, the output from the detector is given by :-

$$S(\tau) = \int_{-\infty}^{\infty} I(t, \tau) dt, \quad (3.3)$$

$$= W[1 + A(\tau)]. \quad (3.4)$$

In the above expression  $W = \int_{-\infty}^{\infty} E_0^2(t) dt$  represents the pulse energy, and  $A(\tau) = \frac{\int_{-\infty}^{\infty} E_0(t) \cdot E_0(t - \tau) dt}{\int_{-\infty}^{\infty} E_0^2(t) dt}$ . (3.5)

When  $\tau = 0$ ,  $A(\tau) = 1$  and  $S(\tau) = 2W$ .

When  $\tau \rightarrow \infty$ ,  $A(\tau) \sim 0$  and  $S(\tau) = W$ .

Thus the signal to background ratio becomes 2:1.

The function  $A(\tau)$  is called the amplitude correlation function.

### 3.1.2. Nonlinear auto-correlation of two pulses - 'slow correlation'.

To carry out a 'slow' correlation of two pulses, the above technique is modified as follows. The two pulses from each arm of the interferometer are rendered parallel but not collinear. They are then focussed on to a second harmonic generating crystal at a suitable phase-matching angle. The second harmonic signal is then detected while the fundamental signal is filtered out. In the following analysis, it is assumed that the phase-matching condition in the nonlinear crystal is maintained over the entire bandwidth of the laser pulse (3).

Let the two output pulses from the interferometer be  $E_1(t)$  and  $E_2(t)$  as above. The second harmonic output field will be given by :-

$${}^{2\omega}E(t) = [E_1(t) + E_2(t - \tau)]^2. \quad (3.6)$$

The output from a slow detector is given by :-

$$\begin{aligned} S(\tau) &= \int_{-\infty}^{\infty} |{}^{2\omega}E(t)|^2 \cdot dt \\ &= {}^{2\omega}W [1 + 2G(\tau)]. \end{aligned} \quad (3.7)$$

Here  ${}^{2\omega}W$  is the second harmonic pulse energy given by :-

$${}^{2\omega}W = \int_{-\infty}^{\infty} E^4(t) \cdot dt. \quad (3.8)$$

$G(\tau)$  is the auto-correlation function of the pulse intensity given by :-

$$G(\tau) = \frac{\int_{-\infty}^{\infty} E^2(t) \cdot E^2(t - \tau) \cdot dt}{\int_{-\infty}^{\infty} E^4(t) \cdot dt} \quad (3.9)$$

When the delay time  $\tau = 0$ ,  $G(\tau) = 1$ , and the ratio

$$S(\tau) : {}^{2\omega}W = 3 : 1.$$

When the delay time  $\tau$  is such that no overlap occurs,

then the ratio  $S(\tau) : {}^{2\omega}W = 1 : 1$ . Thus the signal to background ratio becomes 3 : 1.

The diagram below, figure 3.2, shows the optical paths of the beams during an intensity auto-correlation.

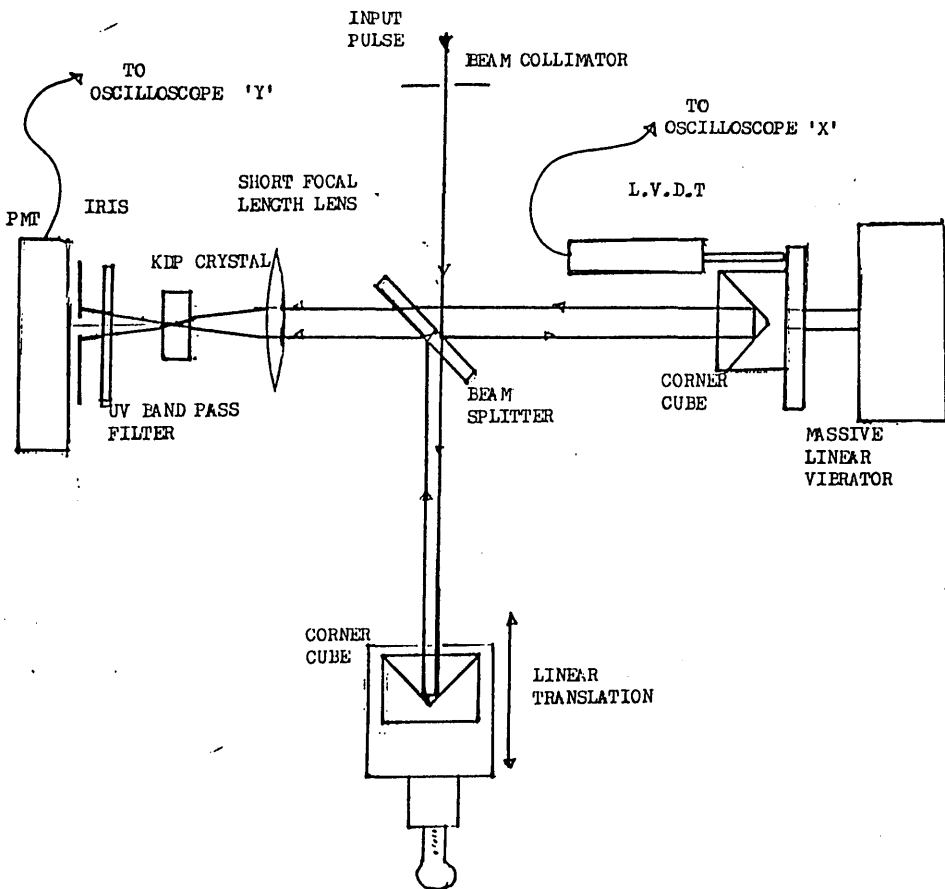


Fig. 3.2. Schematic diagram of an intensity auto-correlator.

### 3.1.3. Background-free correlations. (3)

A nonlinear interferometer can also be constructed to produce a background-free correlation. In this case, when the time delay is such that no overlap occurs between pulses, the background level at the detector falls to zero. This can be achieved in the intensity correlator by the following method.

The second harmonic signal is found for each pulse of the combining pair by blocking each arm of the interferometer in turn and angle tuning the second harmonic generating crystal. These signals lie on either side of the fundamental direction of propagation. The signal from the combined beams is found midway between those of the individual beams. By blocking each beam again in turn, it is verified that no second harmonic is present due to a single beam. Any residual signal at an angle to the combined second harmonic signal is blocked by a suitable aperture.

### 3.1.4. Nonlinear interferometric auto-correlation of two pulses - 'fast' correlation.

The primary interest in the present work was to build an instrument capable of revealing the fine structure in an ultra-short laser pulse. In order to achieve this, a

more sensitive instrument than the intensity auto-correlator is required. The latter does not provide phase information. This is lost in the averaging process. If the correlation is carried out with interferometric accuracy, it may be possible, with the additional information provided by the intensity correlation and spectral analysis, to move closer to the true nature of the pulse (20),(28).

For a measurement carried out with interferometric accuracy, i.e. a 'fast' correlation as described above, the output from the second harmonic generating crystal is produced by parallel and collinear pulse trains from the arms of the interferometer. The crystal is angle tuned to produce maximum output. The output in this case is given by :-

$$I(t) = \int \left\{ E(t)e^{i[\omega t + \phi(t)]} + E(t-\tau)e^{i[\omega(t-\tau) + \phi(t-\tau)]} \right\}^2 dt \quad (3.10)$$

At zero delay, coherent superposition of the fields gives :-

$$I(0) = 2^4 \int E^4(t) dt \quad (3.11)$$

Half a cycle later, the two fields add together with opposite phase producing approximately zero signal. As the pulse delay becomes commensurate with the coherence time, the envelope of constructive and destructive interference will merge into the intensity auto-correlation envelope.

The signal to background ratio then becomes 8:1.

### 3.1.5. Background-free interferometric correlation.

Interferometric correlations can also be rendered background-free by using a second harmonic generating crystal which utilizes a type II phase-matching process. The pulses in each arm of the interferometer are rendered orthogonal by any suitable means. In a type II process the second harmonic is only produced when the input pulses are orthogonal. The crystal is orientated to satisfy this condition. Thus at long delay times, the background falls to zero.

For a crystal such as ammonium dihydrophosphate (ADP), an input combination of vertically and horizontally polarized beams produces a second harmonic output which is horizontally polarized. If the input signal to an ADP crystal is represented by :-

$$E_i(t) = E_h(t)e^{i\omega t} + E_v(t - \tau)e^{i\omega(t-\tau)}, \quad (3.12)$$

then the second harmonic signal output is given by :-

$${}^{2\omega}E_h(t) = E_h(t)E_v(t - \tau)e^{i\omega(2t-\tau)}, \quad (3.13)$$

where  $E_h(t)$  and  $E_v(t - \tau)$  are the slowly varying envelopes of the horizontal and vertical polarized electric fields with respect to  $\omega$ . Note no account has been taken of the conversion efficiency of the crystal.

If  $\tau \gg \Delta\tau$ , then  ${}^{2\omega}E_h = 0$ . If  $\tau = 0$ , then  ${}^{2\omega}E_h$  becomes a maximum. The output signal from a detector having a slow

response time with respect to  $2\omega$ , is given by :-

$$S(\tau) = \int E_h^2(t)E_v^2(t - \tau).dt \quad . \quad (3.14)$$

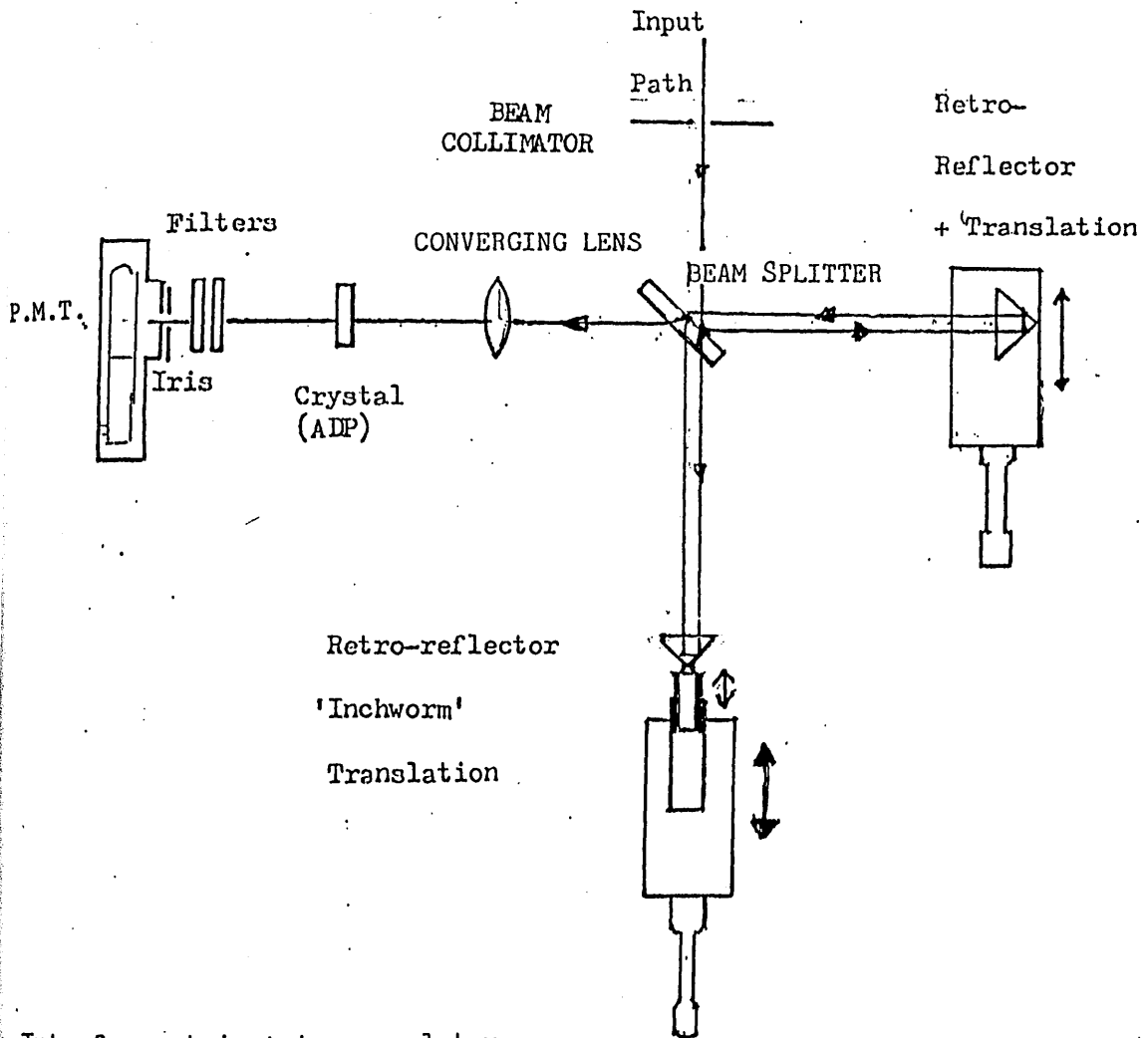
When  $\tau$  is large enough so that no overlap occurs between  $E_h(t)$  and  $E_v(t - \tau)$ , the above signal becomes zero.

In the above analysis it has been assumed that phase-matching in the nonlinear crystal is maintained over the entire bandwidth of the laser pulse. This requires a crystal of limited thickness and sets a lower limit to the time resolution possible. In ADP a thickness of 1mm provides a resolution of about 1ps. Note also that the group velocities of the fundamental and second harmonic frequencies must be approximately equal if the envelope of the second harmonic pulse is to equal that of the square of the fundamental pulse. If these group velocities are not equal then the second harmonic will have a flat top. Its duration will be given by :-

$$\Delta\tau = L_c \left( \frac{1}{v_g(2\omega)} - \frac{1}{v_g(\omega)} \right) \quad , \quad (3.13)$$

where  $L_c$  is the crystal length and  $v_g(\omega)$  and  $v_g(2\omega)$  are the group velocities of the fundamental and second harmonic respectively.

Figure 3.3 below shows the basic components and the optical paths through an interferometric auto-correlator.



Interferometric Auto-correlator.

Fig. 3.3. Schematic diagram showing the basic component layout for an interferometric auto-correlator.

### 3.2. Interferometric correlation and pulse shape.

It has been suggested that an auto-correlation carried out with interferometric accuracy, can yield information regarding the fundamental nature of an ultrashort pulse (20),(28). In particular it can reveal the presence of 'chirp', i.e. frequency changing with time within the pulse. The upper envelope described by the interferometric maxima is much more sensitive to the incident pulse shape since it depends on the fourth power of the electric field and on the phase of the combining fields. The form of the interferometric envelope can be related to the type of chirp within the pulse (28). Interferometric auto-correlations should therefore provide information on the frequency and phase structure within a pulse. Figure 3.4. below shows an interferometric auto-correlation curve and its envelope.

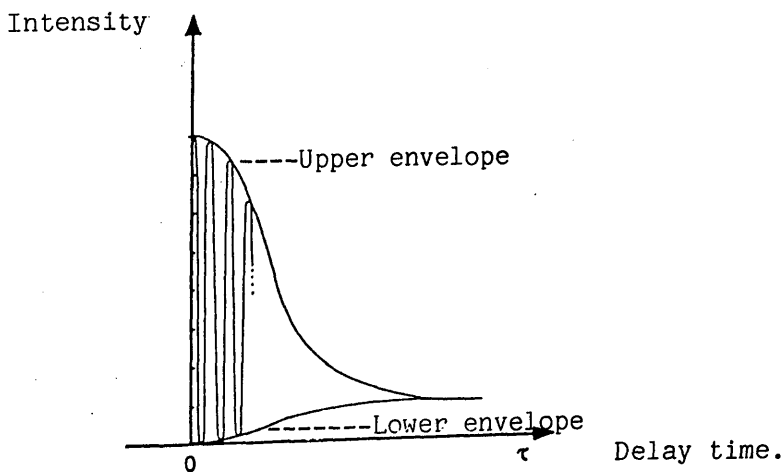


Fig. 3.4. Theoretical curve showing an interferometric auto-correlation. (After ref. 28).

### 3.2.1. Linearly-chirped pulses.

For a linearly chirped pulse, the maxima of the lower envelope recede towards zero delay along a curve close to the intensity correlation curve as the chirp parameter increases. For large phase modulation, the pulse leading edge and tail are no longer coherent. The envelopes of the interferometric and intensity correlations merge for  $T > T_c$  where  $T_c$  represents the position of the lower envelope maximum. The maximum of this envelope, together with  $T_c$ , gives a measure of the chirp parameter, the pulse duration and coherence time.

Note that such a measurement is ambiguous. It depends on assumptions regarding the nature of the chirp. Statistical effects must also be taken into account. For example a train of Gaussian pulses with a Gaussian distribution of frequencies has the same interferometric auto-correlation as a linearly chirped Gaussian pulse (28).

### 3.2.2. Correlation of pulses of unknown chirp.

Analytical expressions can be found for known or assumed pulse shapes. Where the nature of the chirp is unknown, the case is much more difficult to treat. The interferometric auto-correlation of a chirped pulse is itself chirped. This differs from the intensity correlation which is always

symmetric, irrespective of pulse shape. Several techniques have been devised to investigate such pulses. Pulse compression in conjunction with cross correlation can be used, provided that the nature of the chirp allows pulse compression to be carried out.

A down-chirped pulse can be compressed by passing it through a suitable thickness of glass. Within the glass the action of linear dispersion produces pulse compression. If the glass is placed in one arm of a correlator, the compressed pulse from that arm can be cross-correlated with the uncompressed pulse from the other arm. This is illustrated in figure 3.5 below.

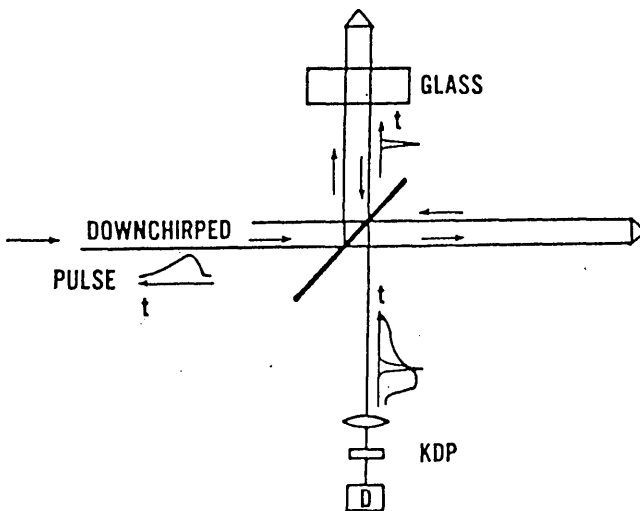


Fig. 3.5. Cross correlation of down-chirped pulses using pulse compression by linear dispersion through glass. (After ref. 28.)

The output observed from the correlator of figure 3.4 can be related to the down-chirp in the original pulse (28).

While this method can be useful for down-chirped pulses, there is no direct method for observing the shape and phase content of a pulse with nonlinear chirp. Pulse analysis may be carried out by postulating a pulse shape, observing the interferometric auto-correlation produced, and comparing it with known auto-correlations. Alternatively, a computer program can be created to simulate the auto-correlation and comparison made (24). Neither method is completely satisfactory.

### 3.3. Summary.

Correlation techniques used in high repetition rate pulsed laser systems, have been introduced. The necessary conditions for obtaining an interferometric correlation have been noted. The information obtainable from a linear correlation was described. The advantages of nonlinear methods for pulse width measurement have been outlined. The necessity for assumptions regarding pulse shape inherent in intensity correlation measurements was noted.

Linear and nonlinear auto-correlation techniques were described in detail. Methods for obtaining background-free correlations were outlined. The relation between interferometric auto-correlations and pulse structure was

discussed. The problem of deriving pulse structure from correlation measurements, with no assumption regarding pulse shape, was introduced.

## CHAPTER FOUR.

### INSTRUMENT CONSTRUCTION AND OPERATION.

#### 4.1. Interferometric measurement.

To carry out an interferometric correlation, the optical path length in one arm of the interferometer must be capable of variation in steps of about one tenth of the minimum wavelength present (32). Assuming an operating wavelength of 500nm, and bearing in mind the doubling of path difference produced by moving one mirror of a Michelson interferometer in the direction of propagation, a resolution of one tenth of a wavelength implies a movement which can be resolved to within 25nm. Mechanical movements driven by a stepper motor are capable of a resolution of 100nm. This represents the smallest step available. The Burleigh "Inchworm" movement, (to be described later), also has a resolution of 100nm. However this does not represent the smallest step available, only the limit of response of the encoder which gives a positional readout.

Single step operation provides a minimum movement of 4nm. The movement can be calibrated by comparison with

a known wavelength standard. Such a movement would appear to allow the possibility of accurate interferometric auto-correlation (16).

#### 4.2. Instrument design.

The instrument was based on the Michelson interferometer. This was originally used to investigate the fine structure of spectral lines by observing changes in the intensity of the output caused by interference between two beams of coherent light from the interferometer arms as the path length in one arm is varied (33).

##### 4.2.1. Basic framework.

The basic framework was made from 'Super Invar' 20mm diameter rod. This metal has an extremely low coefficient of thermal expansion which helped to reduce thermal effects as well as providing a rigid base for the optical components. The rod was welded into the 'T' shape shown in figure 4.1. The plan view shows the frame on which the components were mounted. The side elevation shows the method by which the individual components were located on to the framework in a fixed position. This is further illustrated by the photographs of figure 4.2.

INVAR FRAMEWORK - COEFFICIENT OF LINEAR EXPANSION

$$= 0.9 \times 10^{-6} \text{K}^{-1}$$

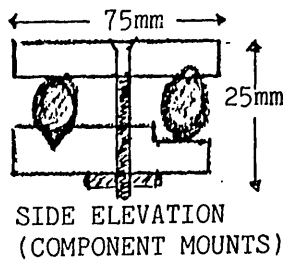
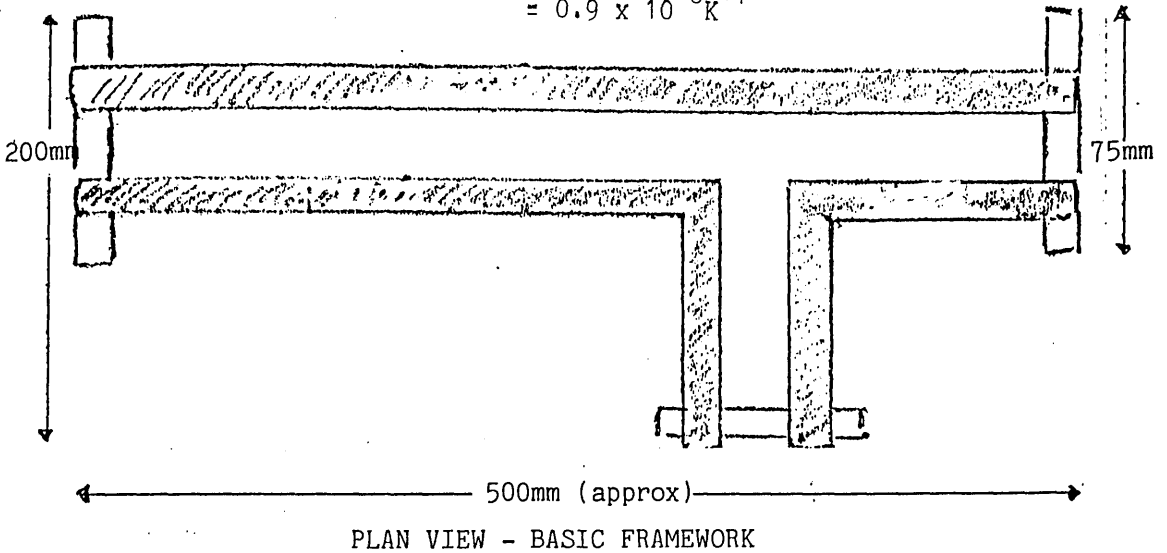


Fig. 4.1. Sketch of the basic invar framework on which the optical components of an interferometric auto-correlator were mounted.

Since the rod supplied could not be regarded as uniformly straight, the mounting fixtures were designed and fabricated as shown in the side elevation of figure 4.1 above. These could be clamped on to the framework at any suitable point and allowed considerable scope for positioning the individual components.

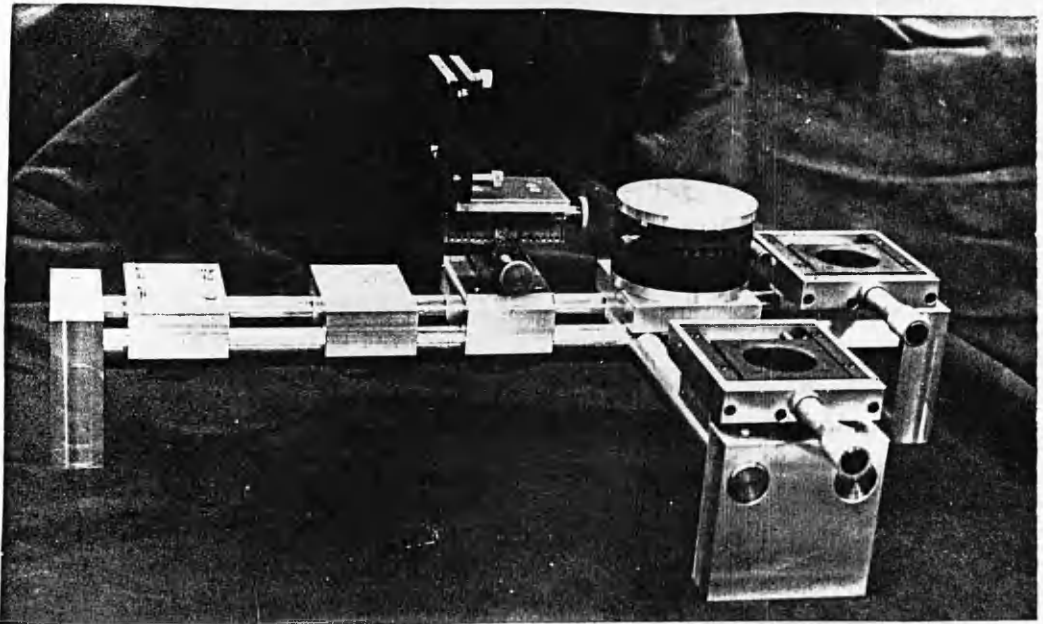
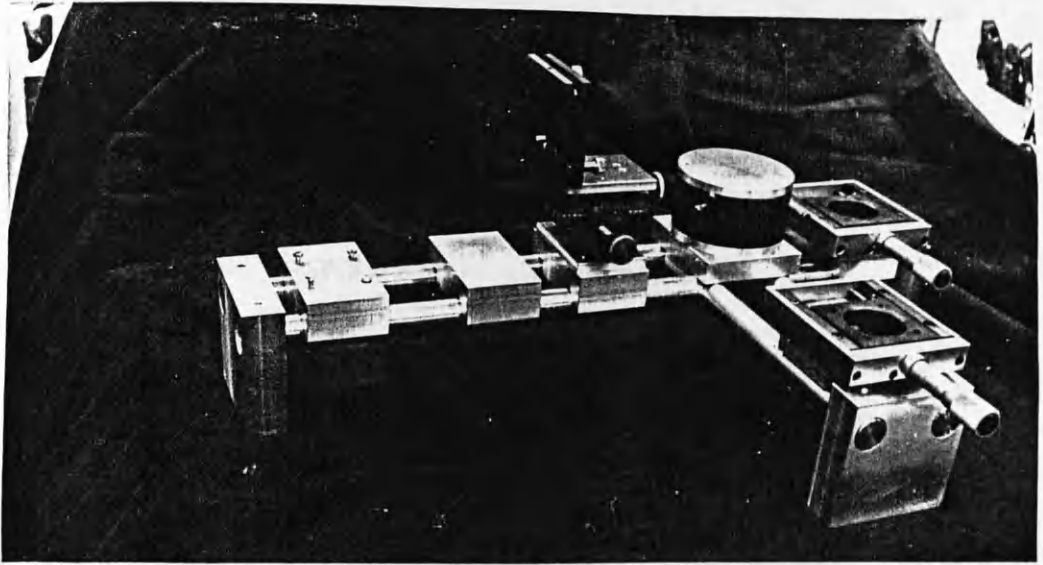


Fig. 4.2. Photographs showing the interferometric auto-correlator at an early stage of construction; the micro-meter movements and some component mounts are shown.

The lengths of the interferometer arms were designed to be a minimum compatible with the component mounts. This kept the physical dimensions of the instrument down to convenient proportions. A pulse of one picosecond duration occupies a length in air of only 0.3mm. Thus there was no requirement to incorporate a distance longer than was convenient for mounting the optical components and which would allow the necessary optical path variation in one arm.

#### 4.3. Components used in the construction of the instrument.

The components used in the construction of the instrument are illustrated in figure 4.3. below. These consist of optical components, mechanical movements and opto-electronic means of detection.

##### 4.3.1 Optical components.

The individual components were as follows, in the order in which the input pulse encountered them.

- (i) "50-50" beam splitter.

The beam splitter was used to split the incident beam or pulse into two parts of equal intensity. The coating on the beam splitter was designed to achieve this over a wavelength range from 400nm to 800nm. It was mounted

on a rotation about the vertical and could also be tilted for alignment purposes. The rotating movement was micrometer controlled, while the tilt was effected by a spring-loaded 40 turns per inch (TPI) screw. The mechanical design and operation were found to be completely satisfactory.

Beam clipping was avoided by using a holder whose width greatly exceeded that of the beam splitter itself. The optical performance was less satisfactory. It was found that the output from each arm of the interferometer was not of equal intensity. This was a result of one beam traversing the glass of the beam splitter three times whilst the other traversed it only once. This is illustrated in figure 4.4

below.

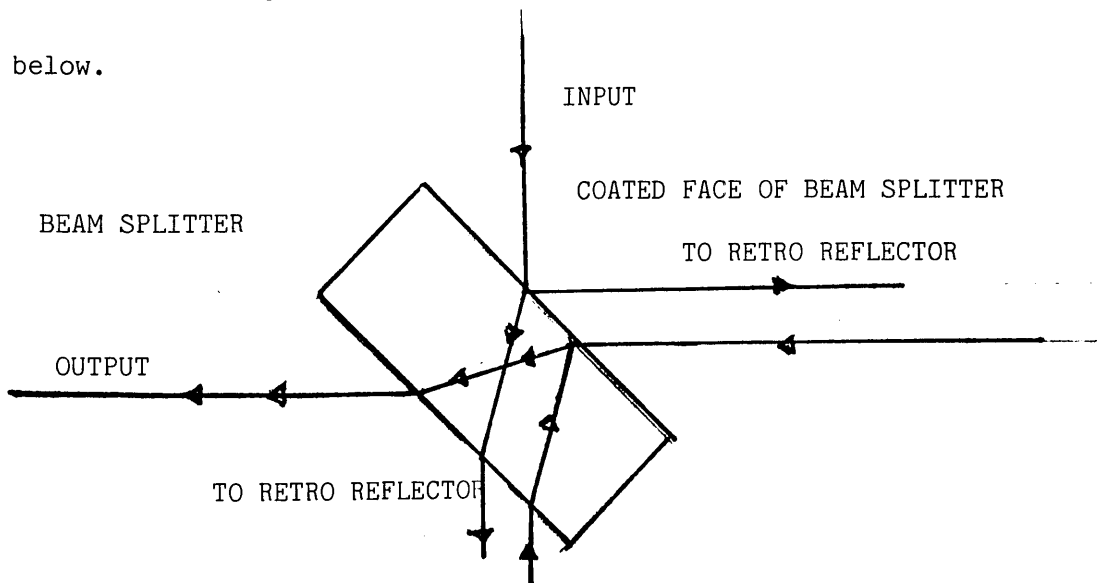


Fig. 4.4. Transmission and reflection within a beam splitter as part of a Michelson interferometer.

The effect of this was to reduce the contrast ratio observed in the interference fringe pattern at the output. The effect on pulse correlation was small.

Previous work has shown that where appreciable thicknesses of glass are traversed by a pulse, its structure can be affected (28). This in turn modifies the observed correlation. A method of avoiding multiple traversals of the beam splitter is by coating the latter half-way on either side. This ensures each beam only traverses the beam splitter glass once.

(ii) Retro-reflectors.

A retro-reflector was used to terminate each arm of the interferometer. These consist of surface-coated mirrors which are assembled in such a manner as to return any incident beam along a path parallel to its original direction and displaced from it. Spurious beams produced at the beam splitter could thus be prevented from returning to the laser cavity by a suitably placed aperture. This removed a possible source of laser instability.

The retro-reflectors used had a tolerance of 30 seconds of arc. As indicated above they were of the mirror type. These minimized dispersion and absorption and eliminated

spurious reflections. One reflector was mounted on a transverse movement which was micrometer controlled. When used in conjunction with the beam splitter rotation and tilt, it could render the output beams parallel or collinear as required by the type of correlation being carried out. For intensity correlations, the beams were parallel but not collinear. For interferometric correlations the beams were collinear.

The other reflector was mounted on the end of an "Inchworm" piezo-electric controlled movement. This was itself mounted on a micrometer-controlled longitudinal movement. The latter was used to find an approximate zero-delay position for the two pulses when their optical path lengths in the interferometer arms are equal. The "Inchworm" movement was then used to scan about this position.

(iii) Focussing lens.

A short focal length lens was required to focus the output from the interferometer arms on to the frequency doubling crystal. In the case of intensity correlations these were parallel but not collinear, as indicated above. The focal length was chosen to achieve the best phase-matching conditions within the crystal. In interferometric work, the lens helped to reduce the spot size within the

crystal. This improved the signal to noise ratio, thus increasing the sensitivity of the correlation.

Any effect due to the lens glass on pulse shape will be present in both pulses. The lens was mounted in a tilt-controlled holder and could be translated in the horizontal plane for alignment and focussing purposes.

(iv) Frequency doubling crystal.

The frequency doubling crystal employed depended on the required wavelength range. For the pulses scanned in this work, a lithium iodide crystal was mounted in a holder which could be rotated in the vertical plane. This allowed selection of the appropriate angle of polarization with respect to the input beams. The crystal was mounted between windows which allowed transmission into the ultra-violet region. These prevented damage to the crystal due to atmospheric moisture or dirt. The crystal was about one millimetre thick. When used in conjunction with a short focal length lens, this ensured uniform phase-matching efficiency over all the frequency components of the pulse (3). If this condition was not maintained, the measured correlation function would be broadened (34).

The frequency doubling crystal was mounted on a horizontal rotating stage to allow the input face of the

crystal to be set for maximum frequency-doubling efficiency.

No difficulty was experienced with this component in practice.

(v) Filters.

After frequency conversion, the output signal fell on to a suitable detector. This signal contained the remainder of the fundamental beam as well as the second harmonic. The fundamental could be removed by the use of suitable narrow bandpass filters. Provision was made to mount two such filters in front of a photomultiplier tube housing. This was also fitted with an iris to stop down the input beam. This removed other beams present during intensity correlations thus providing a 'background free' intensity correlation.

(vi) Detectors.

The detector in normal use was a side-on mounted Hamamatsu photomultiplier tube. A secondary power unit was constructed to supply the basic dc voltage and control. The detector was boxed with the input mounting holding an iris and filter mounts as described above. At some wavelengths a judicious choice of photocathode eliminated the need for filters. Input connexions for the power supply and for the output signal were fitted to this unit.

(i) Micrometer controlled translations.

Both retro-reflectors were mounted on linear micrometer movements. These had a resolution of  $5\mu\text{m}$ . As described earlier they were used for initial positioning.

(ii) "Inchworm movement".

In order to provide the sensitivity necessary for interferometric correlation measurements, a movement capable of sub-micron resolution was required. The movement chosen provided a resolution of  $0.5\mu\text{m}$  and was capable of a minimum step of  $4\text{nm}$ . The "Inchworm" movement used three coupled lead zirconate titanate (PZT) components to perform the fundamental movement. PZT is a ceramic which shows appreciable changes in its linear dimensions on the application of fairly high voltages (35). A specimen can thus be made to expand or contract in any appropriate direction by a suitable application of voltage. The direction of the applied voltage with respect to the structure of the material determines which effect is produced.

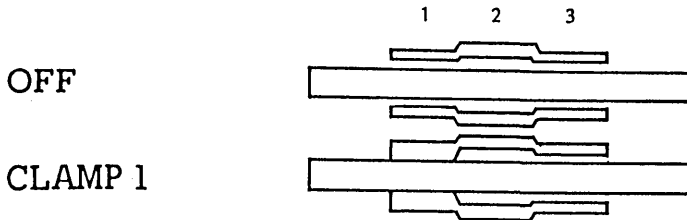
In this application, three cylindrical elements were joined in series to form a collar round the drive shaft which carried the retro-reflector. There was a sliding fit between the shaft and the first and third elements.

The central element had a clearance fit with the shaft.

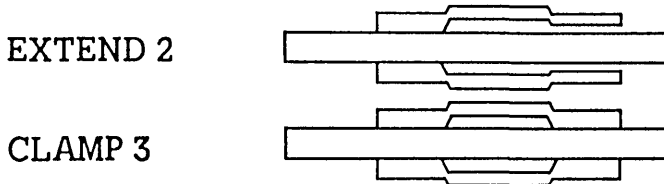
The principle of operation is illustrated by figure 4.5

below.

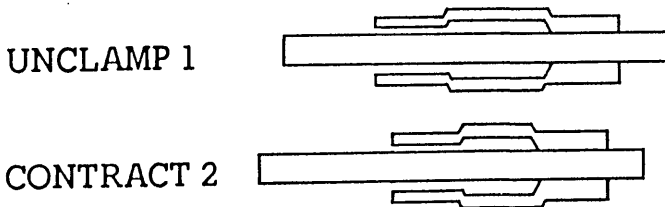
Stage 1. Element 1 is expanded laterally to clamp on to the shaft



Stage 2. Element 2 is expanded longitudinally then element three is expanded laterally to clamp on to the shaft.



Stage 3. Element 1 is unclamped and element 2 is allowed to contract.



Stage 4. Element 1 is clamped and element 3 is unclamped after which the cycle is repeated as necessary.

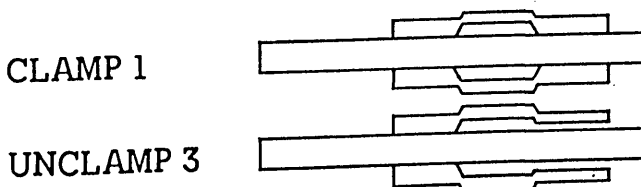


Fig. 4.5. "Inchworm" movement(From the maker's data).

When a voltage was applied to element 1, that element clamped on to the shaft. Then a 'staircase' voltage was applied to the centre element which caused it to expand in the direction of the shaft, in increments of about 4nm. The maximum movement of this element was about 500 such steps. After the upper limit was reached, a voltage applied to the third element caused it to grip the shaft. The voltage to the first element was then removed, and the staircase voltage removed to its lower limit, thus causing the shaft to move through approximately 2 $\mu$ m. The cycle was then repeated until the necessary movement was obtained.

The total movement available was nominally 6.25mm with an encoder resolution of 0.5 $\mu$ m. The speed of application could be varied or the movement stopped or reversed at any time.

#### 4.4. Factors affecting instrumental accuracy.

The accuracy of the instrument was affected by the mechanical operation of the various translations during measurement, and by the performance of the various optical parts.

##### 4.4.1. Mechanical factors.

There were two linear mechanical movements in the arms of the interferometer. One was a transverse movement, used to set the output reflected beams parallel and collinear as required. Since this movement was micrometer controlled to a resolution of  $5\mu\text{m}$ , and the beam width was of the order of  $1\text{mm}$ , no appreciable error was introduced by this movement.

The longitudinal micrometer was used to set the approximate 'zero-delay' condition. Once this was established, the fine tuning was performed using the superposed "Inchworm" movement. Thus the resolution and the accuracy was determined by the latter. The encoder supplied had an accuracy of  $1\mu\text{m}$  and a resolution of  $0.5\mu\text{m}$ . This was calibrated interferometrically against a helium neon laser. Thus it was possible to establish lengths down to a fraction of a wavelength as required by interferometric correlation techniques. The mechanical resolution was  $4\text{nm}$ .

#### 4.4.2. Optical factors.

The deviation produced in either beam due to the retro-reflectors was less than 30" of arc. Over a length of 10cm, which corresponded to the path length used, a lateral displacement of less than  $1\mu\text{m}$  would be produced. This is negligible in comparison with the spot size of 1mm.

As indicated earlier, the passage of the pulse through the beam splitter might produce a degree of asymmetry between the pulse pair. The work of Diels et al. indicated that passage through glass may produce chirp or compensate for some types of chirp. Similarly the focussing lens may have a small effect on the pulse profile, but in this case both pulses would be similarly affected.

The output from the second harmonic-generating crystal depended on good phase-matching over the whole bandwidth of the pulse. The crystal material and thickness were chosen to this end. The micrometer controlled rotation allowed fine setting of the phase-matching angle in the horizontal plane. The rotation in the vertical plane was less satisfactory but adequate.

#### 4.4.3. Signal detection.

The tubes used in the photomultiplier detector were the Hamamatsu R212 or IP28 in the visible region, while in the infra red, an R406 was used. These tubes have a rise time of 2.2ns and an electron transit time of 22ns. In normal operation the output was observed over a large number of pulses so the detector output corresponded to an average value. The speed of operation was not critical to the measurement made. The cathode sensitivity was 20 $\mu$ A per lumen of incident radiation (minimum). One lumen corresponds approximately to 1.5mW at a wavelength of 570nm.

#### 4.5. Instrument operation.

In the normal mode of operation, an input pulse train, originating from a mode-locked laser, was split into two at the beam splitter. These then traversed respective arms of the interferometer before recombining at the beam splitter. The delay between any pair of pulses was varied to within very fine limits by the 4nm step size of the "Inchworm" movement. The pulses were focussed on to a second harmonic-generating crystal. The output from the crystal was filtered if necessary and passed to the detection system. The output

from the detector was displayed on an oscilloscope to assist in improving alignment, and also recorded on a 'Y-T' plotter.

The scanning speed of the plotter was set to a suitable value with respect to the "Inchworm" speed. Very slow scanning speeds obscured individual fringes and left excessive ink on the recording paper. Fast scanning speeds led to very long traces and heavy use of chart paper.

The pulse was scanned around zero-delay, where fringe visibility was maintained. The stability of the system was good, and a clear record of an interferometric correlation could be obtained. This showed a series of maxima and minima as the movement changed the optical path length of the incident radiation by one wavelength. As the pulses passed through one another during scanning, any mismatch in wavelength modified the fringe pattern observed.

#### 4.6 Instrument resolution.

The instrument was based on the Michelson interferometer. The latter can provide the same information as a diffraction grating or a spectrometer, viz. the frequency components present in an optical signal (33). In early applications Michelson was able to estimate the separation of the sodium doublet (6 Angstroms). This was possible because the

resolution of the instrument was proportional to the scanned optical path difference between the two interfering beams.

The maximum path difference which could be achieved using the "Inchworm" movement was about 10mm. Using the accepted definition of resolution as applied to the Michelson interferometer, viz. :-

$$\text{Resolution} = \frac{2 \times \text{path difference}}{\text{wavelength}}, \quad (4.1)$$

leads in the present case to :-

$$\text{Resolution} = \frac{2 \times 0.01}{1\mu\text{m}} = 20000.$$

This assumes an input wavelength of  $1\mu\text{m}$  which is close to that of the Nd:YAG pulses observed. The instrument should be able to resolve a wavelength difference given by :-

$$R = \frac{\lambda}{\delta\lambda}. \quad (4.2)$$

$$\text{Therefore } \delta\lambda = \frac{1\mu\text{m}}{20000}$$

$$= \underline{0.5} \text{ Angstroms.}$$

This treatment assumed that the spectrometer was free from optical aberrations and mechanical defects.

The chirp produced in a pulse was expected to be of the order of 10nm. It was therefore reasonable to expect that the instrument constructed would resolve such features.

#### 4.7. Instrument assembly.

The auto-correlator was assembled using the previously designated parts. No problems were encountered with the basic assembly. The initial alignment tests were performed with a helium-neon laser operating at 633nm cw. The frequency doubling crystal was not mounted for this operation. The movements incorporated in the design were found to be sufficient for good alignment without undue difficulty.

During test scans, the output from the photomultiplier tube was passed to a 'Y-T' plotter. This produced a regular trace of intensity changes corresponding to the phase difference between the beams. The signal to noise ratio was of the order of 7:1. A frequency doubling crystal was mounted in the crystal holder without difficulty or undue stress on the crystal.

#### 4.8. Calibration of the "Inchworm" movement.

Calibration of the "Inchworm" movement incorporated within the auto-correlator was carried out using a helium neon laser operating at 632.8nm cw. This laser has a coherence length of the order of 30cm in single transverse mode operation where more than one axial mode may be present.

It can therefore provide a useful standard of length where interferometric measurements are made over a path difference much shorter than the coherence length. The total path difference which could be introduced between the two arms of the instrument using the "Inchworm" movement alone was nominally 12.5mm. During the calibration check, the total "Inchworm" movement was less than 1mm.

Using the helium-neon laser as source, the output from each arm of the instrument was adjusted parallel and collinear. The combined beams were focussed on a small aperture mounted in front of a photomultiplier tube (Hamamatsu IP28). This isolated the centre of the usual ring pattern so that the output in the scanning mode was a series of maxima and minima varying from twice the average intensity to approximately zero. This pattern was repeated throughout the length of the scan with no apparent change in levels recorded.

The separation of any two successive maxima corresponded to a path difference change of one wavelength of the source light. The output from the photomultiplier tube was recorded on a 'Y-T' plotter. A total of 2274 fringes were recorded in this way. This corresponded to a digital read-out on the Burleigh controller of 0.7220mm.

The total movement was given by :-

$$s = \frac{2274 \times 632.8}{2}$$

$$= 0.7195\text{mm}$$

The apparent movement shown on the controller was :-

$$s' = 0.7220\text{mm}.$$

Therefore the ratio :-  $\frac{s'}{s} = 0.9965$ .

This ratio represents the conversion factor to be applied to any measurement of length made using the "Inchworm" movement.

The percentage error over the distance measured may be expressed as :-

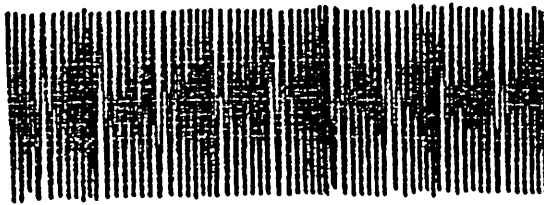
$$\frac{s' - s}{s} \times 100 = 0.35\%.$$

The encoder accuracy stated by the maker Burleigh was +/- 1 $\mu$ m. This represents a percentage error in the above measurement of about 0.14%. The difference in the two results may be due to the presence of a discontinuity or 'glitch' in the "Inchworm" movement..

#### 4.9. 'Glitch' in the "Inchworm" movement.

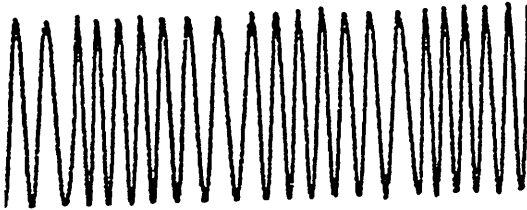
Whilst carrying out preliminary tests, it was observed that a discontinuity appeared about every sixth or seventh fringe when using a helium-neon source. This is apparent in figure 4.6 below.

"Inchworm" speed =  $58\text{nms}^{-1}$ ; paper speed =  $10\text{mm}/\text{min}$ .



----- $25\mu\text{m}$ .-----

"Inchworm" speed =  $37\text{nms}^{-1}$ ; paper speed =  $0.5\text{mms}^{-1}$ .



----- $10\mu\text{m}$ .-----

Fig. 4.6. Test traces formed on a 'Y-T' plotter from the output of the interferometric auto-correlator used as a Michelson interferometer.

It will be recalled that the maximum movement possible using the piezo electric extension alone was about 500 x 4nm steps, i.e. 2 $\mu$ m. Seven fringes at the helium-neon wavelength represent a distance of 2.2 $\mu$ m. Thus the source of the 'glitch' is the need for the "Inchworm" movement to re-orientate itself every 500 steps.

#### 4.10. Summary.

The qualities necessary in an accurate interferometer have been introduced. The instrument design and construction were described in detail. The individual components have been described and their functions and performance discussed. Optical and mechanical factors which affected instrumental accuracy have been outlined and evaluated. Instrument operation was described and instrument resolution estimated. Assembly and calibration of the instrument were described and the test output presented. The presence of a glitch in the test data was noted and its source identified.

## CHAPTER FIVE.

### EXPERIMENTAL INVESTIGATIONS OF THE PERFORMANCE OF THE AUTO-CORRELATOR IN ITS THREE POSSIBLE MODES OF OPERATION.

#### 5.1. Performance evaluation.

In order to evaluate the performance of the auto-correlator, a series of experiments was carried out. The instrument was operated in three distinct configurations. Firstly as a Michelson interferometer, secondly as an intensity auto-correlator and thirdly, as an interferometric auto-correlator. It should be noted that no frequency doubling is employed in the first method of operation. In the second method, the individual fringes produced after frequency doubling by the second harmonic-generating crystal, are averaged out to form an intensity envelope. The first and third methods show individual fringes.

#### 5.2. Applications using the Michelson configuration.

Several investigations were carried out involving the output from a semiconductor laser. The data obtained was used to produce visibility curves and to provide operational parameters such as wavelength and cavity length.

### 5.2.1 Interferogram and visibility curve from the output of a semiconductor laser.

The Michelson interferometer is a suitable instrument for measurement of coherence length and spectral content of quasi-monochromatic sources (32). When Michelson made his original investigations with the instrument adjusted to give circular fringes, he found that the fringes were quite distinct at small path differences. As the path difference increased, the visibility decreased, but not in a simple linear fashion. At large path differences, the fringes disappeared altogether. This result indicated that more than one spectral component was present in apparently monochromatic light. Each component was producing an interference pattern which showed increasing displacement from its neighbours as the path difference increased. The amount of destructive interference between components therefore increased and, in general, the visibility of the fringes decreased with increasing path difference. It should be noted that this result implied that where fringes were visible over a large path difference, the spectral bandwidth was narrow.

It was clear, therefore, that observations made on the variability of fringe visibility with changes in optical path difference must provide information regarding the spectral content of quasi-monochromatic radiation. Furthermore, a coherence length could be defined in terms of the visibility of fringes which could provide a useful parameter in measuring the spectral purity of a light source.

#### 5.2.2. Sharp semiconductor laser LTO 15MF0.

A signal source of great interest for optical communications and a likely source for future developments in integrated optic systems, is the semiconductor laser diode. It is of small physical size, typically  $300 \times 300 \times 10 \text{ } (\mu\text{m})^3$ . While the technology required for its production is not identical to that used in the present semiconductor industry, the facilities and techniques required are similar in nature. Such lasers are capable of continuous or pulsed operation. Their output power, although not comparable with other lasers of much greater physical dimensions, is adequate for digital operations over fibre optic networks of considerable length. Currently available lasers can provide power in excess of 1W (36).

### 5.2.3. Theory of operation of a Sharp semiconductor laser.

The laser diode used in the experimental tests was of the gallium aluminium arsenide type. This consists of a double heterojunction formed by an active layer of  $\text{Ga}_{1-y}\text{Al}_y\text{As}$  surrounded by p-type and n-type  $\text{Ga}_{1-x}\text{Al}_x\text{As}$  cladding layers, (x being greater than y). The construction is illustrated in figure 5.1. below.

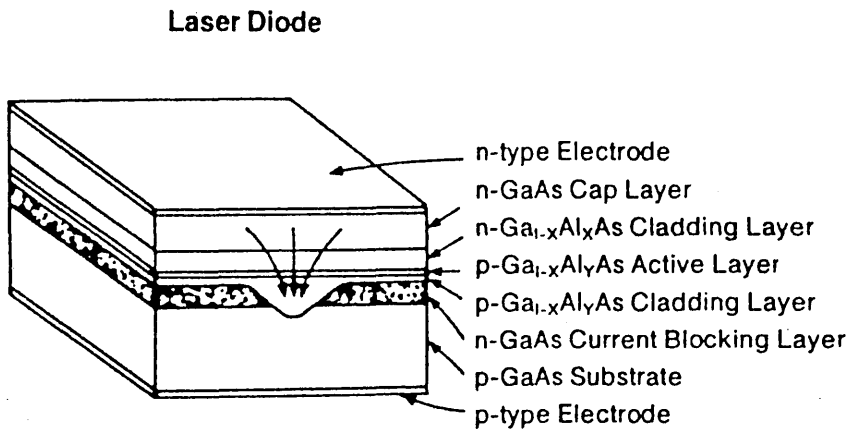


Fig. 5.1. Sharp semiconductor laser construction (after ref. 31).

The laser operates as follows . A forward bias is applied to the diode, causing electrons and holes to be injected into the active layer. The bandgap energy is greater in the cladding layers than in the active layer. Potential barriers are thus set up across the junctions which prevent the injected charge carriers from diffusing into the cladding

layers. In the active layer the charge carriers give off their excess recombination energy in the form of light at a wavelength of approximately 830nm. This makes possible the amplification of light by stimulated emission.

The active layer has a high refractive index in comparison with the cladding layers. This serves to confine the emitted light to the active region. In order to produce a coherent laser beam, a laser oscillator must be formed. Thus the ends of the semiconductor crystal are cleaved to form a resonant cavity between the two parallel reflecting faces. The large difference in refractive index at the interfaces (3.5:1) ensures high reflectivity. The output face of the Sharp laser used in the following experiments had a 1% anti-reflection coating at the operational wavelength. This feature was useful for external cavity operation.

The light produced by the recombination of charge carriers is reflected back and forth within the cavity. Light which is travelling at an appreciable angle to the cavity walls will pass out of the cavity and take no further part in the lasing process. Light which travels in an axial direction will be amplified by further emissions of excess combination energy. Since the cavity length is several hundred times the wavelength of spontaneous emission, the cavity may

support several longitudinal (axial) modes of oscillation.

The preferred mode is where the maximum gain occurs. This depends on the bandgap energy which in turn depends on cavity temperature. Thus changes in temperature will affect the output mode structure.

The possibility also exists for the output of several transverse modes. A transverse mode can be considered as being made up of two components, one parallel to, and the other perpendicular to, the active layer. Since the active layer is very thin, only the fundamental mode is propagated with the perpendicular orientation. In the Sharp laser an attempt to prevent the propagation of more than one transverse mode with parallel orientation is made by forming a 'V' shaped groove in the substrate before the growth of the active layers. This suppresses unwanted oscillations and hopefully confines the oscillation to a single transverse mode. Because the transverse spatial extent of the beam at the output facet is comparable with the emitted wavelength, the beam becomes widely diffracted on leaving the resonant cavity.

5.2.4. Experimental method used in recording a diode laser output.

Figure 5.2 below indicates the component layout used while investigating the output from a semiconductor laser.

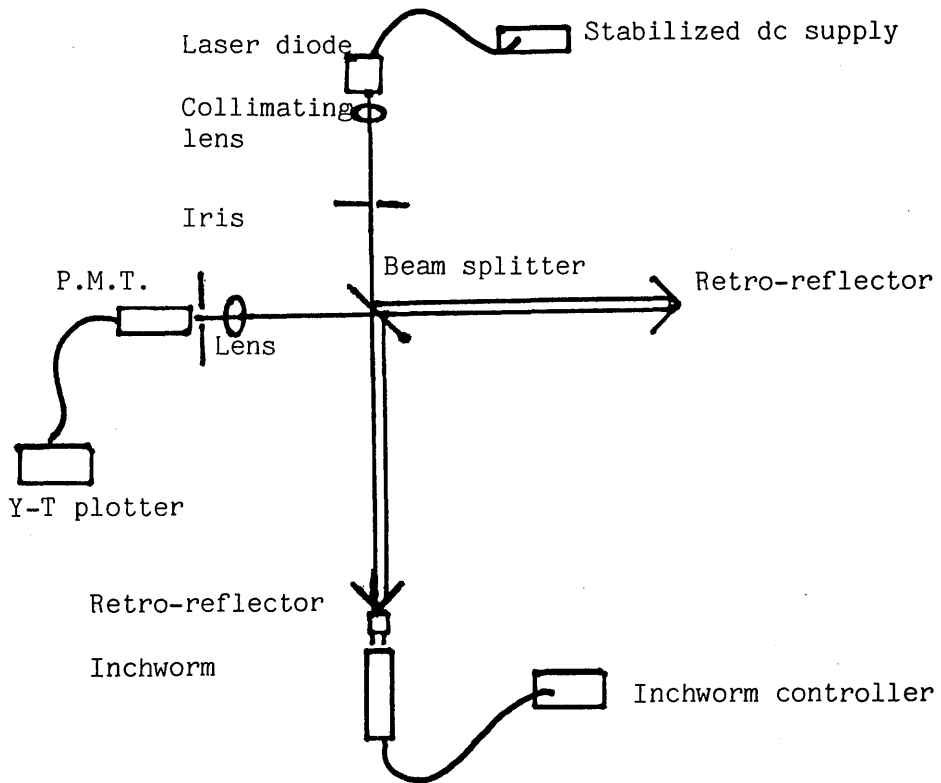


Fig. 5.2. Experimental arrangement for scanning the output of a cw semiconductor laser diode.

As indicated above, the output from the semiconductor laser was divergent at a large angle (of the order of  $30^\circ$  perpendicular, and  $10^\circ$  parallel) to the active layer.

An anti-reflection coated short focal length lens was used to render the laser output parallel. This lens was mounted on an 'X-Y-Z' micrometer controlled movement to facilitate and optimize alignment. The output power from the laser diode was initially set at 15mW as measured by a broadband optical power meter (Spectra-physics 400C). The power level was controlled by a variable dc supply. This supply was designed to provide a constant current and to avoid passing voltage 'spikes' to the diode laser. The operating voltage of the laser was 2V.

The infra-red (830nm) output from the laser was aligned with the interferometer without difficulty. The output from the interferometer was detected by the above broadband power meter which also provided an output analogue voltage. This was passed to a 'Y-T' plotter. Measurements were carried out at a slow scan rate to avoid any limitation on the speed of response of the detector or plotter and to average out random effects. The output was maximized by rendering the outputs from each arm of the interferometer parallel and collinear. The zero-delay position was established approximately by observing the maxima of the interference fringes produced during a preliminary scan. A trace was then made of the interference fringes produced as one

retro-reflector was moved by the "Inchworm" through the zero-delay position. A sample of the fringes obtained is shown in figure 5.3 below. The visibility was poor as the laser was coming to the end of its useful life. The presence of the 'glitch' can be clearly seen.

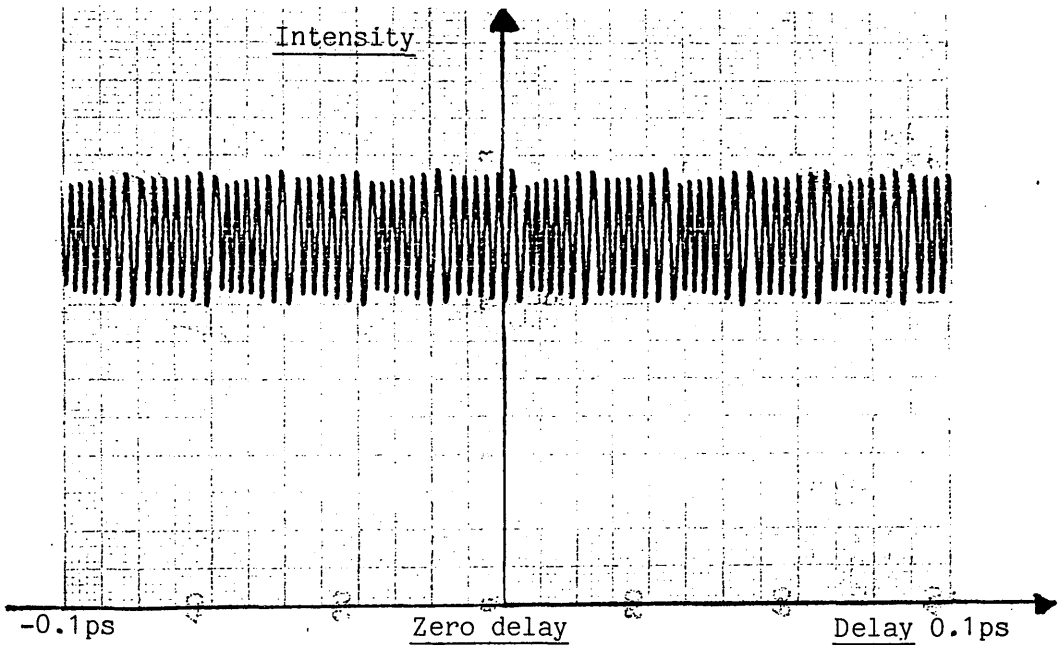


Fig. 5.3. A section of an interferogram of a semiconductor laser output, made using the scanning Michelson configuration.

#### 5.2.5. Visibility curve for a semiconductor laser diode.

From measurements made on the interferogram obtained as above, a visibility curve was produced. This revealed the coherence length of the source, and showed evidence of mode structure.

Fringe visibility is defined as (22) :-

$$V = \frac{I_{\max} - I_{\min}}{I_{\max} + I_{\min}} \quad (5.1)$$

where  $I_{\max}$  and  $I_{\min}$  are the intensities of the output as measured by the maximum and minimum of the interferogram envelope at any given delay.

Plotting  $V$  versus delay or path difference yields the visibility curve. This curve will be symmetrical about zero delay if the light intensities in each arm of the interferometer are equal. Figure 5.4 below shows the visibility curve obtained.

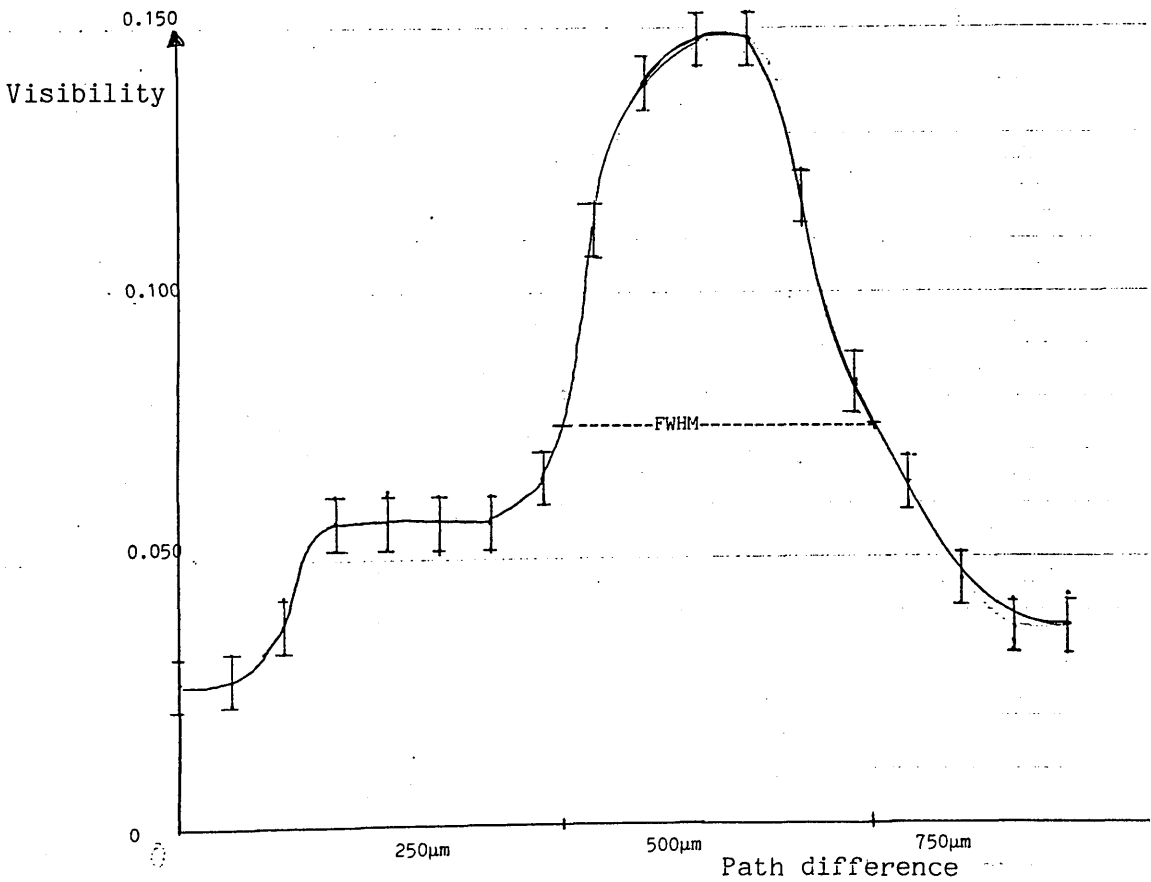


Fig. 5.4. Visibility curve for a Sharp laser diode LTO 15MFO.

Taking the width of the visibility curve at the half-maximum points as a measure of coherence length, the latter was found to be 0.3mm. The plateau on the trace indicates the presence of a second mode of the laser which reduces the coherence length. Since the measurements were made on the fringe envelope, the presence of the movement glitch, although noted, did not affect the result obtained. The visibility was poor as the laser was coming to the end of its useful life (37).

The degree of asymmetry in the curve obtained was due to two factors. The effect of scattering on one beam as it passed through the beam splitter was three times greater than the other as explained above. The beam splitter was designed for the visible range, whereas the laser radiation was at 830nm. Thus a 50% split could not be guaranteed. The first problem could be overcome as outlined above, (4.3.1), or by placing a compensating plate in one arm of the interferometer. The second problem could be overcome by a more suitable choice of beam splitter.

5.2.6. Semiconductor laser as part of a phase-combined array. (- 5.2.8 With the kind co-operation of Brian Graham)

While semiconductor lasers are attractive in many applications because of their small physical dimensions, their relatively low output powers disqualify them from areas where coherent sources of high radiance are required. Laser systems are limited in output power by physical constraints. For example a restriction on the cross section area of the lasing medium may be necessary if single spatial mode operation is required. In semiconductor lasers, facet damage may occur at high light intensities, or breakdown may be induced by high optical field intensities. Where no adequate thermal control is possible, the effects of overheating may restrict operation to low output powers.

In an attempt to overcome these limitations, the output power from several lasers may be combined to act as one source of high radiance. Since it is desirable that such a source produces coherent light, the combination of the individual lasers must be carried out in such a way as to produce and maintain coherence.

One attempt to produce such a source is illustrated in figure 5.5. below.

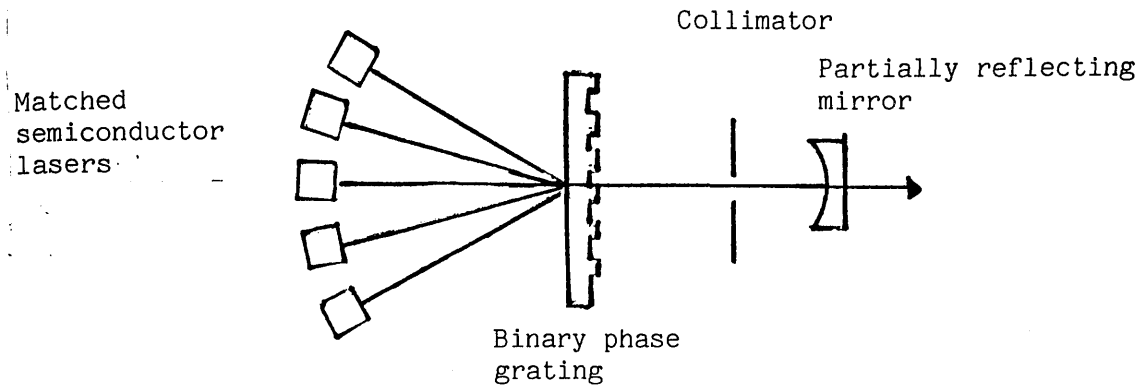


Fig. 5.5. Schematic diagram showing a phase-combined laser array.

The method illustrated above makes use of a binary phase grating which is designed to split a laser beam into several orders of equal intensity. When the individual beams are returned along the same paths, they are recombined to form one beam, with equal efficiency (38). If several lasers are placed in positions corresponding to the grating orders, their output beams will be combined along the same path after passing through the grating. In order to produce a coherent output, the wavelengths and individual phases must be matched. To do this, a cavity is formed by placing a partially reflecting mirror beyond the grating. This acts as an output coupler and also serves to return the combined beam to the lasers via the grating.

Wavelength matching is accomplished by adjusting the temperatures of the individual lasers. Phase-matching depends on the loss conditions within the cavity. If the lasers are not mutually coherent, each laser acts as an individual source. Each produces an angular plane wave spectrum consisting of  $N$  diffraction orders where  $N$  is the number of equal intensity orders which the grating has been designed to produce.

Since only one of the diffraction orders from an individual laser is along the optic axis of the system, the power loss per pass is of the order of  $\frac{1}{N}$ . At the second pass the power loss varies as  $\frac{1}{N^2}$ . This increases dramatically the lasing threshold required by the ensemble. Since any laser system tends to lase in the condition of lowest loss, there will be a natural tendency towards phase-locked operation when the array consists of coherent elements. The lasing condition with the lowest threshold is achieved when the mirror feedback is highest. This occurs when the lasers are coherent and correctly phased for maximum coupling efficiency (38),(39).

As a preliminary to using a monolithic array, where several lasers are produced on the same substrate, an experiment in phase combining two individual lasers was carried out.

### 5.2.7. Phase combination of two semiconductor lasers.

Diode laser 2.

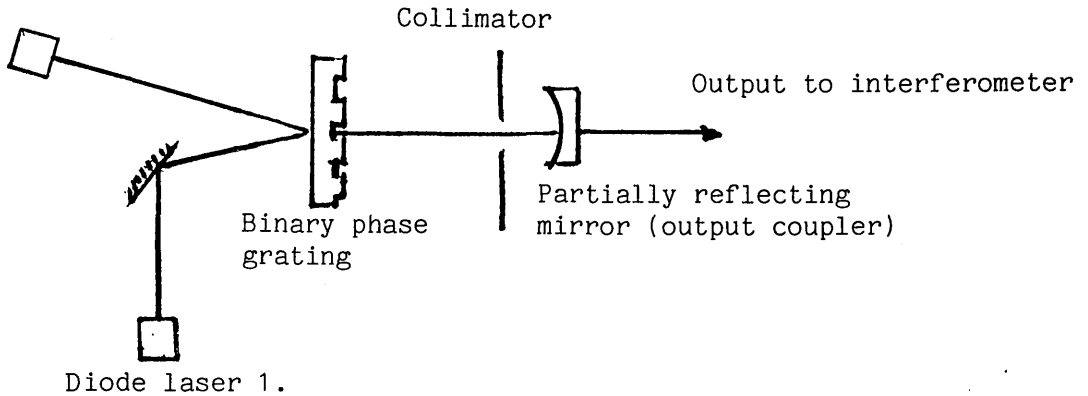


Fig. 5.6. Experimental arrangement for the phase combination of two matched semiconductor lasers.

The individual lasers used in the phase combining experiment illustrated in figure 5.6 above, were mounted on Peltier cooling devices in order to control and adjust the output wavelength (830nm approx.). The output from each laser was observed using a monochromator. The wavelength produced was adjusted to a suitable value by temperature tuning. It was found impossible in some cases to bring the laser wavelengths to matching values. The range of tuning possible in individual lasers did not necessarily correspond in similar laser types. To adjust the phase condition, the lasers were mounted on PZT-controlled translation stages. This allowed very fine tuning

of the individual cavity lengths and helped to give phase matched outputs.

The lasers in this experiment were placed at the positive and negative first-order diffraction positions indicated by the grating. Blocking the individual beams in turn, and noting the diffracted beam positions and intensities, helped ease alignment problems considerably.

It was found possible to produce a phase combined output for very short periods of time only. Since the Michelson interferometer is essentially an integrating instrument, the phase combined output was observed using a scanning Fabry-Perot. Interferometric scans using the Michelson configuration showed a series of weak maxima and poor fringe visibility. Previous workers had used interference fringe visibility as a measure of the mutual coherence of two lasers (39). The result obtained in this instance indicated a distinct lack of coherence.

A possible explanation of the lack of coherence was that it was due to mechanical instability in the system. The system components were individually mounted on an optical table. Inspection of the mounts, and measurements carried out at quiet periods did not yield any indication of mechanical instability.

The poor visibility resulting from incoherently combined beams showed the lasers were operating individually. This may have been due to wavelength mismatch, phase differences between the outputs, the presence of several modes, or instability in the apparatus. Any of these effects or their combination will lead to incoherence in the combined output beam.

In order to try and identify the source of the instability, the output of an individual laser was scanned using the Michelson configuration. The laser was operated within the external cavity arrangement, exactly as it was during phase combining experiments. The instrument was aligned with the output beam from the test laser. The output from the interferometer was detected by a photomultiplier tube and recorded on a 'Y-T' plotter as in the previous experiment.

#### 5.2.8. Interferogram and visibility curve for a semiconductor laser mounted as part of a phase-combining experiment.

The traces obtained showed a series of maxima and minima. These formed two distinct sets, the maxima of one set always exceeding the adjacent maxima of the other. This is clearly shown in the visibility curve of figure 5.7.

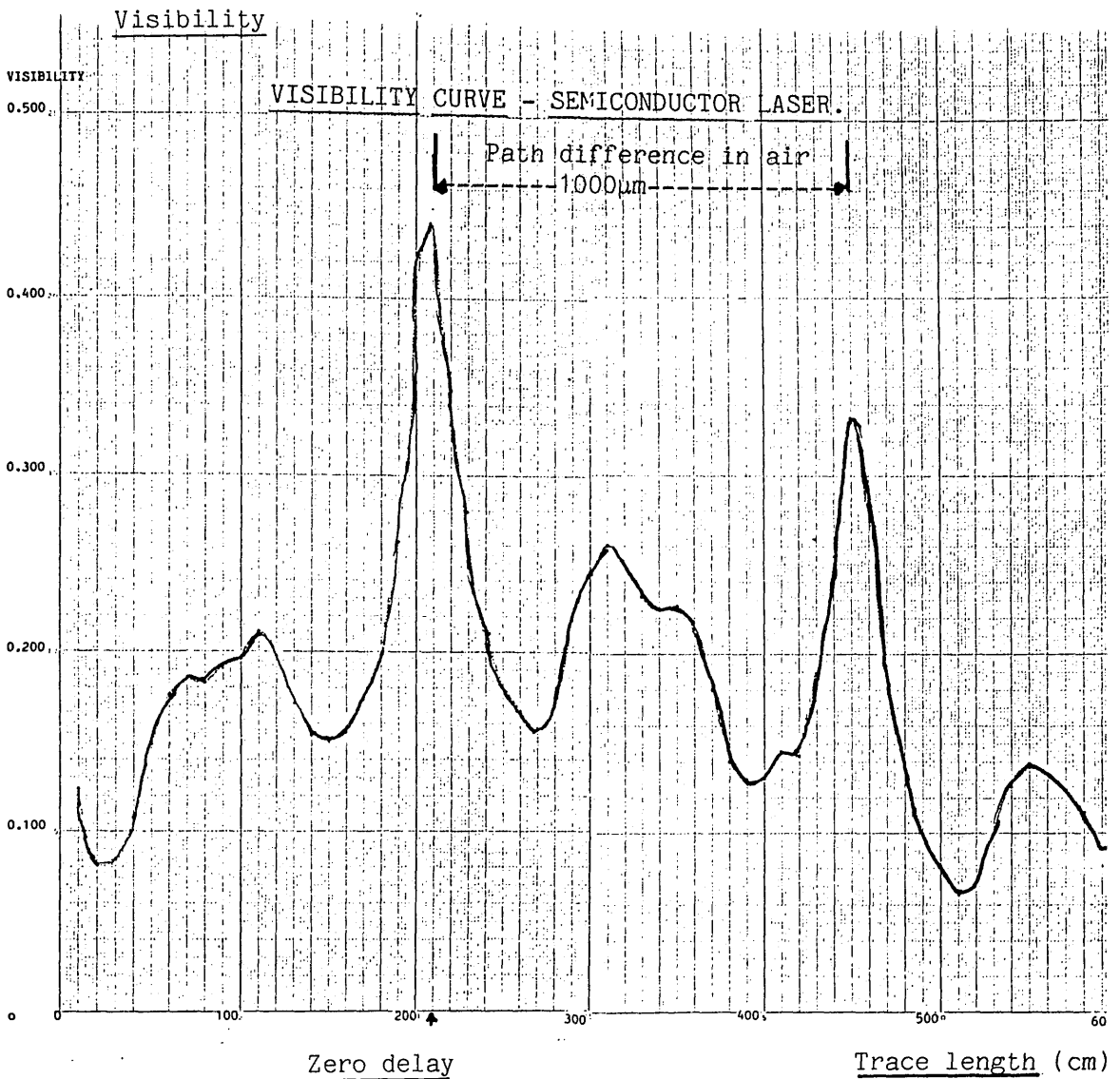


Fig. 5.7. Visibility curve for a semiconductor laser mounted as part of a phase combination experiment.

The major peaks indicate the longitudinal mode separation. This was calculated to be 145GHz. Sample data from the maker's catalogue yields a value of 170GHz although no value is directly quoted. The separation of the minor peaks indicates a mode separation of 60GHz. Calculation

of the transverse mode separation, based on equation 4.6-8 of ref. 44 indicated a much lower value. The maker gave no figure for the possible transverse mode separation as the laser was assumed to operate in a single transverse mode. The deviation of the visibility curve from symmetry about the zero-delay position was due to the factor outlined above, viz. scattering in the beam splitter (41).

A section of the interferogram from which the visibility curve was formed, is shown in figure 5.8 below.

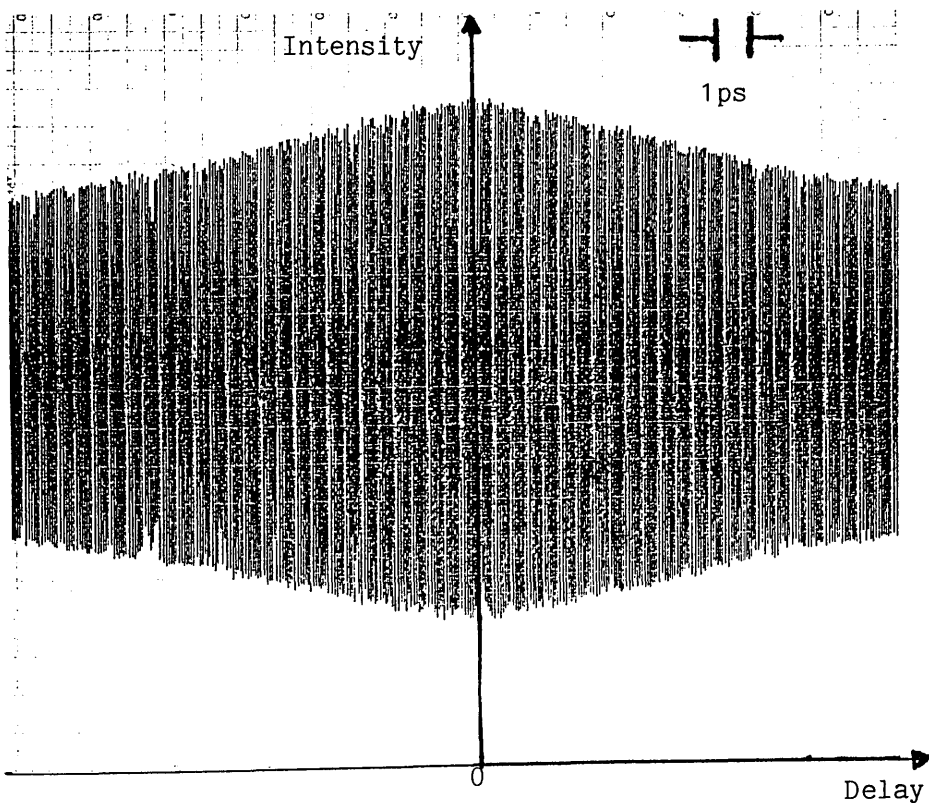


Fig. 5.8. Part of the interferogram obtained by scanning the output of a semiconductor laser.

The signal to background ratio at zero delay was close to 8:1. The following calculations were made from the data obtained from the interferogram.

(i) Calculation of wavelength.

The wavelength of the laser was calculated from a fringe count over a measured length of trace. 300cm on the chart recorder trace contained 3077 fringes. The total trace length of 703.5cm corresponded to an "Inchworm" movement of 3mm. Assuming the fringe spacing represents one half wavelength of laser light, the wavelength was then given by :-

$$\text{Wavelength} = \frac{2 \times 300 \times 3000\text{nm}}{703.5 \times 3077}$$

Applying the correction factor of 0.9965 indicated by the calibration scan above, yielded a wavelength of 828.6nm.

(ii) Calculation of cavity length.

The cavity length of the laser was given by :-

$$\text{Cavity length} = L = \frac{q \times \lambda}{2n} \quad , \quad (5.2)$$

where q represents the number of fringes between adjacent principal maxima,  $\lambda$  is the free-space wavelength of the laser and n is the refractive index of the lasing medium, here taken as 3.5 (31). Since 3077 fringes covered 300cm on the recorded trace, and the principal maxima were separated by 242.5cm on that trace, then :-

$$q = \frac{242.5 \times 3077}{2 \times 3.5}$$

$$= 2487.$$

From equation 5.2 above, the cavity length was therefore :-

$$L = \frac{2487 \times 828.6}{2 \times 3.5}$$

$$= \underline{294\mu\text{m}}.$$

(111) Calculation of mode spacing.

The longitudinal mode spacing was given by :-

$$\frac{\lambda}{q} = \frac{828.6}{2487},$$

$$= \underline{0.33\text{nm}}.$$

The above results may be compared with the manufacturer's sample data which suggests the cavity length to be 250 $\mu\text{m}$  and the longitudinal mode spacing to be 0.35nm.

The room temperature during the above measurements was 20 $^{\circ}\text{C}$  and the drive current was 61mA. The output power was measured to be 15mW.

(iv) Cavity length comparison.

A second laser output was scanned to provide a comparison with the above results. This yielded a wavelength of 825nm and a cavity length of 277.5 $\mu\text{m}$ . During this scan the laser temperature set by a Peltier cooling device was 29.3 $^{\circ}\text{C}$ . The drive current was again 61mA, corresponding to an output power of 15mW.

### 5.2.9. Further experiments using the Michelson configuration.

A 'short' external cavity was constructed from a dural framework, in which a semiconductor laser was mounted about 30cm from a high reflectivity mirror. The output from the cavity was taken via a beam splitter placed near the mirror at an angle of  $45^{\circ}$  to the direction of propagation. A short focal length lens was placed close to the semiconductor laser to collimate its output. This lens was anti-reflection coated at the laser wavelength. The diode mount was controlled by PZT movements in the X, Y and Z directions. A schematic diagram of the optical parts is shown in figure 5.9 below.

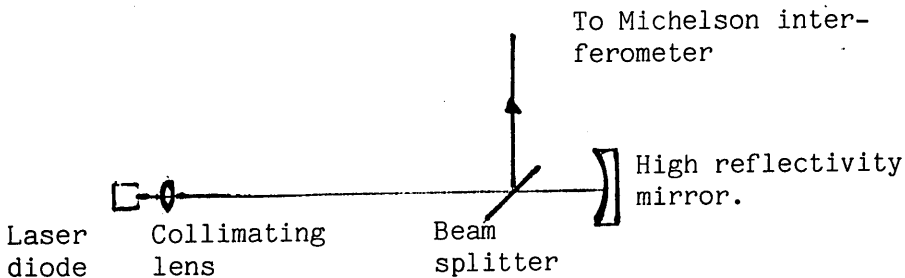


Fig. 5.9. Schematic diagram showing a laser diode mounted to form a short external cavity.

The output beam was aligned with the interferometer by means of a periscope. This was necessary because of

a difference in height levels in the two instruments. The interference fringes produced were detected by a photomultiplier tube and recorded by a 'Y-T' plotter.

#### 5.2.10. Instability and self-pulsing in a semiconductor laser.

When the output from the laser, mounted as described in 5.2.9 above, was scanned immediately after the laser was switched on, the output trace showed signs of considerable instability which persisted for some time. No thermal control was applied to the laser during this experiment, but it was mounted on a heat sink. The following figures 5.10 to 5.13 show the variation of intensity with delay over a time period of more than one hour.

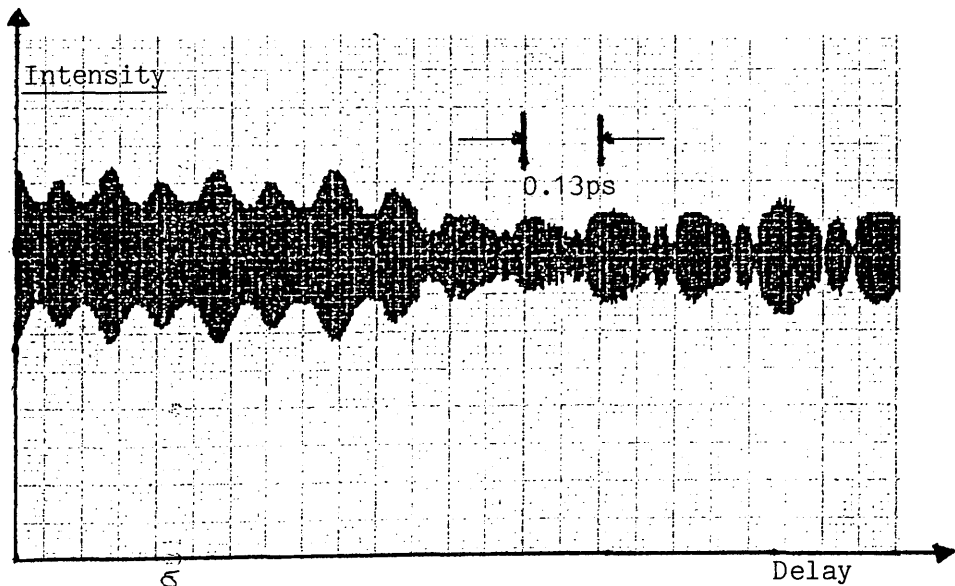


Fig. 5.10. Initial output from a Sharp semiconductor laser mounted in an external cavity, immediately after switch-on.

In figure 5.10, each pair of major and minor peaks are separated by about 0.13ps initially, increasing to about 0.2ps after 5 minutes. The chart speed for this and subsequent figures was 10mm/min., the "Inchworm" scanning rate  $0.25\mu\text{m/s}$  (approx.) which corresponds to a time delay of 0.13ps per cm. of trace.

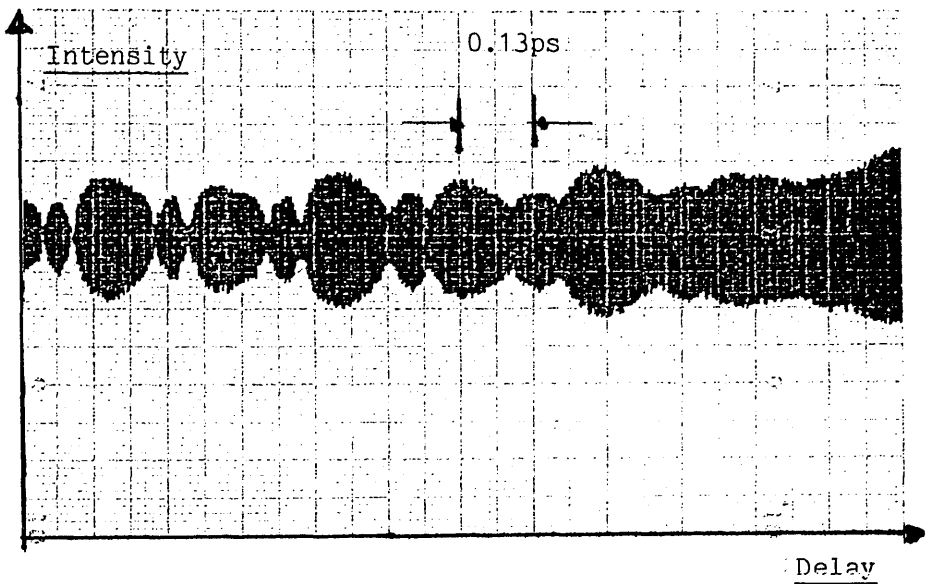


Fig. 5.11. Output from a Sharp semiconductor laser in an external cavity about 12 minutes after switch-on.

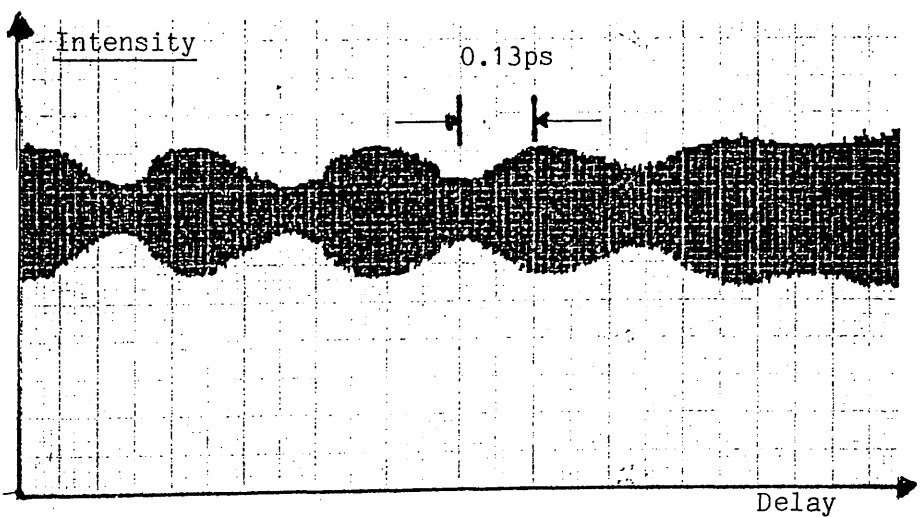


Fig 5.12. Output from a Sharp semiconductor laser in an external cavity about one hour after switch-on.

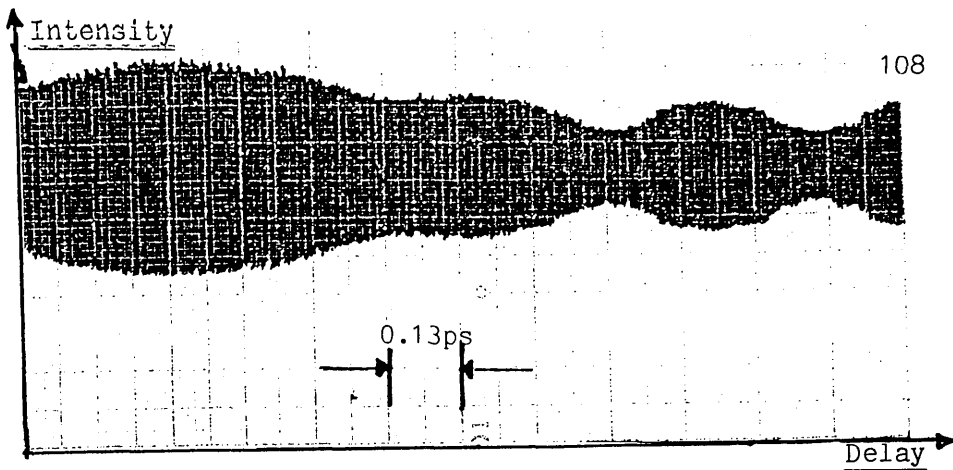


Fig. 5.13. Output from a Sharp semiconductor laser in an external cavity after one and a half hours of operation.

The total scanning movement of the "Inchworm" covered 3mm. The early part of the trace indicated the presence of several competing modes. Saturable absorption is present in many semiconductor devices and often increases with age. This may produce self-pulsing effects and has been exploited for mode-locking purposes (37).

As time increased the laser reverted to more stable operation although some mode structure remained. Taking the separation of the major maxima at this stage to represent the internal cavity length, the latter was calculated to be 283 $\mu\text{m}$ . The visibility of the fringes improved markedly as the laser became more stable. A scan of approximately 1000 fringes made when the laser was operating in a stable condition yielded a wavelength of 824nm and a cavity length of 295 $\mu\text{m}$ .

### 5.2.11. Effect of an external cavity on a semiconductor laser.

The dynamic properties of a semiconductor laser of the type used in the above experiment, are significantly affected by external feedback (42). While this can be used to narrow the spectral bandwidth or for mode-locking, unintentional results can arise from back reflection of light into the laser cavity.

The effect produced can depend on the length of the external cavity. For distances less than the coherence length of the laser, the system behaves like a coupled compound cavity. The resulting output is complex. This is due to several factors. These are :-

- (1) the presence of unstable transverse modes oscillating in several longitudinal modes;
- (2) the broad gain spectrum of the laser which permits the excitement of different longitudinal modes of the laser cavity with very small changes in the external feedback conditions;
- (3) the very sensitive dependence of the crystal refractive index on temperature;
- (4) the strong dependence of the active medium refractive index on the excited carrier density.

If the external cavity length exceeds about 5cm., as was the case in the above experiment, external feedback tends to enhance relaxation oscillations or induce self pulsing. The self pulsing observed in the above experiment, may be due to the effects outlined above, or to saturable absorption as noted earlier. A contributory factor may be local temperature fluctuations in the lasing region. In the laser used, the laser output wavelength increased by approximately 0.23nm per degree celsius. Temperature build-up due to relatively high thermal resistivity will affect the refractive index of the crystal and the carrier density sufficiently to influence the cavity operation. An investigation of these features could form the subject of future investigation.

### 5.3. Intensity auto-correlation.

Intensity auto-correlation is a useful technique for measuring the temporal dimensions of ultra-short pulses. Electronic detectors have sub-nanosecond capabilities when used in conjunction with a sampling oscilloscope. Tektronix currently offer a 11800 series sampling oscilloscope which, when used in conjunction with its corresponding sampling unit (SD46) and sampling head (SD24,SD26), is capable of a 25ps FWHM response. However the cost of such oscilloscopes and necessary accessories is high. Very fast photodetectors are becoming available which can respond to frequencies of 100Ghz but the very fast response required from the signal processing electronics means the photodetector's speed cannot be fully realized.

Intensity auto-correlators are currently being used to measure pulses of 50 femtosecond duration(41). Such an instrument can be constructed from fairly basic optical equipment and requires no sophisticated electronics. The instrument constructed for interferometric auto-correlation measurements had also the capability of making intensity correlation measurements.

### 5.3.1. Intensity auto-correlation of a mode-locked Nd.YAG laser output.

To test the capability of the instrument constructed in making an intensity auto-correlation, the output pulses from a mode-locked Nd.YAG laser were observed. The laser was actively mode-locked by an intra cavity acousto-optic modulator. This produced pulses at a 76MHz reproduction rate. The pulse duration was expected to be about 100 picoseconds.

The spatial extent of a 100ps pulse is about 3cm in air. In order to carry out the correlation measurement one retro-reflector had to be moved at least 1.5cm. The "Inchworm" was capable of a nominal movement of 6.25mm. However, it was mounted on a micrometer controlled translation stage which had a total possible movement of 25mm. It was therefore possible to scan the greater part of the pulse using the micrometer movement. Since there was no requirement to resolve the individual fringes, the "Inchworm" movement was superfluous.

Figure 5.14 below shows the optical layout and the ancillary equipment. The micrometer movement was linked to a stepper motor which was computer controlled. The optical detector

was also linked with the computer via a lock-in amplifier.

This allowed the data to be gathered and processed with a minimum of delay.

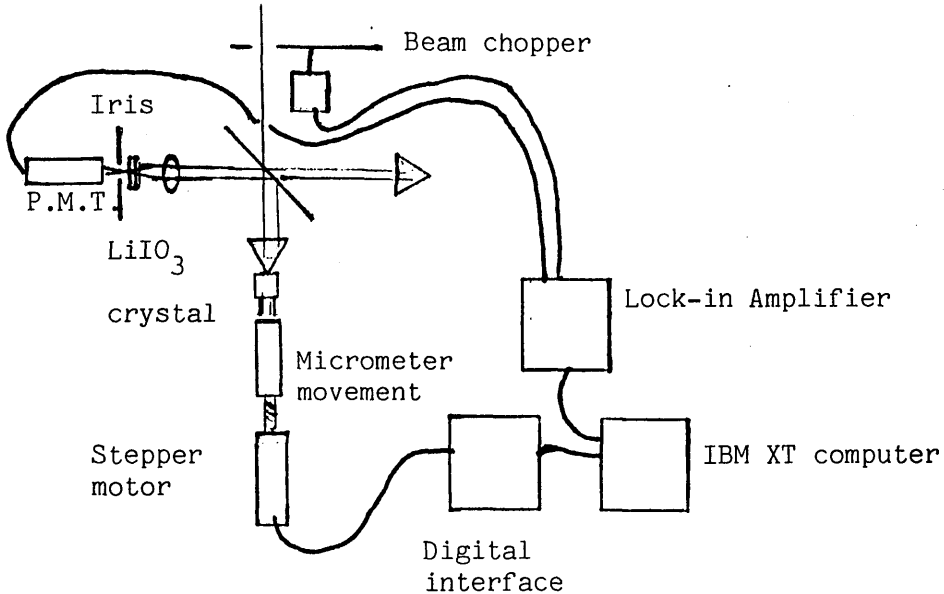


Fig.5.14. Schematic diagram showing the experimental layout for an intensity auto-correlation.

A lithium iodate crystal was used to produce a frequency-doubled output. The bandwidth of this frequency doubling crystal adequately covered the range produced by the Nd:YAG laser. The range of transparency of the crystal was from 310nm to 5500nm, while the laser operated at 1064nm with a room temperature bandwidth of 195GHz (21). The output from the crystal was detected by a photomultiplier tube, IP28 from Hamamatsu, which was insensitive to the infra red pump beam. Therefore an infra red filter was

not required.

(1) Experimental method.

To carry out an intensity correlation, the output beams from each arm of the interferometer were rendered parallel but not collinear. A short focal length lens directed the beam on to the frequency doubling crystal. The crystal was rotated to produce the best phase-matching conditions, as observed by an increase in the visible output. Each beam was blocked in turn to verify that the output was due to both beams combining within the crystal. The focussing lens was also adjusted to produce maximum output.

The micrometer movement, when carrying out a scan, was joined to the stepper drive via a universal coupling. The stepper motor was computer controlled. One revolution of the stepper motor axis was equivalent to half a revolution of the micrometer. The output from the photomultiplier tube was passed to a lock-in amplifier whose reference signal was obtained by 'chopping' the input beam at 1kHz. The output from the lock-in amplifier was passed via a suitable interface to the computer. The data from the photomultiplier and the stepper motor was correlated by the computer and used to give a print-out of the intensity correlation.

## (ii) Intensity auto-correlations and results.

Scans of up to 540 data points could be displayed directly on the computer. Each step of the stepper motor represented  $2.5\mu\text{m}$ . Since there was a 2:1 ratio between the stepper drive and the micrometer translation carrying the retro-reflector, each step of the combined movement represented  $1.25\mu\text{m}$ .

The scan shown in figure 5.15 below shows 540 data points each of which represents 40 steps of the stepper motor.

The width of the scan shown =  $540 \times 40 \times 1.25\mu\text{m}$ .

The path difference =  $2 \times 540 \times 40 \times 1.25\mu\text{m}$ .

This represents a time delay =  $\frac{2 \times 540 \times 40 \times 1.25 \times 10^{-6}}{3 \times 10^8}$   
 = 180ps.

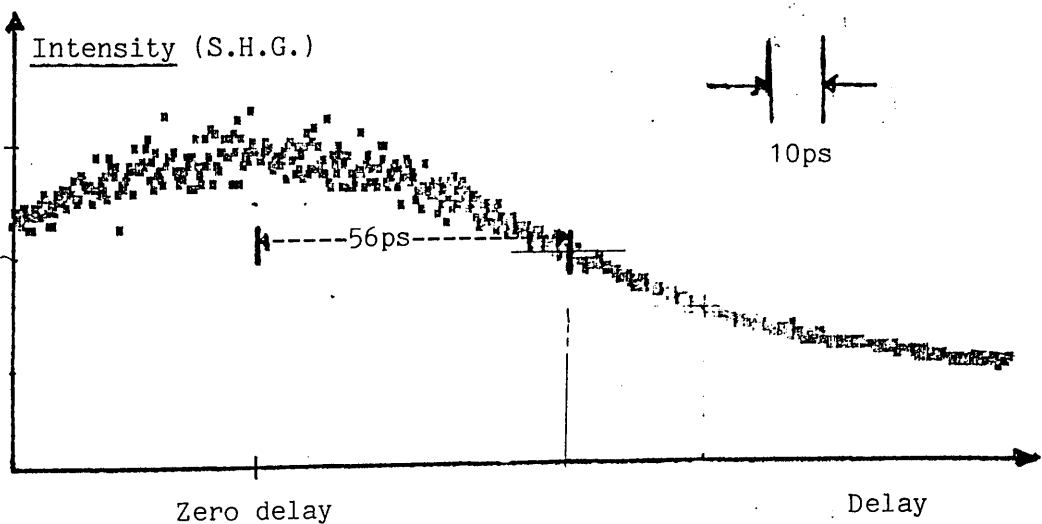


Fig. 5.15. Intensity auto-correlation of a Nd:YAG pulse.

The print-out width was 19.4cm while the width of the curve at half-maximum points was estimated to be 12cm, allowing for background. The apparent pulse width was therefore :-

$$= \frac{12 \times 180}{19.4}$$

$$= \underline{111} \text{ps.}$$

The second scan, shown in figure 5.16 below, covered 500 data points, each of which represented 24 steps of the stepper motor. This yielded an apparent pulse width of 90ps. The discrepancy in the above measurements arose from the difficulty of estimating the background level, and hence the half-maximum points, with accuracy.

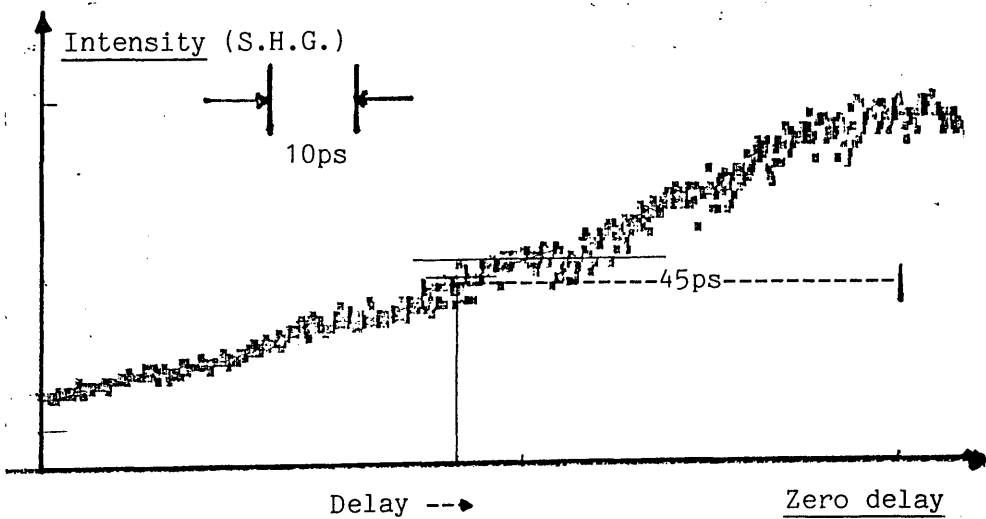


Fig. 5.16. Intensity auto-correlation of a Nd.YAG pulse.

#### 5.4. Interferometric auto-correlation.

The operation of the instrument as an interferometric auto-correlator was tested in two ways. Firstly, a scan of part of the output pulse from the Nd.YAG laser described above, was carried out. Because of the limitation in the extent of the "Inchworm" movement, it was not possible to scan the entire pulse. Secondly, a sampling scan was carried out at millimetre intervals throughout the entire length of the pulse.

##### 5.4.1. Interferometric auto-correlation of part of a Nd.YAG pulse.

In order to carry out the interferometric measurements, the beams from each arm of the interferometer were made parallel and collinear. The position of the frequency doubling crystal was adjusted to give maximum output from the combined beams. It was observed that, in this mode of operation, the output from the crystal showed a cone shape. This is associated with the locus of phase matching paths through the crystal.

The output was detected by a photomultiplier tube as above, and passed to a 'Y-T' plotter. For alignment purposes and for establishing the approximate position of zero-delay,

the output was observed on an oscilloscope.

A short test was carried out using the computer-controlled arrangement of the intensity correlation described in 5.3.1 above. The stepper motor was uncoupled and allowed to run freely. Several fringes were scanned using the "Inchworm" movement. A very slow scan rate was chosen to allow the gathering of sufficient data points which would reproduce the fringe shape with reasonable accuracy. Figure 5.17 below shows the fringes scanned in this manner. It was noted that the fringe spacing increased about every sixth fringe due to the 'glitch' in the "Inchworm" movement described earlier. The background level fell to nearly zero at the fringe minima.

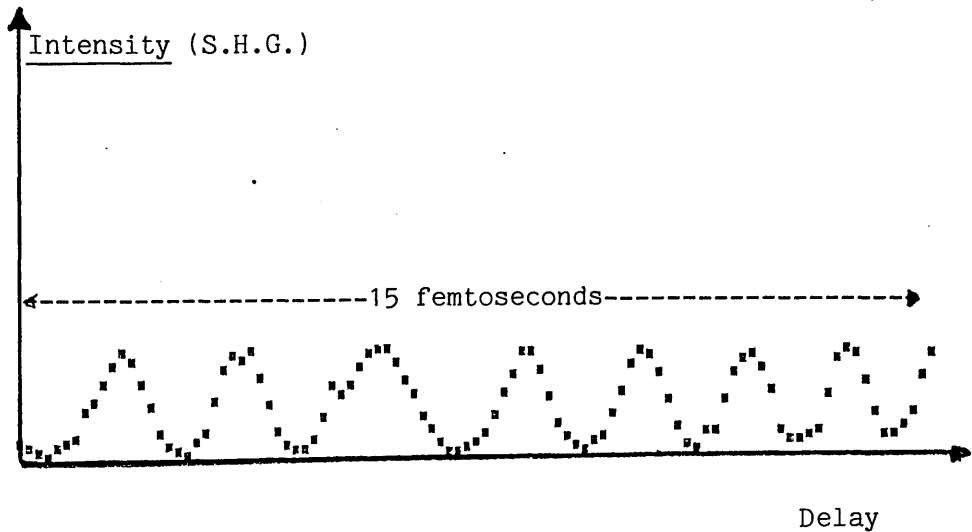


Fig 5.17. Interferometric auto-correlation of a few fringes from a mode-locked Nd.YAG laser.



The flat central region shown in the partial pulse scan of figure 5.18 may have been caused by saturation of the photomultiplier tube. A second scan showed a similar feature. This is illustrated in figure 5.19 below. When taken in conjunction with the intensity correlations, this indicated that the pulse was relatively flat in the central region. However poor phase-matching within the frequency-doubling crystal can also produce the same result (3).

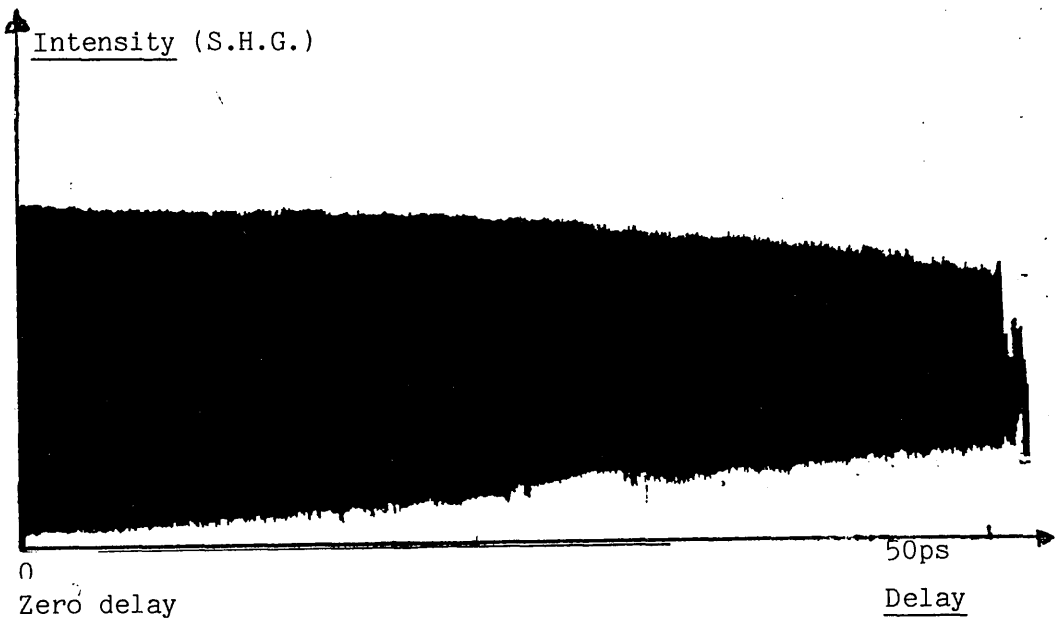


Fig. 5.19. Interferometric auto-correlation of about half the output pulse from a Nd.YAG laser.

The visibility of the fringes at the pulse centre was about 0.91. The visibility at a delay of 50ps from the centre remained at the high value of 0.5. The broad wings

of the pulse indicate that the coherence was high towards the pulse edges (28).

A very slow paper speed was employed during the above scans. This obscured the individual fringes.

#### 5.4.2. Sampling interferometric auto-correlation of sections of a Nd.YAG laser output pulse.

Because the optical path length of a 100ps pulse in air exceeded the maximum possible movement of the "Inchworm", it was not possible to scan the entire pulse length. Furthermore an interferometric scan of a 100ps pulse takes a considerable time using the apparatus outlined above. The Nd.YAG laser used in this work tended to become unstable after several hours of continuous use. In order to overcome these difficulties, it was decided to sample the pulse at regular intervals, recording one thousand fringes at each interval. Any lack of coherency would be indicated by changes in the fringe spacing. The results of this process are shown in table 1 below.

The table shows a shorter apparent wavelength towards the centre of the pulse, which confirms the presence of 'chirp' within the pulse.

TABLE 1. Apparent wavelength at equal delay

increments through a Nd.YAG pulse of about 100ps duration.

<u>SCAN</u>	<u>LENGTH</u>	<u>No. of FRINGES</u>	<u>APPARENT WAVELENGTH</u>
1	534 $\mu$ m	997	1066.7nm
2	534 $\mu$ m	997	1066.7nm
3	534 $\mu$ m	1001	1063.2nm
4	534 $\mu$ m	1000	1064.3nm
5	534 $\mu$ m	1001	1063.2nm
6	534 $\mu$ m	1002	1062.1nm
7	534 $\mu$ m	1001	1063.2nm
8	534 $\mu$ m	1002	1062.1nm
9	534 $\mu$ m	1003	1061.1nm
10	534 $\mu$ m	996	1068.5nm
11	534 $\mu$ m	998	1066.5nm

The following figures, 5.20 to 5.23, show sections of the auto-correlation from the edges where the visibility is extremely poor, towards the zero-delay position where the visibility is high, about 0.8. The individual fringes are apparent in these scans.

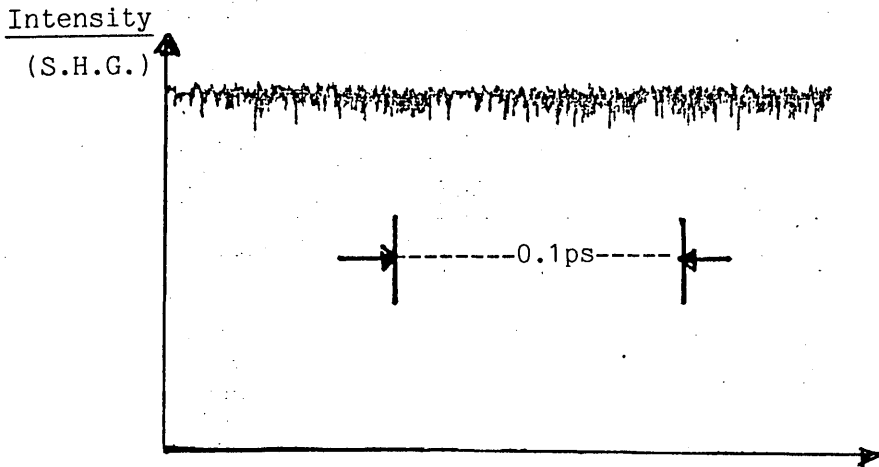


Fig. 5.20. Section of a sampling scan of an Nd.YAG laser

pulse where the delay exceeds the pulse overlap.

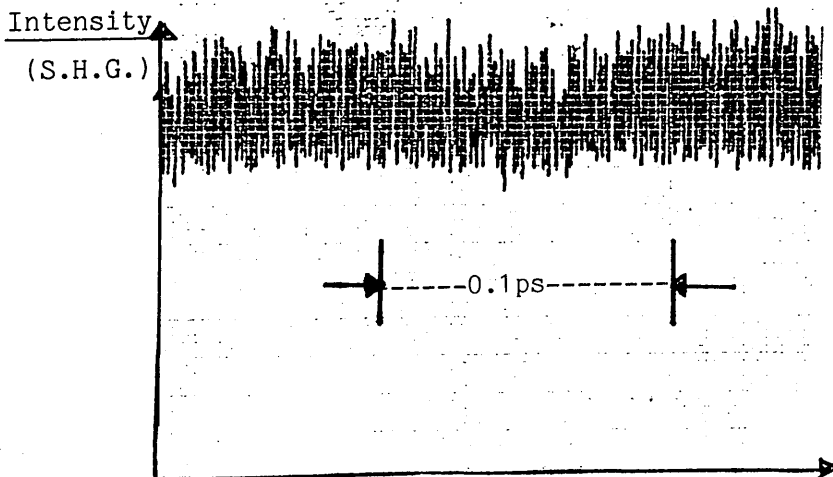


Fig. 5.21. Section of the above sampling scan about

60 ps from zero delay.

Intensity  
(S.H.G.)

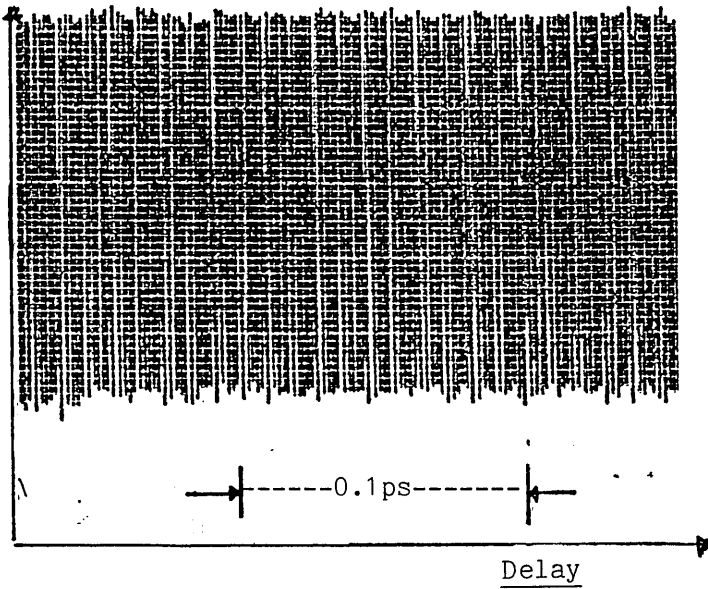


Fig. 5.22. Section of the above sampling scan in the vicinity of zero delay.

Intensity  
(S.H.G.)

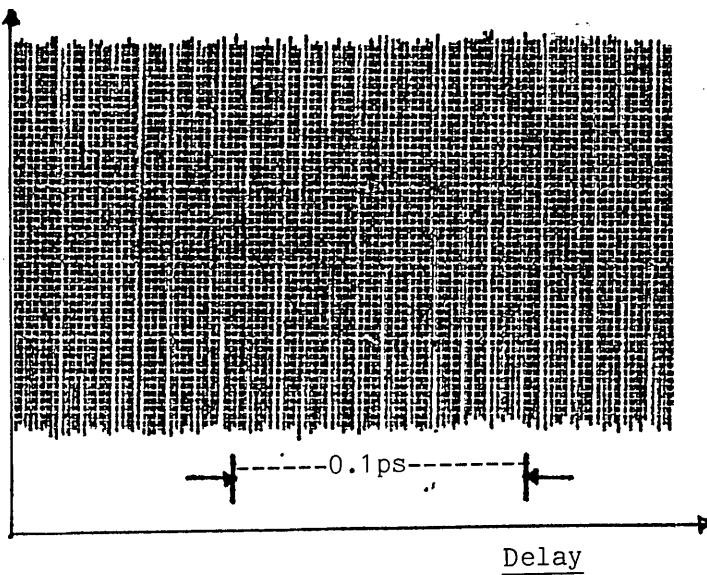


Fig. 5.23. Section of the above sampling scan about 20 ps from zero delay.

### 5.5. Instability in an Nd.YAG laser output.

It had been observed for some time that the Nd.YAG laser used in the above experiments tended to unstable operation after several hours of continuous use. The lower envelope of figure 5.23 above shows the onset of this phenomenon by the appearance of ripple. It was suspected that this might be related to the operation of the mode-locker.

The trace shown in figure 5.24 indicates the effect on the output when the mode-locker was run without, and then with, thermal control. There is a clear improvement from one hour onwards, when the temperature control was switched on. This is indicated by the absence of ripple from the upper and lower envelopes of the trace after that point.

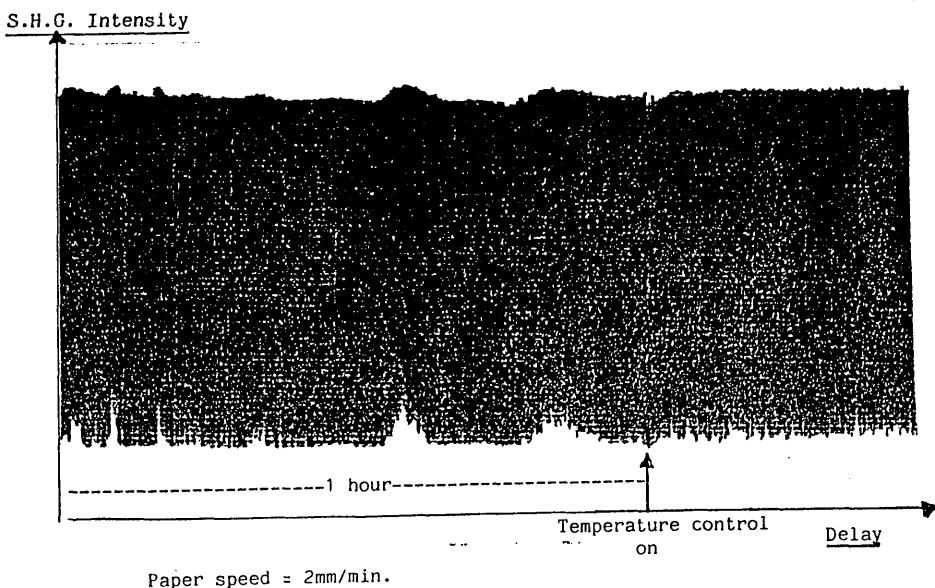


Fig. 5.24. Interferometric scan of a mode-locked Nd.YAG laser showing the effect of applying temperature control to the mode-locker.

The scan shown in figure 5.25 below was made from the output of the Nd:YAG laser after the onset of instability. This showed the type of fluctuation present in figure 5.24 before the application of temperature control to the mode-locker.

Intensity (S.H.G.)

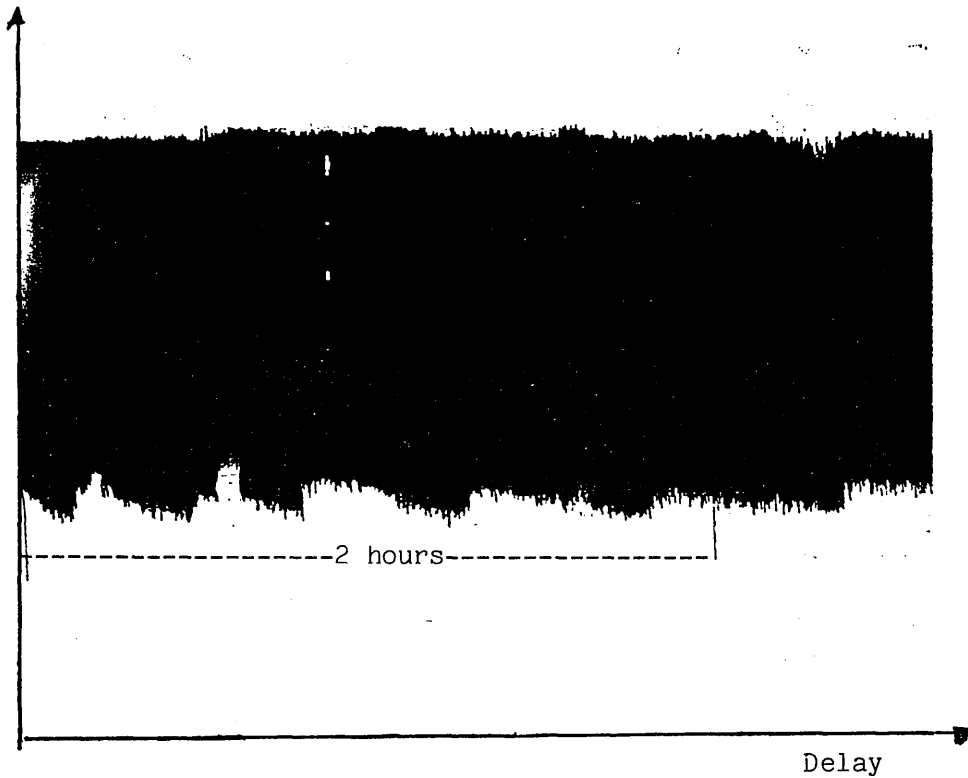


Fig. 5.25. Interferometric scan of a mode-locked Nd:YAG laser after some hours of operation, showing the onset of instability in the laser output

The interferometric auto-correlator was found to be useful in detecting unstable operating conditions which were not readily observable by power measurements or pulse observations on a sampling oscilloscope.

## 5.6. Summary.

The performance of the interferometric auto-correlator was evaluated in three different modes of operation. It was used as a linear interferometer to produce interferograms from the output of several semiconductor lasers operating in a variety of configurations. Visibility curves were produced from these and used to estimate cavity length and coherence length. The interferogram yielded the operating wavelength. The visibility curves also revealed the presence of additional transverse modes in a nominally single mode laser. Evidence of self-pulsing and instability was recorded for an ageing laser mounted in an external cavity. Features in the femto-second region were displayed.

Intensity correlations of 100ps pulses from a mode-locked Nd:YAG laser were made. Estimations of the temporal pulse width were obtained and presented. Interferometric auto-correlations were carried out over half the pulse width. A sampling interferometric scan was carried out over the total pulse width. The presence of chirp was detected.

Instability in the laser operation was observed and recorded by interferometric auto-correlation. This instability was related to problems of thermal control in the mode-locker.

CHAPTER SIX.CONCLUSIONS AND FUTURE WORK.6.1 Conclusions drawn from the work completed.

The growing number of applications of ultra-short pulses and the attainment of ever shorter pulse widths have shown the need for a more complete knowledge of pulse structure (1),(7). A survey of a variety of instruments in current use shows considerable limitations in their abilities to provide the necessary information to unequivocally give a complete description of an ultra-short pulse.

The interferometric auto-correlator has been suggested as an instrument capable of providing information regarding pulse amplitude and phase. An interferometric auto-correlation, taken in conjunction with an intensity correlation and an amplitude correlation should be able to reveal the nature of an ultra-short pulse (20). The only remaining ambiguity would be time inversion.

An instrument has been constructed which is capable of all three functions. It has been operated successfully in all three modes. It has shown the presence of chirp within

a 100ps pulse. In addition it has proved to be a useful diagnostic tool in observing the output of both pulsed and cw lasers. It has identified the operating parameters of semiconductor lasers and revealed the presence of instability and self-pulsing in an ageing semiconductor laser. Features in the femtosecond region were clearly observable.

## 6.2. Suggestions for future applications.

It has been shown that useful information can be obtained in a variety of ways using the interferometric auto-correlator. This information is initially in the form of interferograms, intensity correlations and interferometric correlations. The handling and analysis of this data would be greatly facilitated by direct recording in a host computer. This would allow the direct display of the data gathered, and make it accessible to sophisticated analytical techniques.

### 6.2.1. Fast Fourier Transforms.

When used in the linear mode, the intensity of the output optical signal, measured as a function of path difference or time delay, is the Fourier transform of the frequency spectrum (32). In practice, the ideal transform pair is never realized. The interference pattern (interferogram) is recorded between finite limits. This restricts the resolving power of the instrument. To carry out the Fourier

transform, the optical signal must be sampled at fixed intervals of the order of half the shortest wavelength present in the signal. This avoids the overlap of features within the spectrum.

The optical signal must be digitalized for computerization. For a transformation involving  $N$  sampling points,  $2N^2$  operations are required for a full Fourier transform. This number has been greatly reduced by the application of the 'fast Fourier transform' (F.F.T.).(43). The latter makes use of the symmetry properties due to equal steps in both the interferogram and the spectrum. The number of operations is reduced to  $2N \log_2 N$ . Treatment of the data in this fashion would produce a spectrum where the troublesome glitch in the 'Inchworm' movement noted above would appear as a spectral component well removed from the true spectrum of the optical signal.

#### 6.2.2. Application of F.F.T. to pulse analysis.

F.F.T. techniques have also been suggested as a means of elucidating pulse structure without recourse to assumptions regarding the original nature of the pulse (20). In general there can be no justification for assumptions regarding pulse form. Where such assumptions are made, there can be no assurance that the obtained results represent a unique

solution describing pulse structure. The mathematical foundation of an assumption-free pulse reconstruction has been laid down which is based on auto-correlation techniques. The total data set required consists of the amplitude correlation, the intensity correlation and the interferometric correlation of a pulse. All of these can be obtained using the interferometric auto-correlator constructed for this work. The only remaining ambiguity is that the time direction cannot be obtained.

### 6.2.3. System modifications.

In order to adapt the interferometric auto-correlator to collect the required data set, the following improvements are required. The optical data must be digitalized for passage to a host computer. This was already done during the intensity correlations of the Nd:YAG pulses recorded above. The optical signal must be correlated with the time delay or the linear movement of the 'Inchworm'. The latter's controller already has a facility for control by a host computer which can be activated by the addition of a processor card. The accuracy and reliability of the F.F.T algorithm relies on the equality of steps in the sampling process. In the present instrument the encoder resolution is not sufficiently accurate to provide the necessary step

size for sampling. With the addition of a host computer the scan speed of the 'Inchworm' movement can be controlled to allow sampling to take place at time intervals corresponding to steps of a suitable size.

Some asymmetry was present in the instrument constructed, mainly due to the beam splitter used. This should be replaced by a more suitable type as described in the text. The use of complex Fourier transforms during data analysis can help overcome the effects of any remaining asymmetry.

#### 6.2.4. Research applications.

With the improvements outlined above, the interferometric auto-correlator should provide a convenient instrument for many research applications. Observations of pulse structure before and after interaction with optical fibres and devices should provide useful information regarding pulse degradation in an optical communication system. Laser diagnostics of both pulsed and cw lasers could be carried out. The testing of new semiconductor lasers, establishing their operating characteristics and parameters should assist in theoretical understanding of their operation and in design improvements.

Laser arrays are a subject of current interest. The coherent output from such arrays could be examined to establish the operating parameters and frequency spectrum. The relation-

ship between wavelength, drive current and temperature for a semiconductor laser could be examined since the output spectrum is temperature dependent. Information might be obtained regarding the temperature of the active region of the laser as compared with the heatsink temperature. Lasers used in current research often exhibit very short lifetimes. This may be due to poor thermal conductivity near the active region resulting in a high local temperature.

Extended cavity semiconductor lasers are also of current interest. In such a laser the cavity is extended by fabricating an optical waveguide as a direct extension of the laser diode cavity. This increases the effective cavity length by several millimetres. Such a laser should produce a narrow emission line and is also suitable for mode-locked operation. The examination of the output of such a laser in both cw and pulsed modes could be carried out using the interferometric auto-correlator.

### 6.3 Summary.

It has been concluded that the interferometric auto-correlator built is capable of useful application in several areas of research. Modifications to the instrument have been suggested which would enhance its usefulness and ease of operation. In particular it has been suggested that

computer control of the scanning operation and data gathering would allow direct display of the information obtained and allow the application of sophisticated analysis techniques such as fast Fourier transforms.

The necessary system modifications have been outlined. Possible research applications have been suggested. These include diagnostics of laser systems in current use, investigation of pulse structure from generation to output from optical devices, and investigation of the output of new laser types, both pulsed and cw. It is hoped that the instrument built for this work will find successful application in some of these areas.

REFERENCES GIVEN IN THE TEXT.

1. 'A perspective on ultrafast phenomena.' A. Millet & W. Sibbett; Journal of Modern Optics; 1988, 35; 12; 1871-1890.
2. 'The generation of ultra-short laser pulses'; G. H. C. New; Reports on Progress in Physics; 46; pp877-971, 1983.
3. 'Picosecond Laser Pulses'; A. J. De Maria; Proc. I.E.E.E.; 57; pp2-25; January 1969.
4. 'Optical Fibre - Prognosis and Economic Impact'; C. Kao; Electronic and Wireless World; pp395-396; April 1988.
5. 'Pulse Transmission through a Dielectric Optical Waveguide'; E. P. Kapron & D. B. Keck; Applied Optics; 10; 7; July 1971.
6. 'Picosecond and Femtosecond Fourier Pulse Shape Synthesis'; A. M. Weiner & J. P. Heritage; Revue Physique Applique; 22; pp1619-1628; 1987.
7. 'Frontiers of Femtosecond Research'; Laser Focus/Electro-Optics; April 1985; pp65-76.
8. 'Ultra-short Pulse Measurement'; D. J. Bradley & G. H. C. New; Proc. I.E.E.E.; 62; 3; March 1974; pp313-345.
9. 'Compression of Picosecond Light Pulses'; Physics Letters; 28A; 1; 21 October 1968; pp34,35.

10. 'Measurement of Picosecond Pulse Structure Using Compression Techniques'; E. B. Treacy; Applied Physice Letters; 14; 3, 1 February 1969; pp112-114.
11. 'Direct Demonstration of Picosecond Pulse Frequency Sweep'; E. B. Treacy; Applied Physics Letters; 17; 1; July 1970.
12. 'Measurement and Interpretation of Dynamic Spectrograms of Picosecond Light Pulses'; E. B. Treacy; Journal of Applied Physics; 42; 10; September 1971.
13. Optics Communications; 15; 29; (1975); H. A. Haus et al.
14. 'Dynamic Spectroscopy and Sub-picosecond Pulse Compression'; E. P. Ippen & C. V. Shank; Applied Physics Letters; 27; 9; 1 November 1975..
15. 'Generation and Measurement of 200 femtosecond Optical Pulses'; J. C. Diels et al; Optics Communications; 25; 1; April 1978; pp93-96.
16. ' An Intensity/Phase Autocorrelator for the Use of Ultra-short Pulse Measurements'; Kurobori et al; Optica Communications; 40; 2; 15 December 1981.
17. 'Novel Method of Waveform Evaluation of Ultra-short Optical pulses'; T. Kobayashi et al; Picosecond Phenomena III; Springer-Verlag; 1984.

18. 'Measurement of the Phase of a Frequency-swept Ultra-short Optical Pulse'; Joshua E. Rothenburg & D. Grischowsky; J. Optical Society of America; B; 2; 4; April 1985.
19. 'Measurement of Optical Phase .....'; Joshua E. Rothenberg & D. Grischowsky; Optics Letters; 12; 2; pp99-101; February 1987.
20. 'General Method for Ultra-short Light Pulse Chirp Measurement'; Kazunori Naganuma et al; I.E.E.E. Journal of Quantum Electronics; 25; 6, June 1989.
21. 'Principles of Lasers'; O. Svelto; 2nd edition; Plenum Press; N.Y.
22. 'Principles of Optics'; Max Born & E. Wolf.
23. 'Simultaneous Autocorrelation and Synchroscan Streak Camera Measurement .....'; P. G. May et al.; Optics Communications; 42; 4; 15 July 1982; pp285-290.
24. 'Methods of Pulse-width Measurement'; H. P. Weber; Journal of Applied Physics; 38; pp2231-2234; April 1967.
25. 'Generalized Interference Technique for Ultra-short Pulse Characterization'; Jamal T. Manassah; Applied Optics; 26; 10; 15 May, 1987.
26. 'Solid State Physics'; A. J. Dekker, MacMillan & Co. Ltd., London 1967.

27. 'A Simple Monitoring System .....'; Y. Ishida & T. Yajima; Opt. Communications; 56; 1; 1 November, 1985, pp57-60.
28. 'Control and Measurement of Ultra-short Pulse Shapes'; J. C. Diels et al.; Applied Optics; 24; 9; 1 May 1985.
29. 'Methods of Experimental Physics'; Vol15B; pp185-209.
30. 'Cw. Auto-correlation Measurements of Picosecond Pulses'; K. L. Sala et al.; I.E.E.E. Journal of Quantum Electronics; QE 16; 9; September 1980; pp990-996.
31. Sharp Diode Laser Catalogue.
32. 'Spectrophysics'; A. Thorne.
33. 'Principles of Optics'; Born & Wolf; pp316ff.
34. Review of Modern Physics'; Mandel & Wolf; 37; 2; April 1965.
35. 'Fine Modern Piezoelectric ceramics'; Vernitron Bulletin; January 1976.
36. 'Electronic Communications Systems; George Kennedy; p449; M<sup>C</sup>Graw Hill;1987.
37. 'Generation of Sub-picosecond Coherent Optical Pulses...'; H. Yokayama et al; Applied Physics Letters; 40; 2; pp105-107.
38. 'Coherent Summation of Laser Beams Using Binary Phase Gratings'; W.B.Veldkamp et al.; Optics Letters; 11; 5; May, 1986.

39. 'Coherent Laser Addition Using Binary Phase Gratings';  
James R. Leger, Gary T. Swanson, Wilfred B. Veldekamp;  
Applied Optics; 26; 20; 15 October, 1987.
40. 'Colliding Pulse Femtosecond Lasers .....'; J. C. Diels  
et al.; Ultrafast Phenomena IV, Eds. D. H. Auston & K. B.  
Eisenthal; Springer-Verlag; Berlin 1984; pp30-34.
41. 'Study of a Linear Femtosecond Laser in Passive and Hybrid  
Operation'; Nooshi Jamaski et al.; Journal of Modern Optics;  
35; 12; pp1891-1906.
42. 'External Optical Feedback Effects on Semiconductor  
Injection Laser Properties'; Roy Lang & Kohroh Koboayashi;  
I.E.E.E. Journal of Quantum Electronics; QE-16; 3; March 1980.
43. 'The Fast Fourier Transform'; E. O. Brigham; Prentice  
Hall, Eaglewood Cliffs, N. J. 1974.
44. 'Optical Electronics'; Amnon Yariv 3rd Edition.

Works consulted but not quoted directly in the text :-

Cavity modes.

'Infra-red and Optical Masers'; A.L. Schawlow & C.H. Townes,  
Physical Review, 112, 6; December 15, 1958.

'Confocal Multimode Resonator for Millimetre through Optical  
Wavelength Masers'; G.D. Boyd & J.P. Gordon; The Bell System  
Technical Journal, March 1961.

Auto-correlation.

'Modern Communication Systems'; R. F. W. Coates; 2nd Ed.,  
MacMillan, 1983.

'Simple Distortion-free Real-time Optical Pulse Correlator';  
J.K. Jain et. al., Applied Optics; 21, 22; 15 November 1982.

'Real-time Monitoring of CW Mode-locked Dye Laser Pulses...';  
D. Welford & B. C. Johnson; Optics Communications, 45, 2;  
15 March 1983.

Interferometry.

'Semiconductor Laser Lineshape and Parameter Determination  
from Fringe Visibility Measurements'; E. Eichen & P. Melman,  
Electronics Letters, 20, 20, pp826-828.

'Interaction of Ultrashort Pulses with Etalons'; C. Thomsen  
& Nabil M. Lawandy, Applied Optics, 23, 19; 1 October 1984.

Works consulted....(cont) :-

Pulse width measurement.

'The Effect of Pulse to Pulse Variation on Ultrashort Pulse-width Measurement'; E. W. Van Stryland, Optics Communications, 31, 1; October 1979.

'Determination of the Pulse Response from Intensity Auto-correlation Measurements of Ultrashort Laser Pulses'; T. Andersson & S. T. Eng, Optics Communications, 47, 4, 15 September 1983.

Pulse structure.

'Basis for Picosecond Structure in Mode-locked Laser Pulses'; H. A. Pike & M. Hercher, Journal of Applied Physics, 41, 11; October 1970.

Pulse structure - semiconductor lasers.

'Chirped Picosecond Pulses ....'; D. Marcuse & J. M. Wiesenfeld, Applied Optics, 23, 1; 1 January 1984.

'Temporal Coherence Properties of Picosecond Pulses...'; Per Andersson et al., Journal of Lightwave Technology, Vol. LT2,2; April 1984.

'Sub-picosecond Pulses from a Mode-locked semiconductor Laser'; Y. Silberberg & P. W. Smith, I.E.E.E Journal of Quantum Electronics, QE-22, 6; June 1986.

Works consulted ..... (cont) :-

Mode-locking of semiconductor lasers.

'Pulse Shortening of Actively Mode-locked Diode Lasers by Wavelength Tuning'; Applied Physics Letters, 50, 18; 4 May 1987. M. Serenyi et al.

'Passive Mode-locking of a Semiconductor Diode Laser'; Y. Silberberg et al., Optics Letters, 9, 11; November 1984.

'Sub-picosecond Pulses from Passively Mode-locked GaAs Buried Optical Guide Semiconductor Lasers'; J. P. Van Der Ziel et al., Applied Physics Letters, 39, 7, 1 October 1981.

Coupled cavities.

'Locking of HeNe Laser Modes by Intra-cavity Acoustic Modulation in Coupled Interferometers'; M. D. Domenico & V. Garniewski, Applied Physics Letters, 6, 8, 15 April 1965, pp 150-152.

